STRUCTURE AND FUNCTION OF THE PALMITOYLTRANSFERASE DHHC20 AND THE ACYL COA HYDROLASE MBLAC2

A Dissertation

Presented to the Faculty of the Graduate School

Of Cornell University

In Partial Fulfillment of the Requirements for the Degree of

Doctor of Philosophy

By

Martin Ian Paguio Malgapo

December 2019

STRUCTURE AND FUNCTION OF THE PALMITOYLTRANSFERASE DHHC20

AND THE ACYL COA HYDROLASE MBLAC2

Martin Ian Paguio Malgapo, Ph.D.

Cornell University 2019

My graduate research has focused on the enzymology of protein S-palmitoylation, a reversible posttranslational modification catalyzed by DHHC palmitoyltransferases. When I started my thesis work, the structure of DHHC proteins was not known. I sought to purify and crystallize a DHHC protein, identifying DHHC20 as the best target. While working on this project, I came across a protein of unknown function called metallo-β-lactamase domain-containing protein 2 (MBLAC2). A proteomic screen utilizing affinity capture mass spectrometry suggested an interaction between MBLAC2 (bait) and DHHC20 (hit) in HEK-293 cells. This finding interested me initially from the perspective of finding an interactor that could help stabilize DHHC20 into forming better quality crystals as well as discovering a novel protein substrate for DHHC20. I was intrigued by MBLAC2 upon learning that this protein is predicted to be palmitoylated by multiple proteomic screens. Additionally, sequence analysis predicts MBLAC2 to have thioesterase activity. Taken together, studying a potential new thioesterase that is itself palmitoylated was deemed to be a worthwhile project. When the structure of DHHC20 was published in 2017, I decided to switch my efforts to characterizing MBLAC2.

This dissertation consists of three chapters. Chapter 1 is an introductory chapter surveying the literature on protein S-fatty acylation, with an emphasis on the mechanistic and functional studies on palmitoylation and DHHC proteins. The review also touches on the current status and

advancements in the relatively understudied but equally important field of protein depalmitoylation. Chapter 2 outlines my efforts to crystallize the palmitoyltransferase DHHC20 with the goal of solving its 3D structure. Additionally, I present the results of my investigation of the oligomerization of DHHC20 at a single molecule level. Chapter 3 describes my biochemical study of the uncharacterized MBLAC2 protein. I discuss my findings that MBLAC2 is a palmitoylated protein and is a substrate of DHHC20. My subsequent functional studies reveal that MBLAC2 is a robust acyl CoA thioesterase and contains multiple zinc-binding residues that are important for catalytic activity. Lastly, a book chapter we published in *Methods of Molecular Biology* on purifying recombinant DHHC proteins is included as an appendix.

BIOGRAPHICAL SKETCH

Ian Malgapo was born on February 17, 1990 in Manila, Philippines. As early as high school, he realized his interest the chemical sciences and eventually majored in Chemistry during his undergraduate studies in the University of the Philippines. As a college student, he worked on multiple research projects in the field of Organometallic Chemistry under the supervision of Dr. Jim Minglana. At the time, Ian was fascinated by the applications of green chemistry in renewable energy. For his thesis project, he worked on the synthesis and characterization of novel ruthenium and ruthenium-iridium bimetallic complexes as sensitizers for Dye-sensitized Solar Cells (DSSC's). He presented this work during the Philippine Chemistry Congress in 2010. He was also a trained as a summer student in Energy Development Corporation, the largest producer of geothermal and other renewable energy in the Philippines. During his internship, he devised new methods of extracting oil from seeds of *Jatropha curcas*, a native flowering-plant in the Philippines, for the subsequent synthesis of biodiesel. He then obtained his Bachelor of Science degree, graduating Magna Cum Laude and was one of the two recipients of the Baldomero Olivera–Lourdes Cruz award in the graduating class.

It was in his college senior year that he realized that his greatest passion is teaching. After graduation, he served as a chemistry lecturer and laboratory instructor for two years in the same university. In Fall 2012, he started to pursue his Ph.D, in Chemistry from Cornell University. At Cornell, he also enjoyed his time serving as a teaching assistant in Honors General Chemistry and Physical Chemistry for two years. In 2014, he was given a chance to work with Professor Jane Walcott to develop and teach an Introduction to Chemistry summer course for high school students.

While he was initially registered to do organometallic chemistry research, the incredibly rich scientific community at Cornell enticed him to expand his horizons to other fields. He eventually joined Professor Maurine Linder's lab and worked on the enzymology of protein S-palmitoylation.

After graduation, Ian hopes to do two things. The first thing is to follow his love for teaching and be a lecturer in an undergraduate institution. The second thing is to integrate what he learned so far as an organometallic chemist and a protein biochemist and pursue a professional career in interdisciplinary medicinal research, contributing to the development of important therapeutic products for the public.

ACKNOWLEDGEMENTS

My pursuit of a Ph.D. degree has been the most challenging undertaking I have ever experienced thus far. Over the course of seven years, I have received immeasurable support, encouragement, and help from more people than I can thank in this section.

First, I would like to give my deepest gratitude to my advisor Dr. Maurine Linder for her mentorship since I joined her lab in 2014. I am forever grateful that she took a risk in taking me as a student knowing that I had very little background in biology. She has taught me so many things, the most important of which is how to become a better scientist. Aside from her expertise in the field and unquestionable writing and presentation skills, I am extremely thankful for her patience and encouragement especially whenever I get discouraged by the challenges of scientific research.

I would also like to thank my committee members. Dr. Toshi Kawate for introducing me to membrane protein crystallography and for guiding me throughout my DHHC20 crystallography project. Thank you to Dr. Hening Lin for his generous support. I thoroughly enjoyed working with some of his lab members in connecting lysine palmitoylation with the DHHC enzymes and I am hopeful that our efforts will lead to exciting new discoveries. I am also very grateful to Dr. Rick Cerione for being my committee chair and for always being kind, supportive, and encouraging in every step of the way.

I also thank Wendy Greentree for her immeasurable support in the lab. Her detailed protocols helped me especially when I was a new student in the lab and did not know how to run a gel or *split* and *plate* cells. Thank you for being my go-to person whenever something goes wrong in the lab, but more importantly, thank you for the friendship. I did not mind that our lab was small because you were already the best lab mate I could ask for.

Throughout my stay in the lab, Maurine generously gave me the opportunity to mentor a few undergraduate students. I am thankful for the opportunity to teach and guide younger students. I

consider mentoring them as one of the most fun parts of PhD journey. Thank you for your valued contributions while you were in the lab even though our experiments were not necessarily included in the text: Lingzhen and Toyosi for cloning numerous MBLAC2 mutants, Jenelle for mapping the MBLAC2 palmitoylation sites, and Jordan and Peter for purifying several MBLAC2 and DHHC20 truncation constructs.

I would also like to thank several people who helped me in specific parts of this thesis: Colin Gottlieb for guiding me during my first DHHC protein purification, Kevin Michalski and Dr. Akira Karasawa for sharing your knowledge about FSEC and setting up crystallization trays, Dr. Susan Daniel, Mark Richards and Julia Kumpf for helping me develop a protocol to study the oligomerization of DHHC20, and Dr. Marc Antonyak and Arash Latikfar for teaching me how obtain my first MBLAC2 immunofluorescence images.

Throughout my graduate studies, I have had the pleasure of meeting many wonderful people outside of the laboratory. I would like to thank all of my housemates, past and present, at my co-op housing. I consider living in this house as one of the best decisions I have made as it helped me grow as a person that is open-minded, respectful, and always mindful of how little things can affect the people around me. I am thankful that I have found lifelong friends from all over the world by being in this house.

Lastly, I would like to thank my mom, Ning, and my family for supporting my pursuit of higher education even if that meant that I had to be away from home for a very long time. I am grateful for the constant love and support that they show me even from thousands of miles away.

Table of Contents

LIST OF FIGURES

LIST OF TABLES

LIST OF ABBREVIATIONS

ABHD17: α/β-hydrolase domain 17

ACBP: Acyl-coA binding protein

ACOT: Acyl Coenzyme A thioesterases

APMS: Affinity purification coupled to mass spectrometry

APT1: Acyl protein thioesterase 1

BRET: Bioluminescence resonance energy transfer

BSA: Bovine serine albumin

CCT: Cytosine triphosphate:phosphocholine cytidylyltransferase

CRD: Cysteine-rich domain

CTD: C-terminal domain

CRISPR/Cas9: Clustered regularly interspaced short palindromic repeats/CRISPR-associated protein 9

DHHC-CRD: Cysteine-rich domain characteristic of a DHHC (Asp-His-His-Cys)

DDM: Dodecylmaltoside

DMAB: Dimethylamineborane

DMEM: Dubelco's Modified Eagle Media

DMSO: Dimethylsulfoxide

EDTA: Ethylenediaminetetraacidic acid

EGFR: Epidermal growth factor receptor

ER: Endoplasmic reticulum

Erf2: Effect on Ras function

ETHE1: Ethylmalonic encephalopathy protein 1

FL: Full length

FSEC: Fluorescence size exclusion chromatography

GODZ: Golgi-specific DHHC zinc finger protein

GFP: Green fluorescent protein

GLOII: Glyoxalase II

GPI: Glycosylphosphatidylinositol

GRK5: G protein-coupled receptor kinase 5

HA: Hydroxylamine

HAGH: Hydroxyacylglutathione hydrolase also known as Glyoxalase II

HAGHL: Hydroxyacylglutathione hydrolase-like

HEK-293: Human embryonic kidney cell line

Hhat: Hedgehog acyltransferase

KO: Knockout

LACTB2: β-lactamase-like protein 2

MBOAT: Membrane-bound O-acyltransferase

MBL: Metallo-β-lactamase

MBLAC1/2: Metallo-β-lactamase domain-containing 1/2

MS: Mass spectrometry

MW: Molecular weight

Ni-NTA: Nickel nitriloacetic acid

NTD: N-terminal domain

ODYA: octadecynoic acid

PAT: Protein acyl transferase

PBS: Phosphate-buffered saline

PDMS: Polydimethylsiloxane

PEG: Polyethyleneglycol

PGH: Prostaglandin endoperoxide H synthase

PM: Plasma membrane

PNKD: Paroxysmal nonkinesiogenic dyskinesia

POPC: 1-palmitoyl-2-oleoyl-glycero-3-phosphocholine

RGS: Regulators of G protein signaling

SB: Sample buffer

SDS-PAGE: Sodium dodecyl sulfate polyacrylamide gel electrophoresis

SERZ-β: Sertoli cell gene with a zinc finger domain-β

Sf9: Spodoptera frugiperda cell line

SEM: standard error of the mean

Shh: Sonic hedgehog

SNM1: Survival motor neuron 1

TCEP: Tris (2-carboxyethyl)phosphine

TIRF: Total internal reflection fluorescence

TMD: Transmembrane domains

TNFα: Tumor necrosis factor α

UPLC-MS: Ultra-performance liquid chromatography mass spectrometry

WT: Wild type

Yck2: Yeast casein kinase 2

CHAPTER 1: INTRODUCTION

Protein Lipidation

Protein lipidation is the co- or posttranslational covalent attachment of lipid moieties to a protein. Due to the innate hydrophobic character of lipids, the main outcome of lipidation is an increased binding affinity of modified proteins to biological membranes [1]. In addition, some lipid modifications have been found to modulate protein folding, stability, and interaction with other proteins. This widespread modification is now appreciated to occur on over one thousand proteins through multiple mechanisms involving a variety of lipids [2]. At least four major types of lipids have been observed in proteins: fatty acids, isoprenoids, sterols, and glycosylphosphatidylinositol (GPI) anchors. Some proteins can contain more than one type of lipid. Protein lipidation can be divided into two categories: those modifications that occur in the lumen of the secretory pathway (O-acylation, N-palmitoylation, and GPI anchors) and those that occur in the cytoplasm or on the cytoplasmic face of membranes (S-fatty acylation, N-fatty acylation, and prenylation) [3]. An overview of the various lipid modifications is given in Table 1.

While the focus of this review chapter is on protein S-fatty acylation, the reader is referred to the following articles for reviews of other protein lipid modifications [1, 4-6].

Protein Fatty Acylation

Fatty acids of various lengths and degrees of unsaturation can be attached to the lysine ($^{\varepsilon}$N-fatty acylation), serine (O-fatty acylation), or cysteine (S-fatty acylation) residues of proteins. Among these lipid modifications, S-fatty acylation, in which a protein is post-translationally modified with long chain fatty acids via a thioester linkage, is the most widely studied. Because the most common

fatty acid donor in cells is the 16-carbon palmitoyl Coenzyme A, the process has been more commonly referred to as S-palmitoylation. It must be noted that albeit less common, lysine $^{\epsilon}$N-fatty acylation, N-fatty acylation and O-fatty acylation have also been observed in some proteins.

Protein lysine $^{\epsilon}$N-fatty acylation was discovered over twenty years ago [7-10], but was not fully appreciated until the discovery of sirtuins [11], a class of histone deacetylases the efficiently removes the long-chain fatty acyl group from lysine residues of a protein. Lin and coworkers found that sirtuin 6 (Sirt6), one of seven members of mammalian nicotinamide adenine dinucleotide (NAD)-dependent lysine deacetylases, catalyzes the removal of fatty acid modifications on the lysine residues of tumor necrosis factor-α (TNF-α). Lysine deacylation was shown to regulate the secretion of TNF-α, exemplifying a regulatory role for protein lysine fatty acylation in mammalian cells [12]. Recently, several other proteins are found to be regulated by reversible lysine fatty acylation, including two Ras GTPase proteins R-Ras2 [13] and K-Ras4A [14].

The secreted morphogen hedgehog (Hh) is an example of an N-palmitoylated protein, in which the N-terminus of the protein is palmitoylated. Interestingly, hedgehog exhibits two kinds of lipid modification. Following entry into the lumen of the endoplasmic reticulum, Hedgehog undergoes an autoprocessing event that results in the cleavage between the glycine and the cysteine residues of its Gly-Cys-Phe (GCF) motif. A cholesterol moiety is added to the now C-terminal glycine residue of the N-terminal cleavage product. This same cleavage product is then N-palmitoylated on its N-terminal cysteine residue [15]. Unlike S-palmitoylated proteins, the linkage between palmitate and hedgehog is an amide bond. N-palmitoylation is postulated to occur via a thioester intermediate utilizing the thiol of the cysteine residue, followed by a spontaneous rearrangement to form the amide linkage. The enzyme that catalyzes N-palmitoylation of hedgehog proteins is HHAT (Hedgehog acyltransferase), a member of the membrane bound O-acyl transferases (MBOAT) family.

One well-studied protein that contains O-palmitoylation is Wnt3. The covalent linkage is via an ester bond to a highly conserved Ser-209 residue. Mass spectrometry identified this acyl group to be cis-palmitoleic acid (C16:1 Δ9), a monounsaturated fatty acid. This O-fatty acylation is catalyzed by another MBOAT family member, Porcupine (Porcn) [16] and allows the Wnt protein to exit from the ER for subsequent secretion [17].

One key feature of S-fatty acylation that distinguishes it from other modes of fatty acylation is the lability of the thioester bond formed between the fatty acid and the cysteine residue of a protein substrate during the modification. Both the ester-linked and some amide-linked acyl groups are thought to be essentially irreversible. In contrast, S-palmitoylation is a reversible modification. Often, in response to upstream signals, substrate proteins can cycle between palmitoylated and de-palmitoylated forms on timescales that can range from seconds to hours [18, 19] . Dynamic palmitoylation can impact protein function, subcellular localization, secretion and stability by altering membrane association and dissociation.

Discovery of S-Palmitoylation as a Protein Lipid Modification

Protein fatty acylation was the first covalent lipid modification described in eukaryotic cells. In 1971, Stoffyn and Folch-Pi reported that highly purified brain myelin proteolipid protein contained covalently attached fatty acids [20]. While the exact chemical nature of the fatty acylation was unknown, the authors characterized the mode of lipid linkage as either an ester or a thioester. In their analysis, a mixture of palmitate (C16:0), stearate (C18:0), and oleate (C20:1) fatty acids were found. Several years later, while studying tissue culture cells infected with the Sinbis virus, Schlesinger made a serendipitous observation that viral membrane glycoproteins retained a small amount of lipid during isolation [21]. Using exogenous radioactive palmitate labeling, it was shown that [^{3}H] palmitate was

incorporated into the glycoprotein. SDS-PAGE and proteolysis were unable to remove the radioactive signal from the glycoprotein, indicating that the palmitate was covalently bound. In 1985, it was reported that treatment with hydroxylamine (HA) removes the covalently bound palmitate and converts it into palmitohydroxamate, suggesting that the palmitate is conjugated to cysteine residues via a thioester bond [22, 23]. Soon thereafter, palmitoylation was regarded as a widespread modification of eukaryotic proteins.

The members of the p21Ras family, previously characterized guanine triphosphate hydrolases (GTPases) are some of the first proteins to be added in the library of palmitoylated proteins. Ras proteins are prototypical small G-proteins that play a key role in signal transduction, proliferation, and malignant transformation. Interestingly, the frequency of *RAS* mutations is among the highest for any gene in human cancers [24]. Mutations that cause a loss of GTP hydrolysis in p21Ras frequently result in constitutively active signaling, driving unregulated growth and proliferation in a variety of cell types. In 1989, mutagenic experiments showed that the hypervariable domains of the H-Ras and N-Ras isoforms of p21Ras were isoprenylated at the cysteine of a conserved C-terminal Cys-aliphatic-aliphatic-X (CaaX) motif and palmitoylated at nearby upstream cysteines [25]. It is now understood that prenylation alone cannot stably anchor Ras proteins to lipid bilayers. N-Ras and H-Ras are further modified with palmitate moieties that are attached to one or two cysteines, respectively. Mutation of these palmitoylation sites significantly reduced membrane affinity and transforming potential of both proteins. More specifically, both the addition and subsequent removal of palmitate were necessary to support the localization of H-Ras and N-Ras. In 2005, Bastiaens showed that a dynamic cycle of palmitoylation and depalmitoylation, operates on H-Ras and N-Ras, driving their rapid exchange between the Golgi apparatus and the plasma membrane [26]. This continuous cycle prevents nonspecific redistribution of Ras on endomembranes across the cell. The role of palmitoylation in Ras signaling inspired a growing interest in identifying and characterizing protein acyl transferases (PATs),

the enzymatic writers of palmitoylation, with the goal of potentially targeting them to treat Ras signaling-dependent cancers.

Discovery of the First Protein Acyl Transferases

While the library of identified palmitoylated proteins quickly grew since the initial discovery of palmitoylation, it took over three more decades for the identity of the enzymatic writers of palmitoylation to come to light. Traditional biochemical approaches at determining the molecular identity of these enzymes were limited, if not unsuccessful. It is now widely appreciated that the majority of S-palmitoylation is catalyzed by an evolutionarily conserved family of enzymes called DHHC protein fatty acyl transferases.

A yeast genetics approach in the context of palmitoylation-dependent Ras signaling identified the first legitimate PAT. At the time, it was already established that subcellular targeting of Ras proteins requires a series of posttranslational modifications in the C-terminal C*aaX* motif. These modifications include isoprenylation, -*aaX* proteolysis, and carboxy methylation. Additionally, a final step involves either palmitoylation of an upstream cysteine or interaction of a series of basic amino acid residues in the Ras sequence that allows attachment of the protein to the membrane. In 1999, Deschenes and coworkers performed a genetic screen in *Saccharomyces cerevisiae*, a yeast strain that expresses two Ras proteins, Ras1 and Ras2 [27, 28]. They generated a strain whose viability was dependent on Ras palmitoylation by knocking out the endogenous copy of Ras 1 and modifying the genomic sequence of RAS2 [27]. This modified RAS2 allele has two important characteristics. First, it was unable to be prenylated due to the mutation of the cysteine in the CaaX box. Second, it was fused to an ectopic polybasic domain at the C-terminus. These two characteristics allowed Ras2 to adhere to the membrane and support viability of the yeast strain. Using this strain, the genes required for the

palmitoylation of Ras were identified. One of the mutants identified in this screen was given the name Effector of Ras Function (Erf) 2. Erf2 is an integral membrane protein that localizes to the endoplasmic reticulum. Additional studies showed that Erf2 function required a binding partner, Effector of Ras Function (Erf) 4. Together they formed an endoplasmic reticulum-associated complex [29]. In 2002, the Erf2/Erf4 complex was successfully purified and shown to catalyze the transfer of radioactive palmitate from palmitoyl CoA to a yeast Ras2 substrate *in vitro*, demonstrating Erf2 as the first *bona fide* PAT to be characterized [30].

At the same time, a second yeast protein was also reported to have PAT activity. Davis identified Ankyrin repeat (Akr) 1 protein to be a yeast PAT enzyme required to palmitoylate and support the plasma membrane localization of the yeast casein kinase (Yck) 2 protein [31]. Comparing the amino acid sequences of Erf2 and Akr1 revealed a substantial difference in size, composition, and predicted topology. While both enzymes are integral membrane proteins, Erf2 has four transmembrane domains and Akr1 contains six. In addition, Akr1 has a much longer N-terminal domain that includes several ankyrin repeats not seen in Erf2. Yet, one striking similarity between these two PATs is the presence of a highly conserved Asp-His-His-Cys (DHHC) motif within a larger cysteine-rich domain (CRD). The alignment of the DHHC-CRD in Erf2 and Akr1 proved useful as a template for bioinformatics search, leading to the discovery of DHHC proteins, a family of biologically significant enzymes that act as writers of protein S-palmitoylation [32].

DHHC proteins make up a family of enzymes conserved in eukaryotes. Genome databases annotate 7 DHHC proteins in *Saccharomyces cerevisiae*, 5 in *Schizosaccharomyces pombe*, 16 in *Caenorhabditis elegans*, 9 in Trypanosoma brucei, 23 in Arabidopsis thaliana [33], 22 in *Drosophila melanogaster* [34], and 23 in mammals [32]. Prokaryotes do not express any DHHC enzymes, but some bacterial proteins are S-fatty acylated in a eukaryotic host [35, 36].

The DHHC Family of Protein Acyl Transferases

Topology of DHHC Proteins

The predicted topology of DHHC proteins highlights notable conserved elements (Figure 1.1). All DHHC enzymes contain multiple transmembrane domains (TMDs), with four being the most common**.** For most DHHC proteins, the DHHC motif sits on the cytoplasmic loop between TMD 2 and TMD 3. A few DHHC proteins like DHHC13, DHHC17, DHHC23, and yeast Akr 1 and 2 contain six TMDs, with the DHHC motif located between TMD 4 and TMD 5. Additionally, DHHC17 and yeast Akr1 contain a chain of ankyrin repeats in the N-terminus. There are only two DHHC enzymes known to have five TMDs, making their topological organizations unique: DHHC4 and DHHC24 contain an extra TMD near the N- and the C-terminus, respectively, making the N-terminal end of DHHC4 and the C-terminal end of DHHC24 luminal [37]. Interestingly, the yeast Erf2 requires the formation of a heteromeric complex with its binding partner, Erf4 for PAT activity. Additional topological features recently identified in DHHC proteins include these three short conserved sequences: a Asp-Pro-Gly (DPG) motif, a Thr-Thr-Xxx-Glu (TTxE) motif, palmitoyltransferase conserved C-terminal (PaCCT) motif [38]. The DPG motif sits on the cytoplasmic side of the protein and shortly precedes the DHHC-CRD, while the TTxE and the PaCCT motifs are in the far C-terminal end of the DHHC. The N- and C-terminal domains might also contain protein-protein interaction domains/motifs involved in substrate recruitment [39].

DHHC enzymes are so-called due to the presence of a canonical Asp-His-His-Cys (DHHC) tetrapeptide motif [40]. This motif sits within a larger cysteine-rich domain (CRD) of 51-amino acid residues [41]. Together, this domain is referred to as the DHHC-CRD. The DHHC-CRD is situated in the cytoplasmic loop, following one TMD and extending several amino acids into the next TMD. Bioinformatic analysis reveals that this domain has the following consensus sequence:

$CX_2CX_9HCX_2CX_2CX_4DHHCX_5CX_4NX_3F$ (Figure 1.2). The cysteine in the DHHC motif is found to be required for the PAT activity of almost all DHHC proteins [40, 42]. The remaining cysteines in the CRD are thought to be involved in zinc binding due to the high similarity of the CRD fold to that of the C2H2 zinc finger motif [41, 43]. Mutation of these cysteines generally results in an unstable protein with compromised structural integrity and abolition of PAT activity [41]. Notably, some DHHC proteins are predicted to exclude a zinc binding domain, suggesting that for some DHHC proteins, structural integrity can be achieved without the ability to bind zinc [44]. The remaining residues in the DHHC-CRD are predicted to play a role in in the catalytic binding pocket that affects fatty acyl CoA binding and selectivity.

Sequence Diversity in DHHC Proteins

The DHHC proteins show significant divergence beyond the DHHC cysteine-rich domain. This is reflected by the wide range in amino acid sequence lengths within the family. For example, human DHHC22 has 263 residues, DHHC20 has 365, and DHHC8 has 765. Despite this variability in size, virtually all DHHC proteins are *bona fide* PATs. Except for the yeast Akr2, a paralog of yeast Akr1, all of the yeast and mammalian DHHC proteins have shown evidence of PAT activity [45]. The catalytic activity of the DHHC protein family with high diversity outside of the DHHC-CRD suggests that the critical elements necessary for enzymatic activity are located in this region. Nonetheless, there are slight variabilities in the primary sequence of the DHHC-CRD worth noting (Figure 1.2). In humans, most DHHC proteins contain seven cysteine residues with a conserved arrangement relative to the DHHHC motif. The only exception to this is the DHHC22 which lacks the 2nd and the 5th cysteine in its CRD. Additionally, in DHHC13, the first histidine in the canonical Asp-His-His-Cys is replaced with a glutamine. This sequence variability in the DHHC-CRD is more prominent in yeast. While all seven

yeast DHHC enzymes have the canonical DHHC cysteine retained, Akr1, Akr2, and Pfa5 have replaced the third histidine in the motif with a tyrosine. Additionally, Pfa5 contains only four of the conserved cysteines, while Akr1 and Akr2 have only two. These minor sequence variations in the DHHC-CRD of the DHHC family suggest that the catalytic mechanism of these yeast enzymes can operate independently of some of the conserved cysteines and histidines present in human DHHC proteins.

Subcellular Localization of DHHC Proteins

In addition to sequence diversity, DHHC proteins have been found to localize to multiple membranes throughout the cell. In 2006, Igarashi cloned all the human and yeast DHHC genes and investigated the intracellular localization of the ectopically overexpressed, epitope-tagged DHHC proteins. [46]. Their investigation showed that the majority of the DHHC proteins displayed ER and/or Golgi localization. Human DHHC5, 20, and 21, and yeast Pfa5 were found to be an exception and localized at the plasma membrane. Notably, DHHC20 has also been detected in the perinuclear region and intracellular organelles like the Golgi [47]. Interestingly, the yeast Pfa3 alone was found to be localized in the vacuole, and no human DHHC protein was detected in the equivalent mammalian organelle, the lysosome. However, a number of these results were inconsistent with work from others that looked at endogenous proteins. For example, Igarashi reported overexpressed DHHC2 as being in the ER and Golgi. However, multiple groups have found DHHC2 localized to the PM and recycling endosome [48-50]. DHHC21 also displayed different localization patterns in various cell types; it was located on the plasma membrane in HEK-293 cells [46] and to the Golgi in primary keratinocytes [51]. In COS-7 cells, DHHC21 was found predominantly in the Golgi, but still detectable in the plasma membrane [52].

The exact mechanism of spatial distribution and organelle sorting of DHHC proteins remains unknown. However, some studies have pointed to the role of distinct sorting signals to protein localization. A study in 2011 identified and characterized lysine-based sorting signals that determine the restricted localization of DHHC4 and DHHC6 to ER membranes [53]. The ER targeting signals were found to be a Lys-Xxx-Xxx (KXX) motif for DHHC4 and a Lys-Lys-Xxx-Xxx (KKXX) motif for DHHC6. Remarkably, adding the same targeting signal to the C-terminus of the typically Golgi-localized DHHC3 redistributes the enzyme to the ER, signifying that the dilysine signals are sufficient to dictate ER localization. Moreover, the organelle redistribution of DHHC3 did not affect its ability to palmitoylate its substrate Synaptosome Associated Protein 25 (SNAP-25). Another study showed that the C-terminal region of DHHC2 and DHHC15 regulate the localization of these two distinctly localized PATs. DHHC2 was found to cycle between endosomes and the plasma membrane, with the localization regulated by its C-terminal domain [48]. Remarkably, swapping the C-terminal region of DHHC2 to DHHC15 altered the localization of the chimeric DHHC15 to regions similar to those of the DHHC2 enzyme [48].

It was also shown that external stimuli may alter the localization of the DHHC2 enzyme [54]. In neurons, DHHC2 translocates from dendritic shaft vesicles to post-synaptic densities (PSDs) at the PM of dendritic spines in response to activity blockade. This DHHC2 translocation increases the palmitoylation levels of PSD-95 in the spines. This leads to an upregulation of 2-amino-3-(hydroxy-5-methyl-4-isoxazole) propionic acid type glutamate receptor activity, eventually restoring homeostasis.

Taken together, these studies suggest that defined membrane targeting of active DHHC proteins may be an important factor contributing to spatially restricted patterns of substrate palmitoylation.

Substrate Specificity and DHHC Protein-Protein Interactions

While several specific DHHC enzyme-substrate pairs have been identified, a vast majority of palmitoylation events have yet to be assigned to the enzymatic activity of a specific DHHC enzyme. There are no indications that a universal mechanism dictates how DHHC enzymes recognize specific protein substrates. Enzyme-substrate interacting domains, subcellular localization, and the amino acid composition of the modification site have all been found to play a role [4].

In the first proteomic survey of palmitoylated proteins performed in yeast, over 50 proteins were identified to be palmitoylated [55]. While palmitoylation of some of these proteins were found to be dependent on specific DHHC enzymes, the knockout of individual DHHC proteins more often had only modest effect on the overall yeast palmitoyl-proteome. Interestingly, several proteins in this study maintained similar palmitoylation levels even in the absence of five of the seven yeast DHHC proteins, suggesting a limited specificity and an extensive overlap in enzyme-substrate recognition pairs in yeast.

In 2006, Fukata introduced a mammalian-based systematic cell-based screening method to identify specific enzyme-substrate pairs. In this technique, individual DHHC enzymes are ectopically overexpressed with a potential substrate in HEK-293 cells. The cells are then metabolically labelled with [^{3}H] palmitate. Following the labeling period, the cells are lysed and the immunoprecipitated substrate is assayed for palmitoylation levels. This process generates a panel of DHHC enzymes that increased the palmitoylation level of the substrate. Afterwards, these candidate enzymes are individually knocked down. A decrease in palmitoylation of the substrate after knockdown verifies the legitimacy of the enzyme-substrate pair [56]. This method successfully identified an overlapping substrate specificity for DHHC3 and DHHC7 towards PSD-95, SNAP-25, and Growth Associated Protein 43 (GAP-43). Moreover, it showed that DHHC9 and DHHC17 had PAT activity only toward H-Ras and

SNAP-25. However, the Fukata method has been found to be unreliable due to its inherent flaws. Overproduction of a protein may cause it to spill out of its native compartments, as observed for the DHHC3 enzyme. This may explain why a decrease in PSD-95 palmitoylation levels was not observed in the DHHC3 knockout mice, even though overexpression of the DHHC3 enzyme with PSD-95 was shown to increase substrate palmitoylation [57]. The mislocalized DHHC enzyme likely retained its catalytic activity which could palmitoylate non-natural substrates resulting in false positive enzyme-substrate pairs. Additionally, knockdown of a specific DHHC protein does not always completely abolish substrate palmitoylation due to the palmitoylation activity being carried out by the remaining DHHC enzymes. For example, N-Ras retained a low level palmitoylation level in vivo even when DHHC9 was knocked out [58]. The Fukata screens demonstrate two confounding features of the DHHC PAT family. First is the broad substrate specificities of several of its member enzymes. Second is the inherent redundancies that allow for other DHHC enzymes to palmitoylate a protein substrate in the absence of the primary DHHC enzyme. These characteristics are likely a critical evolutionary adaptation and a hint to the significance of palmitoylation events in over-all cell function and signaling. Moreover, this divergence from a single enzyme-single substrate paradigm shows the complexity of cellular palmitoylation and the challenges in elucidating its mechanism and regulation.

The sequence elements found in the N- and C-terminal domains of the DHHC enzymes have also been shown to contribute to protein substrate specificity. Several DHHC enzymes have been reported to contain PDZ-interacting domains that allow for enzyme-substrate interactions. The PSD-95/discs large/ZO-1 (PDZ) domain is a common structural domain of 80-90 amino acids found in a variety of signaling proteins and often recognize short amino acid motifs at the C-termini of target proteins [59]. Both DHHC5 and DHHC8 contain a PDZ-interacting domain in the C-terminus [60]. In DHHC8, this domain was found to be essential for the recruitment of the substrate protein interacting with C-kinase 1 (Pick-1) whose palmitoylation is important for long-term synaptic depression (LTD) in

cultured mouse cerebellar Purkinje neurons [61]. Similarly, the PDZ-interacting domain of DHHC5 is required for the palmitoylation of the neuronal PDZ domain protein, glutamate receptor interacting protein 1 (Grip-1). Another binding domain observed in many eukaryotic DHHC proteins is a conserved 16 amino acid sequence in the C-terminus known as the PaCCT motif (Figure 1.1). The mutation of Tyr-323 located within the PaCCT motif of spore wall formation 1 (Swf-1) in yeast abolishes Swf-1 palmitoylation activity *in vivo*. Similarly, a diminished activity of another yeast DHHC, protein fatty acyltransferase 3 (Pfa-3) was observed when Phe-250 in its PaCCT motif was mutated to alanine [38]. The DHHC6 protein is unique in that it is the only DHHC protein that contains a Src homology 3 (SH3) domain in the C-terminus. This domain allows DHHC6 to interact with selenoprotein K, another SH3 domain-containing protein. Multiple studies suggest that selenoprotein K may be a binding partner of DHHC6, but its exact role in facilitating palmitoylation has not yet been determined. Nonetheless, multiple reports have shown that the formation of a DHHC6-selenoprotein complex is required for the palmitoylation of several protein substrates like inositol 1,4,5-triphosphate receptor (IP3R) [62] and the low density lipoprotein receptor CD36 [63].

Another well-studied domain situated in the N-terminus of a few DHHC proteins has been reported to mediate DHHC-substrate interaction. DHHC17 (Figure 1.1), also known as huntingtin-interacting protein 14 (HIP-14), interacts with the huntingtin protein through its ankyrin repeat (Akr) domain [64]. When this Akr domain was fused to the N-terminus of DHHC3, the chimeric Akr-DHHC3 protein was found to interact with the huntingtin protein, a feat that is absent in wild-type (WT) DHHC3. Moreover, Akr-DHHC3 redistributed Huntingtin to the perinuclear region through palmitoylation-dependent vesicular trafficking. The interactions between a DHHC enzyme and its protein substrate are thought to be weak and transient, but recent investigations suggest that the Akr domain present in both DHHC17 and DHHC13 confers a stronger interaction between the DHHC enzyme and its protein substrate. Recently, a previously overlooked [VIAP][VIT]XXQP motif was found

in known DHHC13 and DHHC17 substrates SNAP-25, SNAP-23, cysteine string protein, and Huntingtin [65]. Crystal structures of the ankyrin repeat domain of DHHC17 and a truncated form of SNAP-25b have elucidated the nature of this interaction, attributing it primarily to hydrogen bonding and hydrophobic interactions involving the [VIAP][VIT]XXQP motif of SNAP25b [66]. Not surprisingly, the loss of this motif in huntingtin heavily disrupted DHHC17 binding.

Surprisingly, the literature consensus is that the catalytic DHHC-CRD plays very little role in the protein substrate specificity of DHHC enzymes. A chimeric DHHC15 construct containing the DHHC-CRD of DHHC3 failed to palmitoylate SNAP-23, a substrate modified by WT DHHC3 but not by WT DHHC15, suggesting that the CRD of DHHC3 is not sufficient to confer substrate specificity to SNAP-25 [49].

Acyl CoA Selectivity of DHHC Proteins

The DHHC enzymes not only have a broad specificity for protein substrates but also display a wide specificity for different acyl CoA substrates. Pioneering *in vitro* experiments indicate that the DHHC2 enzyme exhibits a broad acyl-CoA specificity, efficiently transferring acyl chains with lengths of 14 carbons and longer with varying degrees of unsaturation [67]. Remarkably, despite being similar and grouped together in a phylogenetic analysis, DHHC3 and DHHC7 have very different acyl-CoA substrate preferences: DHHC3 only efficiently transfers C14:0, C16:0, and C16:1 acyl group, while DHHC7 prefers the longer C18:0 group. This surprising difference is attributed to an isoleucine residue in the TMD3 of DHHC3 which is bulkier than the corresponding serine found in DHHC7. When this isoleucine on DHHC3 was mutated to serine, the mutant was able to utilize the C18:0 fatty acid [68]. This observation was validated by the crystal structure of *h*DHHC20 with a fatty acid chain covalently bound to its active site cysteine. The structure showed a hydrophobic cavity, formed by its four

transmembrane helices, enclosing the acyl chain. In *h*DHHC20, the homologous residue to the DHHC3 Ile in TM3 is Tyr181, which forms an H-bond with Ser29 at TM1. Together, the Tyr-Ser hydrogen bond pair closes off one side of the top face of the cavity. Mutation of Tyr181 to a less bulky alanine, allows hDHHC20 to utilize the longer stearoyl-CoA (C18), while mutation of the serine to a bulky phenylalanine increases preference for a shorter chain acyl-CoA. However, sequence alignment analysis shows that the cavity lining residues vary among different DHHC enzymes in a complex manner, suggesting alternative mechanisms for acyl CoA selectivity exist in other DHHC enzymes [69].

It is worth noting that there is a general lack of mass spectrometry data directly confirming the molecular identity of the fatty acids transferred by individual DHHC enzymes. This leaves open the possibility that acyl groups other than palmitate may also act as physiological lipid modifiers in some proteins. An analysis of the acyl groups in the pool of acylated proteins in platelets revealed that 74% were palmitate (C16:0), 22% were stearate (C18:0), and 4% were oleate (C18:1) [70]. In addition, differences in fatty acid profiles of S-acylated proteins in various cell types have been observed. For example, very long chain fatty acyl CoAs constitute 10% of the total fatty acyl pool of RAW246.7 and 50% of the fatty acyl pool in MCF7 cells [71]. Interestingly, heterogeneous fatty acylation of Src-family kinases has been detected, with the nature of the attached fatty acid influencing raft-mediated signal transduction [72].

Mechanisms of DHHC-Mediated S-Palmitoylation

The thioester bond formed between a cysteine residue and palmitate during palmitoylation has the same bond energy as that of the donor molecule, palmitoyl CoA, indicating that the reaction is energy neutral. Indeed, *in vitro* palmitoylation assays does not require any additional energy sources such as ATP [73]. [^{3}H]-palmitate labeling experiments performed on yeast Erf2/Erf4 and mammalian

DHHC2 and DHHC3 revealed that DHHC enzymes share a two-step catalytic mechanism [67, 74]. The first step, autopalmitoylation, is a fast transfer of palmitate to the DHHC cysteine resulting to the formation of a palmitoyl–enzyme intermediate. This is followed by a slower second step, in which the palmitate moiety is transferred to the substrate protein (Figure 1.3). This mechanism is supported by early experiments in which purified DHHC3 was labeled with [^{3}H]-palmitate in the absence of a protein substrate. After a second purification step that removed excess radioactive palmitoyl CoA, the enzyme was incubated with its known protein substrate, Gαi. Over time, the radioactive palmitate was either transferred from DHHC3 to Gαi or at a slower rate lost to the enzyme by hydrolysis. Notably, only 50% of radioactivity was lost despite long incubation times with the substrate, suggesting that [^{3}H]-palmitate may also be present in other cysteine residues not directly involved in the catalysis. However, no other sites of palmitoylation were detected with a significant stoichiometry [67]. Mutagenesis studies suggest that the autopalmitoylated residue is the cysteine of the DHHC motif because autopalmitoylation is abolished in the DHH**S**3 mutant enzyme. In 2015, Gottlieb and Linder reported the first mass spectrometry evidence of the DHHC cysteine being modified by palmitate [41]. Most recently, the crystal structure of *h*DHHC20 showed alkylation on its catalytic DHHC cysteine by the common palmitoylation inhibitor 2-bromopalmitate (2-BP) [69], further demonstrating that the catalytic DHHC cysteine is the relevant palmitoylation site.

The functions of the aspartate and the two histidines in the DHHC motif of the enzyme are less clear. In Erf2, mutation of the first histidine to alanine retained autopalmitoylation of the enzyme but abolished palmitate transfer to Ras2 [30] suggesting that the role of the first histidine is in activating the cysteine protein substrate, but not the DHHC active site cysteine [75]. Interestingly, the yeast Swf1 with a natural DQHC motif retains partial palmitate transfer activity despite not having the first histidine residue. Similarly, DHHC13 which also possesses DQHC, while has low levels of autoacylation, remains able to palmitoylate the huntingtin protein. Mutating the glutamine in

DHHC13 to histidine to reconstitute the canonical DHHC motif did not impart any extra catalytic ability to DHHC13. Conversely, replacing DHHC with DQHC in the closely related DHHC17 enzyme abolished its activity [65]. Studies of yeast Swf1 and Pfa4 enzymes, in which the active site cysteine was mutated to arginine to give DHHR, were found to be active. Most likely, the palmitoyl-DHHC intermediate would not form with the Swf1 DHHR mutant. The authors proposed a plausible mechanism in which the first histidine of the DHHC motif favors the formation of the thiolate in the substrate protein, leading to direct nucleophilic attack of the substrate on palmitoyl-CoA [76]. To date, the absolute requirement for an autoacylated intermediate in DHHC enzyme-mediated S-fatty acylation remains an unsolved question [42].

Mechanisms Regulating DHHC Activity

To date, there is no consensus as to how cells regulate DHHC-catalyzed palmitoylation. Numerous studies suggest that multiple factors may play a role. Palmitate cycling on both small and heterotrimeric GTPases was found to increase significantly upon activation of G-protein coupled receptors (GPCRs), suggesting that protein palmitoylation is regulated in response to external stimuli. [77]. In addition, several DHHC proteins are known to interact with non-substrate proteins. The yeast Erf2 requires a binding partner Erf4 to palmitoylate Ras2 [29]. A similar prerequisite is observed in its human orthologue, DHH9 with its binding partner Golgi complex-associated protein of 16 kDa (GCP16) [78]. Both Erf4 and GCP16 increase the ability of their partner DHHC enzyme to palmitoylate its substrates through the formation of a stable DHHC-cofactor complex. Similarly, DHHC6 associates with and requires Selenoprotein K to palmitoylate its substrates. However, the exact role of its cofactor has not yet been reported [62].

Regulation of DHHC PAT activity by controlling cellular DHHC protein levels has also been proposed. In 2013, Hang reported that the global palmitoyl-proteome in *Schizosaccharomyces pombe* is significantly different between vegetative growth and meiotic phases. During meiosis, a substantial upregulation of the Erf2 PAT enzyme was observed. The increased Erf2 expression corresponded to an increased palmitoylation of the Ras Homolog 3 (Rho3) protein, which in turn stimulated meiotic entry of the fission yeast [79].

Another potential regulatory mechanism is control of the access site of DHHC proteins to cysteine thiols on protein substrates. The phosphorylation of phosphodiesterase 10A (PDE10A) in its Thr16 residue was shown to interfere with the palmitoylation of Cys11, which would otherwise be palmitoylated by DHHC7 and/or DHH19 [80]. Interestingly, DHHC3 was also shown to be phosphorylated and regulated by endogenously expressed fibroblast growth factor receptor (FGFR) and Src proteins. Abolition of tyrosine phosphorylation resulted in an increase in both the DHHC3 autopalmitoylation and the palmitoylation of neural cell adhesion molecule (NCAM) [81].

Lastly, there is evidence that some DHHC enzymes exist in a dynamic monomer:oligomer equilibrium with different catalytic activities for different states. In DHHC3, activation with palmitoyl CoA preserves the more active monomer form whereas mutation of the cysteine in the DHHC motif promotes the formation of the less active dimer [82]. However, the kinetic properties of the different oligomeric forms of DHHC have not been evaluated. Moreover, this model not supported by the crystal structures of DHHC2 [69]. In the structure, a head-to-tail dimer of the enzyme was observed, which is presumed to be an artifact of crystallization.

Examples of Biological Functions of S-Palmitoylation

In general, the addition of a fatty acid like palmitate to a protein increases its hydrophobicity. This can have different functional consequences depending on the protein being modified. Palmitoylation is shown to occur on a diverse set of proteins, from cytosolic proteins to peripheral and integral membrane proteins. The roles that palmitoylation plays in the cell are just as diverse.

As a membrane anchor, palmitoylation can influence protein localization and trafficking. A prototypical illustration of this is the palmitoylation of the Ras GTPases. After prenylation and processing, H-Ras is either mono- or dually-acylated at Cys-181 and Cys-184. Monoacylation at Cys-181 is required and sufficient for efficient trafficking to the plasma membrane. On the other hand, monoacylation at Cys-184 results in trafficking to the Golgi but not beyond [25]. After depalmitoylation at the plasma membrane by APT enzymes, H-Ras diffuses back into the cytosol until it is repalmitoylated at the Golgi and directed back to the PM. This continuous cycle prevents nonspecific redistribution of Ras on endomembranes across the cell. Similarly, palmitoylation facilitates proper shuttling of the ATP-binding cassette transporter (ABCA1). ABC(A1) lipidates apolipoprotein A-I both directly at the plasma membrane and uses lipids from the late endosomal or lysosomal compartment. Removal of palmitoylation of ABCA1 by results in a reduction of ABCA1 localization at the PM and a reduction in the ability of ABCA1 to efflux lipids to apolipoprotein A-I [83].

The membrane microdomain distribution of a protein can also be influenced by palmitoylation as in the case of A-kinase anchoring protein (AKAP79). AKAP79 is a human anchoring protein that organizes cAMP-dependent protein kinase (PKA), Ca^{2+}/calmodulin (CaM)-dependent protein phosphatase (PP2B), and protein kinase C (PKC) for efficient cAMP signaling [84]. Mutation of the palmitoylation sites in AKAP79 excludes it from lipid rafts and prevents it from regulating adenylyl cyclase 8 (AC8) activity [85].

Another crucial biological function of palmitoylation is the regulation of protein stability. This is exemplified in the context of the Huntington's disease. A wild type huntingtin protein typically contains a chain of 6-35 repeated glutamine residues in its N-terminus. In Huntington's disease, the huntingtin protein has 5-10 additional glutamine residues. Expansion of this polyglutamine tract causes the huntingtin protein to aggregate, which leads to the disease. In neurons, the huntingtin protein is palmitoylated by DHHC17 (HIP14) and DHHC13 (HIP14L) on Cys214. Palmitoylation is shown to reduce huntingtin protein aggregation while knockdown of the DHHC gene induces neuronal cell death [86].

Palmitoylation can also affect protein-protein interaction and stabilize oligomeric complexes. For example, non-palmitoylated Gαo protein exists mostly as higher order oligomers which could disaggregate completely into monomers by GTPγS stimulation. Palmitoylated Gαo on the other hand, exist only as oligomers and is resistant to GTPγS-dependent stimulation [87]. Similarly, mutation in the palmitoylation site of the huntingtin protein accelerates aggregate and inclusion formation, causing neuronal toxicity [88]. Interestingly, palmitoylation of the α-amino-3-hydroxy-5-methyl-4-isoxazole propionate (AMPA) receptor, GluR1 inhibits its interaction with the 4.1N protein. This reduced interaction blocks the endocytosis internalization of 4.1N protein at the PM [89].

Enzymatic Protein Depalmitoylation

Protein S-palmitoylation is a highly dynamic process. This was first demonstrated in 1987 with reports that the p21 N-Ras and ankyrin proteins undergo an active acylation-deacylation cycle with a fast palmitate turnover [90, 91]. Additionally, the agonist activation-induced removal of palmitate in stimulatory G protein α-subunit (Gαs) was found to prompt a localization shift of the Gαs protein from

the membranes to the cytosol [77]. These findings were early indications that a tightly regulated palmitoylation cycle plays a role in protein sorting and signaling cascades in cells.

While the vast majority of studies in the field has advanced the understanding of how palmitate is added to cysteines in proteins, relatively little is known about how it is removed. In 1993, the first enzyme initially thought to catalyze intracellular protein depalmitoylation was discovered. Hoffman purified palmitoyl protein thioesterase 1 (PPT1) from a soluble fraction of bovine brain and demonstrated its ability to remove the palmitate of both H-Ras and Gα *in vitro* [92]. The crystal structure of PPT1 revealed motifs also present in known mammalian thioesterases at the time: an N-terminal Gly-Xxx-Ser-Xxx-Gly motif, a C-terminal Ser-Asp-His catalytic triad, and an α/β-hydrolase fold harboring a hydrophobic groove that could accommodate a palmitate lipid chain [93, 94]. However, subsequent cloning of PPT1 revealed a signal sequence and ultimately linked its main physiological role to the lysosome as a lysosomal depalmitoylase that removes fatty acids from proteins undergoing degradation in the lysosomal lumen [95, 96]. Interestingly, mutations in the PPT1 gene have been shown to cause infantile neuronal ceroid lipofuscinosis (INCL), a fatal childhood neurodegenerative lysosomal storage disorder. Individuals with INCL accumulate cysteine-containing lipid moieties, presumably the endogenous substrates of PPT1 in brain tissues [97]. This suggests that PPT1 may play an important role in postnatal development or maintenance of cortical neurons.

Distinguishing legitimate protein depalmitoylases from a pool of impostors like the PPT1 enzyme has been a challenge in the field. To date, only two groups of proteins have been identified as *bona fide* cytosolic protein depalmitoylases: the acyl protein thioesterases and the α/β hydrolase domain 17 (ABHD17) family of proteins.

Acyl Protein Thioesterases

In 1988, Duncan and coworkers isolated APT1 from soluble rat liver homogenates while screening for cysteine depalmitoylase activity on G proteins [98]. Sequence analysis revealed that the enzyme had been previously purified and characterized as a lysophospholipase and designated as LYPLA1 [99]. Subsequent kinetic analyses and competition studies showed that APT1 has at least a twenty-fold higher enzymatic activity towards thioacylated proteins than lysophospholipid substrates *in vitro* [98, 100]. More importantly, ectopically expressed APT1 was found to be primarily cytosolic and able to catalytically remove palmitate from Gαs in cells, supporting APT1 as a legitimate protein thioesterase. In 2000, the crystal structure of human APT1 was solved revealing an α/β-hydrolase fold, Gly-Xxx-Ser-Xxx-Gly motif, and a Ser-Asp-His catalytic triad. These structural elements characterized APT1 as a member of the ubiquitous α/β-hydrolase family that includes other acyl hydrolases such as PPT1 [101].

Several proteins have since been tested as potential substrates for APT1. Upon incubation with the substrate, recombinant APT1 purified from *E. coli* cells was able to remove the palmitate from SNAP-23 and several viral membrane glycoproteins [102, 103]. Overexpression of APT1 in various cell lines was shown to accelerate the depalmitoylation of the Gα protein [98], small GTPase H-Ras [104, 105] and endothelial nitric oxide synthase (eNOS) [106]. Interestingly, APT1 had no effect on the palmitoylation levels of the raft protein caveolin [106], suggesting that APT1 exhibits some degree of substrate specificity.

A second mammalian enzyme also formerly annotated as a lysophospholipase has been studied for its depalmitoylase activity. Sequence comparison shows about 68% sequence identity between APT1 and APT2, but both enzymes contain the canonical lipase motif seen in other thioesterases [101]. Despite this similarity, recent evidence suggests that APT1 and APT2 may

hydrolyze distinct substrates. For example, only APT2 has been demonstrated to hydrolyze prostaglandin glycerol esters in human cancer cell lines [107]. Another report showed that APT2 overexpression, but not APT1 promotes an accelerated GAP-43 depalmitoylation. Similarly, overexpression of APT2 HeLa cells was found to be essential for the depalmitoylation and stabilization of DHHC6, whereas APT1 did not have any effect [108]. Another study showed that agonist-dependent palmitoylation of the β2-adrenergic receptor is reversed by APT1, but not APT2 [109]. Nonetheless, APT1 and APT2 showed the ability to remove palmitate from semisynthetic N-Ras *in vitro*, suggesting some substrate overlap between the two enzymes [110].

Notably, APT1 and APT2 themselves are palmitoylated. The site of palmitoylation for both enzymes is the N-terminal Cys-2 residue. Interestingly, APT1 can depalmitoylate both itself and APT2. One report suggests that palmitoylation gives the APT enzymes transient membrane affinity to access the membrane-anchored palmitate moiety in their membrane-bound substrates [111]. In addition, blocking the palmitoylation of these depalmitoylases adversely affects their membrane localization as well as that of their purported substrates, H-Ras and GAP-43, respectively [105]. An independent report proposed another model in which the autodepalmitoylation of APTs creates two interconverting thioesterase pools with distinct functionalities: depalmitoylated APTs in the cytoplasm and palmitoylated APTs in the Golgi. Using dynamic imaging of APT-substrate catalytic intermediates, the study demonstrated that it is the depalmitoylated soluble APT pool that removes palmitate on substrates on endomembranes [111], supporting earlier reports of a rapid and ubiquitous depalmitoylation [18].

Contrary to the initial studies showing APT1 primarily localized in the cytosol and the Golgi apparatus [98, 105, 111], recent immunostaining and fractionation experiments reveal that APT1 is predominantly localized in the mitochondria [112], challenging previous reports of APT1 being a true

cytosolic cysteine depalmitoylase. The mitochondrial localization of APT1 is supported by two quantitative proteomic studies showing a similar mitochondrial residency of APT1 analogs in *Trypanosoma brucei* and *S. cerevisiae [113, 114]*. This discovery allows for the discovery of the functional roles of APT1 to include the regulation of the S-palmitoylation of the mitochondrial proteome. To date, identification of mitochondrial targets of APT1 remains complicated as genetic perturbation and pharmacological inhibition of APT1 affect the overall function of APT1 throughout the cell.

A third acyl protein thioesterase, APT1-like (APT1L) also exists but has not been thoroughly characterized. This enzyme is unique because of its high expression profile in adipose tissues. Mutations in APT1L protein are associated with obesity in a number of genome-wide association studies, suggesting a role in lipid metabolism [115, 116]. The crystal structure of APT1L reveals an overall fold similar to APT1 and APT2. However, the active site of APT1L is shallow and precludes binding of long-chain substrates. Consistent with the solved structure, biochemical data revealed that APT1L was unable to depalmitoylate palmitoylated N-Ras. Additionally, APT1L exhibited neither phospholipase nor triacylglycerol lipase activity [117].

Inhibitors of Protein Depalmitoylation

The development of small molecule inhibitors of APT1 and APT2 was highly instrumental in the advancement of our understanding of the roles of these acyl protein thioesterases. Palmostatin B and its more potent analogue, Palmostatin M, were the first dual APT1/2 inhibitors to be synthesized and have since been routinely used in many depalmitoylation studies (Figure 1.4). Both are β-lactone mechanism-based inhibitors that inactivate APT1/2 by reversible covalent modification of the enzyme active site, initiated by a nucleophilic ring opening of the β-lactone electrophile. While initially thought

to be specific for APT1, APT2, and PPT1, subsequent activity-based protein profiling (ABPP) studies demonstrated that Palmostatin B inactivates a number of other lipid processing serine hydrolases with somewhat weaker potency [118]. This finding not only necessitated a reevaluation of earlier conclusions utilizing this inhibitor, but also paved a way for the consequent discovery of ABHD17 enzymes, a novel family of cysteine depalmitoylases.

Recently, a new generation of selective APT inhibitors has been engineered. These inhibitors share a common piperazine-amide scaffold and contain additional modifications to impart substrate selectivity. The APT1 inhibitor, ML348, has piperazine amide adjacent to a furanyl group, while the APT2 inhibitor, ML349, has a thiophene conjugated to thiochromane 1,1-dioxide. Of note, one study utilizing these new inhibitors showed that APT1 and APT2 do not affect signaling downstream of N-Ras, thereby correcting a previous report obtained with the non-specific inhibitor, Palmostatin B [119]. Additionally, APT2-selective inhibition by ML349 showed that APT2 depalmitoylates the Scribble protein, affecting its membrane localization [120].

α/β Hydrolase Domain 17 Family Thioesterases

APT1 and APT2 were regarded as the primary depalmitoylases in cells. However, multiple experiments have engendered cogent evidences hinting at the existence of other undiscovered depalmitoylases. For example, genetic ablation on APT1 in yeast, Drosophila, and C. elegans did not lead to a significant growth phenotype, suggesting that either depalmitoylation is dispensable for viability or that multiple additional protein acyl thioesterases exist. Moreover, H-Ras depalmitoylase activity was found exclusively in the insoluble cell fraction and not with APT1 in the soluble fraction [121]. In 2015, a study demonstrated that knocking down APT1 and APT2 blocked depalmitoylation of Huntingtin but did not affect palmitate turnover on PSD-95 and N-Ras. Evidently, some

depalmitoylation events in the plasma membrane are not attributable to APT1 and APT2. To address this, Conibear performed activity-based protein profiling on the combined novel targets of the non-specific serine hyrodrolase inhibitor, Palmostatin B, and general lipase inhibitor, hexadecylfluorophosphonate, HDFP [118]. Among the candidate proteins identified by the profiling screen are members of the α/β hydrolase domain 17 (ABHD17) protein family. Remarkably, expression of ABHD17A, ABHD17B, or ABHD17C accelerated palmitate cycling on both N-Ras and PSD-95. Cysteine depalmitoylation by ABHD17 proteins were found to regulate the re-localization to internal cellular membranes of N-Ras [118]. In addition, the ABHD17 proteins were reported as the physiological PSD-95 depalmitoylating enzymes that regulate PSD-95 palmitoylation cycles in neurons. This study describes the first direct evidence for the neuronal depalmitoylating enzyme and provides a new aspect of the dynamic regulatory mechanisms of synaptic development and synaptic plasticity. The discovery of the ABHD depalmitoylating enzymes expands the small list of *bona fide* cellular cysteine depalmitoylases and suggests that the depalmitoylation process is both substrate-selective and compartment-specific [118]. Notably, the serine hydrolase superfamily of enzymes has 116 members in humans, but only half of them have an annotated biological function [122]. It will not be surprising if several more cysteine depalmitoylases will soon be discovered from this list.

Conclusions

The field of protein S-palmitoylation and its devoted scientific community have both grown tremendously since the discovery of the first palmitoylated protein over 40 years ago. As of 2019, the SwissPalm database has catalogued over 10,000 unique putative palmitoylated proteins [123]. This number is expected to continue to rise along with the rapid advancement in the techniques used to identify lipid-modified proteins. In conjunction with the expansion of the palmitoylome is the

substantial progress made in the biochemical and mechanistic characterization of the DHHC enzymes. The biomedical importance of DHHC proteins is highlighted by their association with human disease found using DHHC-deficient mouse models.

Perhaps the most critical recent development in the field happened in 2018 with the determination of the first three-dimensional structure of a human DHHC enzyme. This discovery provides a structural framework that allows a more informed investigation of the nuances in the molecular mechanism governing DHHC-catalyzed palmitoylation. Fine-grained mechanistic hypotheses based on the known structures can now be made, tested, and validated using both *in vitro* and *in vivo* systems. More importantly, this breakthrough likely ushers a new molecular era of palmitoylation. One immediate goal is to develop structurally precise and specific small molecule inhibitors that allow modulation of this dynamic process. Looking ahead, it will not be surprising if the next few decades see the development of drugs for therapeutic use for human diseases with a palmitoylation component.

This chapter of my dissertation gives a literature overview of the evolution of field of S-palmitoylation since its initial discovery several decades ago. The two next chapters discuss my study of two S-palmitoylated proteins. In chapter 2, I outline my efforts to crystallize the palmitoyltransferase enzyme DHHC20 with the goal of solving its 3D structure. I also discuss the results of my investigation of the oligomerization of DHHC20 at a single molecule level. In chapter 3, I describe my examination of the palmitoylation and the catalytic activity of the MBLAC2 protein. I discuss my findings that MBLAC2 is a palmitoylated protein and is a substrate of DHHC20. I also report my data indicating that MBLAC2 is a robust acyl CoA thioesterase and contains multiple zinc-binding residues that are important for catalytic activity. Finally, In the appendix, I include a chapter in *Methods of Molecular Biology* that I wrote about the purification of recombinant DHHC proteins.

Table 1. Overview of Various Protein Lipid Modifications.

Type of Lipid	Modification	Modifying Group	Attachment Site	Enzyme (substrate)	Linkage
Fatty Acid	S-Acylation	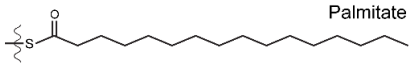	Cysteine	DHHC	Thioester to Cys
	N-Myristoylation	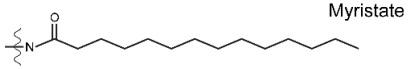	(M)GXXXS/T-	NMT	Amide to N-Gly
	O-Acylation	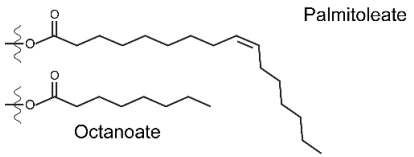	-CKCHGXSGSCXXKTCW- (-MAMA)GSSFLSP-	Porcn (Wnt-3a) GOAT (pro-ghrelin)	Oxyester
	N-Palmitoylation	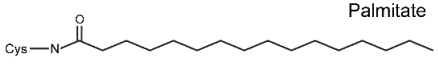	CGPGRGFGKRRHPKKL-	Hhat (Shh) Unknown (Gαs)	Amide to N-Cys
	εN-Palmitoylation	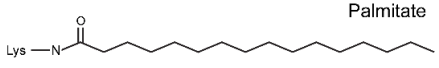	Lysine	Unknown	Amide to Lys
Isoprenoid	Farnesylation	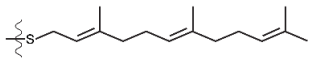	-CaaX	FTase	Thioether to Cys
	Geranylgeranylation	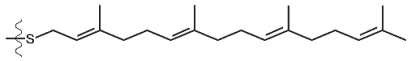	-CaaL, -CXC, -CCX$_{1-3}$	GGTaseI GGTaseII	Thioether to Cys
Sterol	Cholesterol	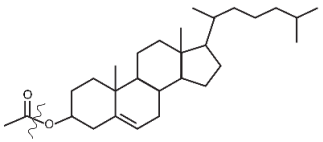	-G(CF--)	Non-enzymatic (Hh/Shh)	Cholesterol ester
Glycolipid	Glycosylphosphatidyl Inositol (GPI) Anchor	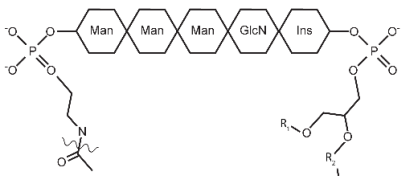	C-terminal carboxyl group	GPI - transamidase complex	Amide to carboxyl

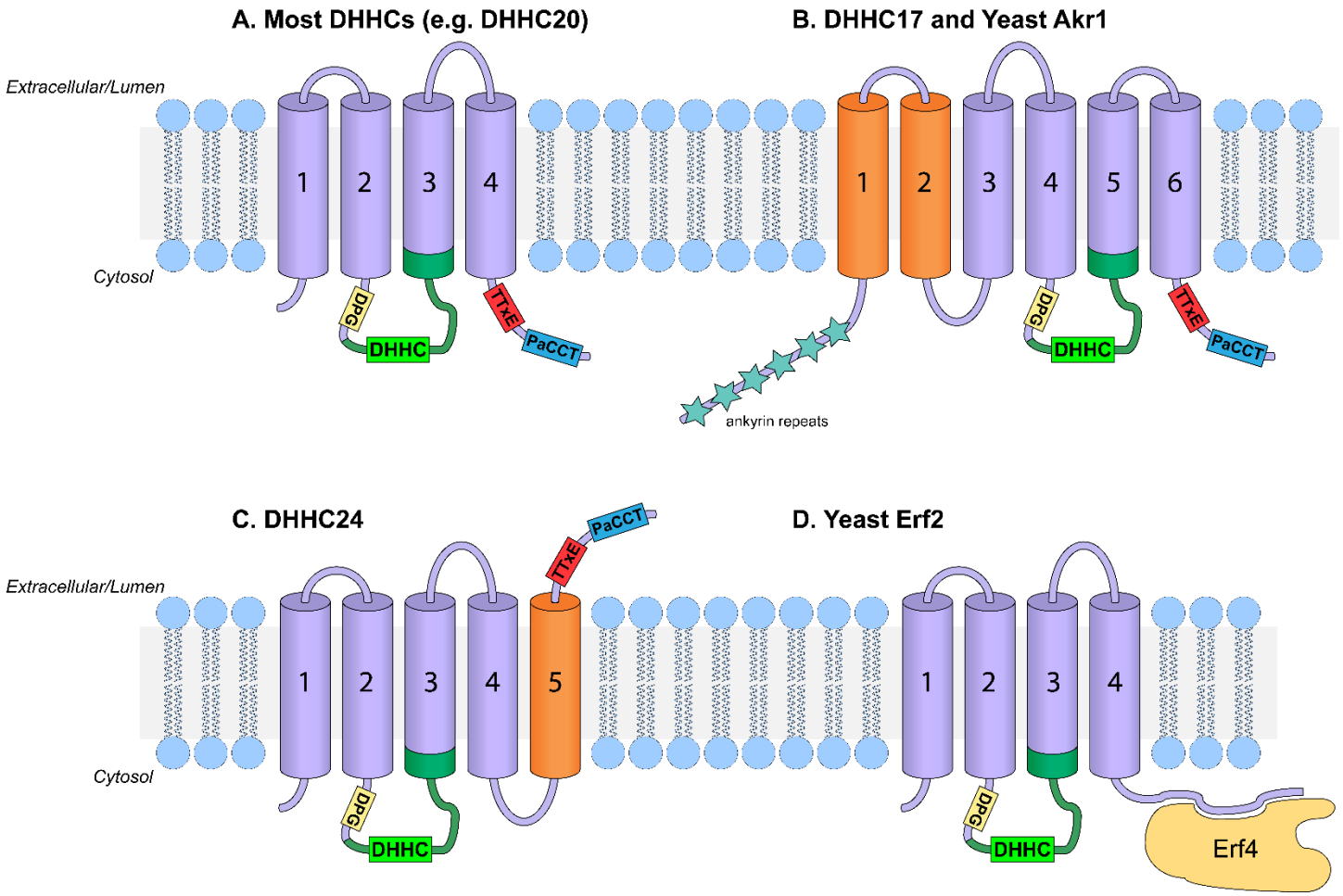

Figure 1.1 Diverse membrane topology and conserved motifs in the DHHC enzyme family.

A. Most DHHC proteins contain four TMDs. The DHHC-CRD (dark green) harbors the canonical DHHC motif (light green) situated on the cytoplasmic face of the lipid bilayer between TMD 2 and 3.

B. DHHC17 and Akr 1 contain six TMDs with six ankyrin repeats at the N-terminus.

C. Only two DHHC proteins contain five TMDs. DHHC24 has the C-terminus facing the lumenal side of the lipid bilayer.

D. The yeast Erf4 requires a binding partner, Erf4 for PAT activity.

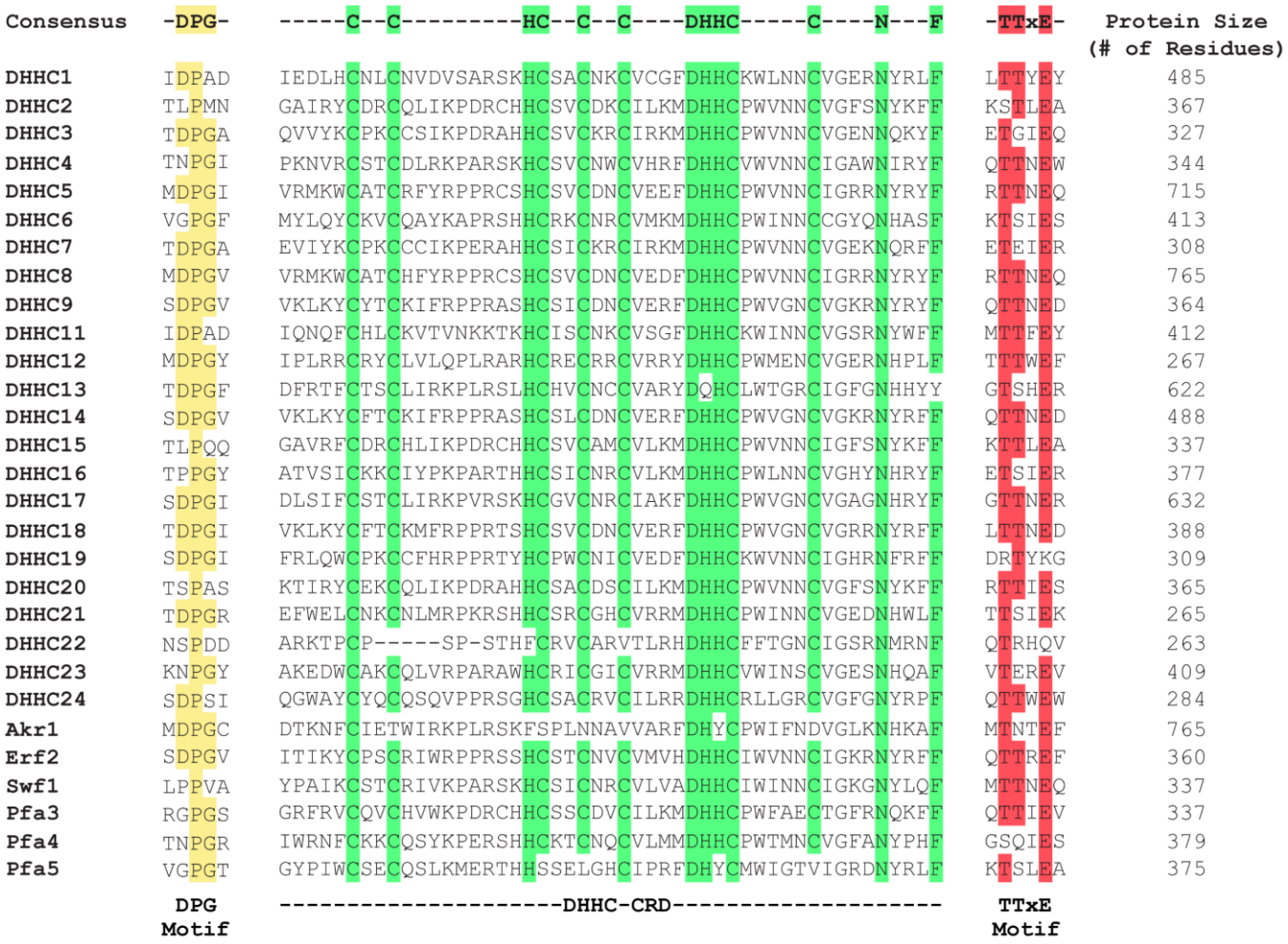

Figure 1.2 Sequence conservation in the DHHC-CRD and conserved motifs in the N- and C-termini of human and yeast DHHC enzymes.

Conserved residues are shown in yellow (DPG motif), green (DHHC-CRD), and red (TTxE motif)

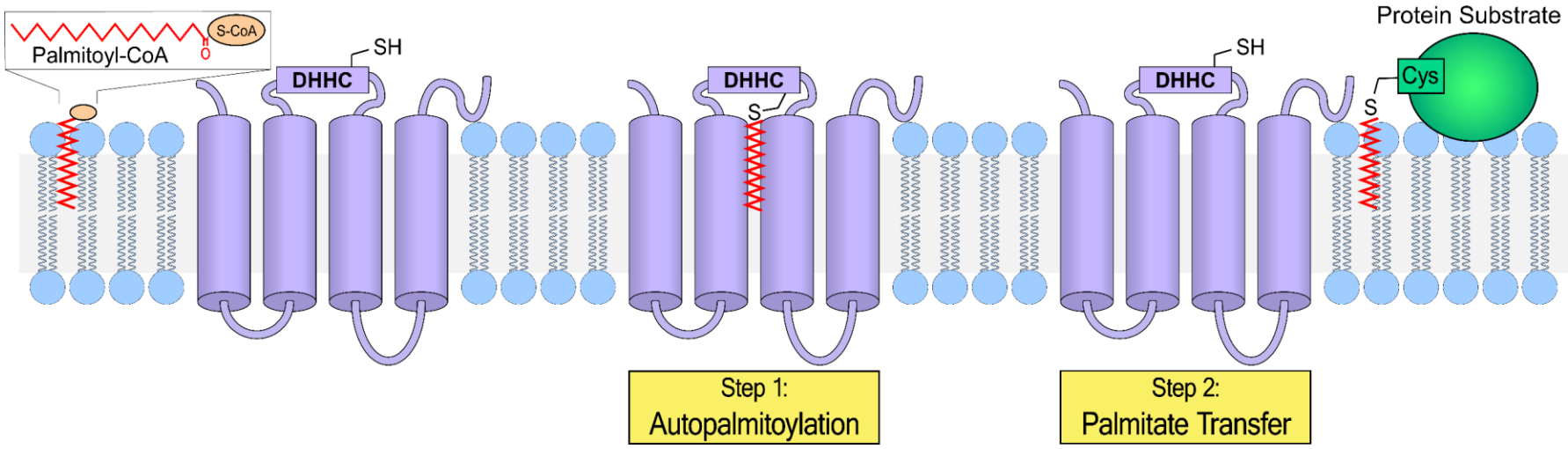

Figure 1.3 Two-step "Ping Pong" mechanism of DHHC-mediated protein S-palmitoylation.

Using palmitoyl CoA as a donor molecule, the DHHC enzyme first modifies the cysteine of the DHHC motif with palmitate, and then transfers the palmitate from itself to the protein substrate.

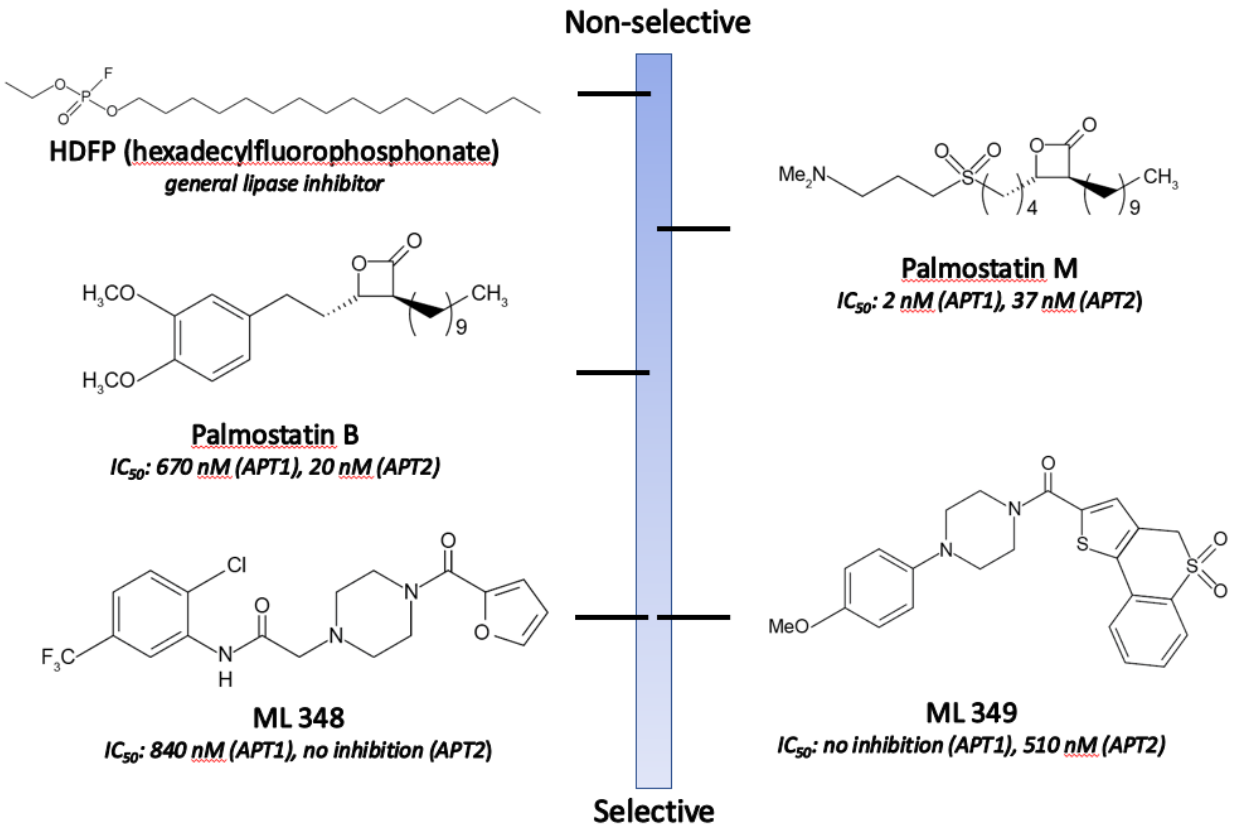

Figure 1.4 Common inhibitors used in the study of protein depalmitoylation and their half maximal inhibitory concentrations (IC_{50}) [4, 124].

CHAPTER 2: CRYSTALLIZATION ATTEMPTS AND OLIGOMERIZATION STUDIES OF DHHC PALMITOYLTRANSFERASES

INTRODUCTION

Protein S-palmitoylation refers to the post-translational attachment of fatty acids (16-carbon palmitate being the most common) to proteins. In 2002, the identity of the enzymes that catalyze protein palmitoylation was revealed [30]. Referred to as the DHHC palmitoyltransferases, these enzymes comprise a highly diverse family with 23 members in humans. The biomedical importance of the members of this family is underscored by its association with a variety of human diseases, including intellectual disability, Huntington's Disease, schizophrenia, and cancer [80, 125-130]. Essential and unique roles for DHHC proteins have been identified using DHHC-deficient mouse models [131]. Phenotypes observed include neurodevelopmental deficits, defective learning and memory, and neurodegeneration [127, 132-134]. Accordingly, there is significant interest in understanding the mechanism and regulation of DHHC enzymes.

At the beginning of my graduate studies, the knowledge of the structure of DHHC proteins was limited. However, several key structural elements had already been identified. The signature feature is a nearly invariant Asp-His-His-Cys (DHHC) cysteine rich domain (CRD) harboring the catalytic center of the enzyme [32]. DHHC proteins are predicted to share a core topology of at least four transmembrane domains (TMDs). The 51-amino acid DHHC-CRD begins in the cytoplasmic loop between the second and third TMDs and extends into the third TMD. Based on the highly conserved pattern of cysteine and histidine residues within the DHHC-CRD, some DHHC enzymes are also predicted to bind zinc [135]. During my graduate studies, this prediction was confirmed for mouse DHHC3, in which two zinc ions are tightly bound within the DHHC-CRD. The zinc metals were found to

be necessary for the structural integrity of the enzyme, but not for its catalytic activity [41]. Elucidating the atomic-level structure of a DHHC protein is an essential step in understanding how this family of enzymes carries out their functions, promoting a more guided design of small molecule inhibitors or activators that can modulate PAT activity.

The first part of this chapter describes my attempts to crystallize a DHHC enzyme. Although my initial experiments used the DHHC3 enzyme, the bulk of the crystallization optimization work was done in the context of the DHHC20 enzyme. DHHC20 overexpression was previously shown to cause cellular transformation [47] and had also been implicated in a variety of cancers. The Cancer Genome Atlas reveals that variations in DHHC20 expression including deletions, amplifications, and mutations occur in breast, lung, and prostate cancers. More recently, DHHC20 was found to be a palmitoyltransferase for the epidermal growth factor receptor (EGFR), a receptor tyrosine kinase known to facilitate tumorigenesis and cancer progression [136].

I also present in this chapter my data assessing the oligomerization status of DHHC proteins. Prior studies in the Linder lab suggest that DHHC proteins may exist in a monomer:dimer equilibrium that reflects high and low activity states, respectively. The model in which oligomer formation modulates DHHC palmitoyltransferase activity is supported both by cell-based and *in-vitro* assays. Using Bioluminescence Resonance Energy Transfer (BRET) experiments, Lai and Linder showed that DHHC3 and DHHC2, and to a higher extent the catalytically inactive mutants, DHH**S**3 and DHH**S**2, self-associate in intact HEK-293 cells [82]. Their BRET experiments suggest that DHHC2 and DHHC3 are not stable multimeric complexes but are in fact highly dynamic in cells. However, BRET experiments are limited by the inability to directly count the number of subunits in different oligomeric states. Highly purified recombinant DHHC3 dimer made by fusing two DHHC3 molecules via a covalent bond linker displayed lower activity compared than the monomeric DHHC3. Enzymatic activity was shown to be

recovered upon cleavage of the covalent bond to release the individual DHHC3 monomers [82]. While this in-vitro experiment provided cogent evidence for the difference in enzymatic activities between the monomeric and dimeric enzymes, the possibility that detergent solubilization during purification promotes oligomer dissociation cannot be discounted. In my study, I sought to address these fundamental challenges by using a recently discovered technique called Total Internal Reflection Fluorescence (TIRF) microscopy. Because of its unique ability to analyze fluorescence at a single molecule level, TIRF microscopy allows the quantification of the stoichiometry of individual GFP-tagged DHHC molecules in the context of a phospholipid bilayer.

RESULTS AND DISCUSSION

Full length mouse DHHC3 and DHHS3 enzymes purify well but aggregate at high concentrations

My first year in the Linder laboratory involved the optimization of the large-scale purification of the mouse ortholog of DHHC3. At the time, the bulk of DHHC enzymology done in our lab was in the context of the DHHC3 protein. Both DHHC3 and its catalytically inactive mutant, DHH**S**3, in which the catalytic cysteine is mutated into a serine, are biochemically tractable, highly purifiable, and stable in detergent solution (Figure 2.1). While both proteins yielded promising size exclusion chromatography (SEC) profiles following a two-step affinity purification, concentrating either protein to above 1 mg/mL resulted in significant protein aggregation. Not surprisingly, I was unsuccessful in growing protein crystals of both the *m*DHHC3 and *m*DHH**S**3 proteins. Interestingly, these initial experiments showed consistently higher yields for the DHH**S**3 enzyme compared to the wild type, which prompted me to use the mutant in the succeeding optimization experiments.

We sought to solve the aggregation problem of the *m*DHHC3 protein by designing and screening several truncation constructs that excluded flexible and disordered regions in the protein. However, instead of following the traditional approach of purifying all the candidate constructs using a baculovirus insect-cell expression system, we took advantage of an efficient pre-crystallization screening strategy that only required transient transfection in HEK cells [137]. In this technique, individual candidate protein constructs are covalently fused to green fluorescent protein (GFP) and transiently expressed in HEK cells. After cell lysis, the total cell lysate containing the candidate protein is analyzed by fluorescence size-exclusion chromatography (FSEC), in which the conventional SEC column is coupled to a fluorometer to give a GFP fluorescence-based chromatogram. The resulting chromatograms are evaluated by the following: the number of peaks indicates protein homogeneity, the height of each peak corresponds to protein expression level, the sharpness of each peak demonstrates monodispersity, and the elution volume approximates the molecular mass of the protein (Figure 2.2A). Following this technique, I cloned several N- and C- terminal truncations of *m*DHH**S**3 into the pCGFP-EU2 vector that encoded a covalently linked GFP at the C-terminus of the protein (Figure 2.2B). Among the candidate constructs tested, only *m*DHH**S**3 Δ1-34 gave an FSEC profile of similar quality to that of the full length (FL) DHH**S**3. (Figure 2.3A). Interestingly, the two C-terminal truncations of DHH**S**3 resulted in a significant reduction in the expression level of the protein suggesting that the C-terminal residues may be important for the structural integrity of the protein. Notably, a similar sensitivity in C-terminal truncations was observed for the N-terminally GFP-tagged DHH**S**3, which showed lower expression levels compared to C-terminally GFP-tagged DHH**S**3 (data not shown). Unfortunately, like the full-length construct, purified *m*DHH**S**3 Δ1-34 resulted in an aggregated protein upon concentration to 1 mg/mL (Figure 2.3B).

Another approach we took was designing *m*DHH**S**3 chimeras that add the highly-crystallizable T4 lysozyme (T4L) protein in the internal loops of protein. This technique was demonstrated to

successfully promote the crystallization of some G protein coupled receptors (GPCRs) including the β2-adrenergic receptor [138]. Among the four *m*DHH**S**3-T4L fusion proteins we designed (Figure 2.2B), T4L-1 and T4L-2 expressed well in HEK cells. However, just like the previous *m*DHH**S**3 constructs, purifying and concentrating these fusion proteins resulted in a highly aggregated protein (Figure 2.3C,D).

Human DHHC20 stands out among other DHHC PATs as a candidate for crystallization

Due to the demonstrated general propensity of the DHHC3 protein to aggregate at concentrations amenable to protein crystal formation, we decided to screen other members of the mammalian DHHC family for a new candidate DHHC protein. The conserved DHHC-CRD and a common kinetic mechanism among the highly divergent DHHC proteins suggests that the information gleaned from solving the structure of any of the DHHC proteins is relevant to the entire DHHC family. To identify the best candidate for crystallization, we used a similar FSEC approach to evaluate expression, stability, and monodispersity of 16 *human* or *mouse* DHHC proteins. In this screen, *human* DHHC20 came out as the most promising candidate, demonstrating a single sharp, monodisperse FSEC peak. As expected, DHHC3 also showed a monodisperse peak (Figure 2.4). Unfortunately, as in the case of the *m*DHHC3 protein, protein preparations of WT DHHC20, the catalytically inactive DHH**S**20 mutant, and the N- and C-terminal DHHC/**S**20 truncation constructs all led to an aggregated protein at high concentrations.

Frog DHHC20 does not aggregate at high concentrations

The persistent aggregation problem seen in *m*DHHC3 and *h*DHHC20 upon concentration compelled us to then search for new crystallization candidates in other DHHC species. To identify the

optimal species for crystallization, we screened orthologs of both DHHC3 and DHHC20 enzymes. The species included in the screen contained 40-90% sequence identity to either the *mouse* DHHC3 or *human* DHHC20 (Figure 2.5 and 2.6). While none of the DHHC3 orthologs included in the screen gave good SEC profiles, the *frog* DHHC20 construct with 73% sequence identity to the human protein, displayed robust expression, stability, and monodispersity by SEC (Figure 2.7). More importantly, FL *fr*DHHC20 fused at the C-terminus to a strep tag, a thrombin protease cleavage site, and a GFP tag purified at high yield from insect cells (2.5 mg/L insect cell culture). After cleavage with thrombin protease to remove the GFP and Strep tags, FL *fr*DHHC20 concentrated to 10-12 mg/ml with minimal aggregation. We then sought to remove the unstructured N- and C-terminal loops in the context of *fr*DHH**S**20. Among these truncations, the best SEC profile was seen for *fr*DHH**S**20 Δ1-5 ΔR1-68 (hereby referred to as *fr*D**S**20Δ), in which the first 5 residues in the N-terminus and the last 68 residues in the C-terminus are removed from the protein (Figure 2.8). Interestingly, the catalytically inactive *fr*DHH**S**20 construct displayed a more symmetric peak compared to wild type construct. Further characterization of the WT *fr*DHHC20 protein by Multi-angle Light Scattering (MALS) suggests that the *fr*DHHC20 protein exists predominantly as a dimer in detergent solution (data not shown).

Functional characterization of frDHHC20 constructs

Because there was no biochemical characterization of *fr*DHHC20 in the literature, I sought to examine if my *fr*DHHC20 enzyme preparations are active. I used N-myristoylated SH4-GFP fusion protein as a substrate for my enzymes in a radioactive PAT assay. The Src homology 4 (SH4) domain is defined as the membrane-targeting domain of Src-family kinases and is contained within a peptide sequence encoding N-myristoylation and S-palmitoylation sites. The SH4-GFP fusion protein contains three cysteine residues available for palmitoylation and is a substrate for a diverse set of DHHC

proteins [139]. Both FL *fr*DHHC20 and *fr*DHHC20 Δ1-5 ΔR1-68 displayed PAT activity. As expected, FL and truncated *fr*DHH**S**20 were catalytically inactive (Figure 2.9).

***Manipulating the cysteine residues of frDHHS20* Δ1-5 ΔR1-68**

In order to reduce protein heterogeneity, we sought to remove potential non-specific palmitoylation sites by mutating cysteine residues into a serine residue. The FL frDHH**S**20 protein has a total of 16 cysteines in its amino acid sequence. Two of which are embedded in the transmembrane domains and one faces the lumenal side of the lipid membrane; these cysteines were assumed to not participate in catalysis and were not tested. Among the remaining cysteines, 5 were situated outside of the DHHC-CRD. The mutations C82S, C229S, and C287S did not cause significant changes in the SEC profile of *fr*DS**2**0Δ. However, a double cysteine mutation in the N-terminus C9,10S led to a significantly reduced protein expression level (Figure 2.10).

Additionally, there are 8 cysteine residues within the DHHC-CRD of *fr*D**S**20Δ. Cys-153 is the catalytic cysteine, which was found to be necessary for enzymatic activity (Figure 2.9). Mutation of this cysteine into a serine did not affect the structural integrity of the protein. Sequence comparison to *m*DHHC3 suggests that Cys-125, Cys-128, and Cys-142 are bound to one zinc ion while Cys-139, Cys-145, and Cys-159 are bound to another zinc in a zinc finger fashion for the structural integrity of the protein. Indeed, mutation of any of these cysteines into a serine residue caused either a dramatic decrease in protein expression level or an aggregated protein. On the other hand, mutation of Cys-136, an unconserved cysteine within the DHHC-CRD maintained a monodisperse chromatogram similar to the parent construct (Figure 2.10).

***Optimizing the crystallization of frDHHS20* Δ1-5 ΔR1-68**

After an iterative process of screening several hundred DHHC protein constructs, I determined that *fr*DHH**S**20 Δ1-5 ΔR1-68 was the most viable candidate for crystallization. A series of optimization experiments was then undertaken to generate diffracting crystals of this protein construct. These include detergent screening, addition of lipids (e.g. bicelles, lipidic cubic phase) and small molecules (metal ions, myristate, palmitoyl CoA). Interestingly, most of the protein crystals formed were in the context of solubilizing the enzyme in different detergent solutions and by hanging-drop method of crystallization. In these conditions, the crystal appearance ranged from amorphous to needle-like of varying sizes. Finally, weakly diffracting crystals (≈ 18 Å) of *fr*DHH**S**20 Δ1-5 ΔR1-68 were obtained in 18% PEG 2000, 0.15 sodium formate, and 0.10 M Tris pH 8.5.

Determination of the oligomeric state of DHHC proteins

The existence of different oligomeric states of the DHHC proteins was first described in coimmunoprecipitation experiments showing that catalytically inactive DHH**S**3 (also named GODZ (Golgi-specific DHHC zinc finger protein)) multimerizes and interacts with itself and its close paralog DHHC7 (also named sertoli cell gene with a zinc finger domain-β (SERZ-β)) [140]. The observed oligomerization of DHH**S**3 provided a possible rationale for previous reports that DHH**S** acts as a dominant negative when expressed in cultured cells [73, 140, 141]. Since then, oligomerization of DHHC proteins was hypothesized as one mechanism by which DHHC activity is regulated in cells.

In 2013, Lai and Linder provided cell-based and *in-vitro* data supporting that DHHC oligomerization modulates DHHC enzyme activity. While it was suggested that DHHC porteins esist mostly as dimers and monomers, the exact stoichiometry of the DHHC oligomerization has not been resolved. I approached this problem using Total Internal Reflection Fluorescence (TIRF) microscopy.

TIRF microscopy allows the quantification of the stoichiometry of individual GFP-tagged DHHC molecules in the context of a phospholipid bilayer. This technique was demonstrated to successfully resolve the subunit composition of the membrane protein N-methyl-D-aspartate (NMDA) receptor [142].

With the help of Mark Richards from Dr. Susan Daniel's laboratory and Julia Kumpf from Dr. Toshi Kawate's laboratory, I sought to determine the subunit composition of human DHHC20, a plasma membrane-localized DHHC protein and its catalytically-inactive mutant in which the cysteine in the DHHC motif is mutated into a serine residue (DHH**S**20). To do this, I made recombinant DHHC constructs that contained a GFP tag on either the N- or the C-terminus of the protein and expressed them in HeLa cells. This cell line was chosen because of its ability to spontaneously release plasma membrane vesicles called blebs when incubated in serum-free media. After transfection, PM blebs harboring the GFP-tagged DHHC molecules shed from the cell surface and were collected and separated from contaminating microsomes. The solution was then plated on supported 1-palmitoyl-2-oleoyl-sn-glycero-3-phosphocholine (POPC) lipid bilayers and imaged using a TIRF microscope. Photobleaching events were collected and analyzed using the MATLAB programming software. The resulting raw images contained photobleaching traces of multiple fluorescent spots. The use of the genetically encoded GFP tag is important to ensure that every tagged subunit carried exactly one chromophore. Since photobleaching of a single GFP is a discrete process, the fluorescence intensity of a protein complex with one or several GFP molecules drops in a stepwise fashion. The number of photobleaching steps reveals the number of GFP-fluorescing subunits, and hence, the number of subunits in each fluorescing complex [142]. For example, a monomeric DHHC molecule will show one photobleaching step, whereas a dimeric one will show two discrete steps (Figure 2.11).

My results indicate that both N- and C-terminally GFP-tagged DHHC20 exist mostly in a monomeric or a dimeric state, demonstrating that the placement of the GFP tag had no effect on the oligomeric distribution of the protein. More importantly, for both N-terminally and C-terminally GFP-tagged constructs, a higher dimer to monomer ratio was observed for the catalytically inactive DHH**S**20 than for the wild type. This result strongly parallels the observations reported by Lai in which the amount of dimer detected using purified enzyme preparation in detergent solution was modest relative to the monomeric protein. While experiments using detergent-purified protein preparations are confounded by the possibility that detergent solution may promote oligomer dissociation, my analysis of oligomerization on a single molecule level in natural lipid bilayer provides a better representation of the protein status in cellular membranes.

There have been multiple reports of higher order oligomers in DHHC proteins, albeit inconsistently [41, 82, 140]. While 90% of the DHHC20 and DHH**S**20 molecules detected by TIRF microscopy were either monomers or dimers, roughly 10% of the DHHC species indicated an oligomeric state higher than n = 2. Notably, one caveat of this technique is that for complexes containing more than three subunits, the distributions of photobleaching steps for n and n + 1 subunits look quite similar or are distorted, making the detection and assignment of discrete steps very challenging. Hence, the small fraction of higher order oligomer species was annotated as n > 2-mer.

CONCLUSIONS

While my efforts did not ultimately result in the first crystal structure of a DHHC protein, Banerjee and coworkers successfully solved the crystal structures of *human* DHHC20 and the catalytically inactive mutant of *zebrafish* DHHC15 [69]. Their diffraction data successfully resolved the atomic structures of residues 5-299 of *h*DHHC20 and of residues 8-298 of *zf*DHH**S**15. The *h*DHHC20 protein crystallizes in two different crystal forms in LCP: a P63 form with an antiparallel dimer and a P21 form with a loose parallel dimer in the asymmetric unit. Conversely, zfDHH**S**15 crystallizes in P42212 space group with an antiparallel dimer in the asymmetric unit.

Variations in protein preparations can lead to substantial changes in the quality of protein crystals

Highly diffracting crystals of human DHHC20 were obtained by utilizing the lipidic cubic phase (LCP) method of crystallizing proteins [143]. While I tried this technique in the context of the truncated *frog* DHHC20 constructs, incorporating these proteins into monoolein and cholesterol lipids, I did not test the utility of this technique with the full length (FL) *frog* and *human* DHHC20 proteins. Interestingly, two key pre-crystallization steps were identified to be critical in improving the quality of DHHC20 protein crystals: the addition of lipids during protein purification (lipid identity was not specified) and the reductive methylation of DHHC20 using formaldehyde and dimethylamineborane (DMAB) complex prior to the removal of the GFP tag and subsequent SEC. These two key pre-crystallization steps were absent in all of my DHHC protein preparations. Addition of lipids might have helped with the protein aggregation issue of most of the DHHC constructs by increasing the stability of the protein-lipid-detergent complex during protein purification. Moreover, as in the case of the myosin subfragment-1 protein, improved crystal formation kinetics might have been obtained upon

methylation of the solvent exposed lysine residues that contribute to an increased entropy of the protein [144].

The overall structure of hDHHC20 and zfDHHC15 is similar to what was predicted for DHHC enzymes

Consistent with common DHHC protein sequence topology predictions, the four TMDs of *h*DHHC20 forms a tepee-like cavity where the acyl chain of the acyl CoA co-substrate is inserted. The residues lining this cavity determine acyl CoA chain length selectivity. The lumenal side of the membrane contains short loops that connect TM1 and TM2, and TM3 and TM4, while the cytosolic side harbors the highly conserved DHHC-CRD connecting TM2 and TM3. The positioning of this active site at the membrane-cytosol interface supports previous predictions that candidate cysteines for palmitoylation are usually proximal to the membrane [145]. The active site consists of an Asp-His-Ser catalytic triad-like arrangement that activates the catalytic cysteine as a nucleophile.

Two zinc ions serve a structural function in the cysteine-rich domain of DHHC20

The cysteine-rich domain of DHHC20 indeed binds two zinc ions. As expected of zinc finger motifs, both Zn^{2+} adopt a tetrahedral coordination composed of three cysteines and a histidine. My characterization of *fr*DHH**S**20 cysteine mutants supports this structural data. In my SEC experiments, a significant reduction in protein expression level or an increase in protein aggregation levels was observed when any of the Zn-binding cysteine residues were mutated into serine; whereas mutation of a nearby unconserved cysteine (Cys-136) did not affect the structural integrity of the enzyme.

The C-terminal domain of DHHC20 contains residues that interact with the active site of the enzyme

Despite being highly variable among the different members of the DHHC protein family, the C-terminal domain (CTD) of DHHC proteins has two conserved non-catalytic structural features: the Thr-Thr-Xxx-Glu (TTxE) motif and the palmitoyltransferase conserved C-terminus (PaCCT) motif. The structure of *h*DHHC20 demonstrates for the first time that the residues in these two motifs form critical interactions with the DHHC-CRD and the TMDs. The glutamate of TTxE forms a salt bridge with a conserved arginine in the DHHC-CRD. The second threonine of the TTxE motif forms a hydrogen bond with the aspartic acid of the DHHC motif, although the exact chemical role of this contact in catalysis is unclear. Mutation of these two threonine residues into alanine drastically reduces enzymatic activity. Interestingly, in *fr*DHHC20, the TTxE motif exists as Ser-Thr-Ile-Glu (STIE). Moreover, a highly active DHHC3 enzyme has a Thr-Gly-Xxx-Glu (TGxE) motif. The highly conserved Asn-266 of the PaCCT motif of *h*DHHC20 forms extensive hydrogen bonds with neighboring residues in TM3 and TM4 and is important for the structural integrity of the enzyme. Mutation of this asparagine residue into alanine drastically reduces enzymatic activity.

Lastly, the structure showed an unanticipated amphipathic helix formed by W278, L279, L280, P281, and I282 in the CTD of *h*DHHC20 forming contact with TM3 and TM4 and likely provides local stability. The amphipathic helix is followed by a hydrophobic loop that is stabilized by highly conserved lysine and proline residues. The hydrophobic residues in this loop inserts into the putative lipid bilayer and forms additional contacts with TM3 and TM2. In *fr*DHHC20, these residues correspond to W275, L276, L277, P278, and M279. This might explain why my truncation construct *fr*DHH**S**20 Δ1-5 ΔR1-80 in which part of this amphipathic helix is removed resulted in a drastic reduction of protein expression.

Outstanding questions on the mechanism of the DHHC proteins

The recent structures of the human DHHC20 and zebrafish DHH**S**15 provide a structural framework to understand the mechanism governing DHHC-mediated S-palmitoylation. We now appreciate that the DHHC enzyme active site contains an atypically arranged catalytic triad, in which the three active site residues (Aps153, His154, and Cys156), are arranged sequentially and linearly. In this mechanism, His-154 is polarized by Asp-153 and acts as a general base to activate Cys-156 into a thiolate nucleophile. This thiolate then attacks the carbonyl carbon of the fatty acyl Coenzyme A forming the DHHC-palmitate intermediate that was previously proposed and detected by mass spectrometry. Subsequently, the fatty acyl chain is transferred to the protein substrate thus regenerating the DHHC enzyme for another round of catalysis. While this mechanism stood for both DHHC20 and DHHC15, other mechanisms of palmitoylation remain possible. For example, the yeast ERF2–ERF4 protein complex with a D**A**HC mutation was found to autoacylate but not acylate protein substrate, suggesting that the role of the first histidine is in activating the cysteine protein substrate, but not the DHHC active site cysteine [74]. This implies an alternate mechanism for the ERF2 enzyme that probably relies heavily on its association with the ERF4 subunit. Additionally, the yeast Swf1 and Pfa4 both remain active palmitoyltransferases as DHH**R** proteins, suggesting that S-palmitoylation does not necessarily require an autoacylated DHHC intermediate [76].

It has been predicted that the C-terminal residues of the DHHC proteins are important for substrate binding. However, the solved structures do not clearly identify substrate binding sites in the protein. Of note, the last ∼30 residues, predicted to be unstructured, are missing from the structure. Because the C-terminal domain wraps halfway around the protein, it is unclear if the missing residues are important in positioning the protein substrate close to the active site for fatty acylation. It is possible that DHHC enzymes can adopt a different conformation in which the C-terminal domain is rearranged closer to the transmembrane domains in the active site. Another proposed site for

substrate recruitment is the zinc-finger motifs situated right below the active site and compose a plausible interface to mediate protein–protein interactions [146]. However, domain swap experiments suggest that at least for a subset of DHHC-PATs, the DHHC-CRD is unlikely to impart substrate specificity [49]. To date, it can not be ruled out that there are different modes of DHHC enzyme-protein substrate interactions and even transient DHHC enzyme-substrate interactions can still be productive. In cells, these interactions occur close to the membrane which could be a critical third component in these enzyme-substrate interactions.

Although the catalytic domains and the fatty acid-binding domain are expected to be similar, the structures of other DHHC enzymes containing more than four transmembrane domains remain of interest. While the current structures provide significant snapshots on the mechanism of the DHHC enzymes, the structures of intermediate DHHC species at different stages of the palmitoylation cycle are currently unavailable. Combined with molecular dynamics studies, these important structures are expected to answer more detailed mechanistic questions that can be validated by experiments.

Oligomerization of DHHC Proteins

The dimer interface seen in the crystal structures of *h*DHHC20 and *zf*DHHC15 is oriented in a head-to-tail manner. This odd dimer arrangement, if physiologically relevant, would imply that one of the dimeric subunits had its catalytic DHHC motif sitting in the lumen. Based on the assumption that palmitoylation exclusively occurs on the cytoplasmic face of the membrane, which would entail that the DHHC motif is always cytosolic, the authors interpreted the dimeric interface as adventitious protein-protein interactions similar to what was seen in the crystal structures of rhodopsin [147] and the chemokine receptor type 9 (CCR 9) receptor [148].

To exclude the possibility that DHHC20 or DHHC15 adopts an inverted topology, the authors carried out a fluorescence protease protection assay in which both constructs were tagged with GFP at the C-terminus and expressed in HEK-293 cells. Upon permeabilization of the plasma membrane with digitonin and addition of trypsin, the fluorescent tags on the C terminus of both DHHC20 and DHHC15 were removed, whereas a control with a fluorescent tag in the lumen of the Golgi was retained, ruling out any physiologically relevant topology of DHHC20 or DHHC15 that positions the DHHC loop in the lumen of the Golgi.

The finding that DHHC proteins can form head-to-tail dimers in the crystal structure raises questions as to whether the previous results of Lai and Linder demonstrating that DHHC3 and DHHC2 oligomerize in intact cells and *in-vitro* also represent a non-physiological conformation. While it is tempting to assume that the lack of physiological dimer in the crystal structure of the DHHC proteins precludes the formation of DHHC oligomers in cells, it is possible that detergent solubilization during protein purification causes a dissociation of the DHHC oligomers into monomers which crystallize as dimers in the head-to-tail conformation. In Lai's *in-vitro* experiments, an artificial dimer composed of two DHHC3 molecules linked together by a thrombin cleavage site was used as a model for a DHHC3 dimer. The PAT activity of this dimeric DHHC3 was seen to increase over the time course of thrombin cleavage, which was presumed to be a result of the more active monomers being released by the thrombin cleavage. However, it is also possible that the spike in activity was merely due to the relief of any conformational constraint caused by the fusion of two DHHC3 monomers in forming the artificial dimer. My investigation of the oligomeric states of DHHC20 using TIRF microscopy experiments averted this complication by looking at individual DHHC molecules in supported lipid membranes, which is more representative of a native membrane than detergent micelles. These results support Lai's experiments in intact cells showing self-association of DHHC2 and DHHC3 using BRET reporters.

My findings demonstrate the occurrence of monomers and dimers of DHHC20, which together with the previously studied DHHC2 and DHHC3 constitute the list of DHHC proteins with evidence of oligomerization. It will be interesting to test if other proteins exhibit similar behavior. It has been reported that DHHC3 forms heteromultimers with DHHC7 [140]. The formation of DHHC heteromultimers has been hypothesized to account for the dominant negative effects when catalytically inactive DHHC proteins are expressed in cells [140]. If DHHC oligomers indeed represent a less active state of the enzyme, then sequestration of a DHHC protein in inactive oligomers may provide a possible mechanism to explain its dominant inhibitory behavior.

EXPERIMENTAL PROCEDURES

Reagents – Anti-FLAG® M2 affinity gel was purchased from Strategene. A 1000x polyethylenimine (PEI) transfection reagent (Sigma) was made in water. A 1000x protease inhibitor cocktail of 5 mg/mL leupeptin (Sigma-Aldrich, St. Louis, MO), 3 mg/mL aprotinin (Sigma), 1 M PMSF (MP Biomedicals, LLC, Solon, OH) and 1 mM pepstatin A (Amresco, Solon, OH) was mized from individual components. Alexa-flour®647 azide was purchased from Invitrogen (San Diego, CA). [^{3}H]-palmitoyl CoA was synthesized as previously described [82]. HEK-293 cells were cultured in DMEM (Gibco) media with 10% fetal bovine serum (Life Technologies). Cells were maintained at 37 ^{o}C in a humidified incubator supplemented with 5% CO_2.

Two-step Affinity Purification of DHHC3 and DHHS3 enzymes – WT DHHC3-FLAG-His6 and DHH**S**3-FLAG-His6 constructs were made using Bac-to-Bac baculovirus insect-cell expression system and expressed in Sf9 cells as described before [149]. Purified proteins were concentrated using Amicon® Ultra filter units (Millipore-sigma).

Fluorescence Detection Size Exclusion Chromatography (FSEC) Screening – DHHC constructs used for the FSEC screening experiments were cloned into the pNGFP-EU2 or pCGFP-EU2 vectors to include an N-terminal GFP or a C-terminal GFP tag respectively. The day before transfection, HEK-293 cells were plated onto six-well plates at 40-50% confluency. The cells were incubated overnight at 37 °C. The next day, the cells were transfected with 5 µg of DNA and 15 µg of PEI transfection reagent. After 48 h, the DMEM media was aspirated, and the cells were suspended and washed with 2 mL of ice-cold PBS. The cells were then lysed with 150 µL of lysis buffer (1x PBS, 1% DMM, and 1x protease inhibitor) for 30 minutes at 4 °C while rotating. The whole cell detergent extract was then centrifuged at 17,000 x g for 20 minutes at 4 °C. 30-50 µL was applied to FSEC. 50 µl of each supernatant was injected into a Superose Increase 10/300 GL column preequilibrated with running buffer (1x PBS supplemented with 0.5 mM DDM) using a flow rate of 0.5 ml/min. The eluate was monitored using a fluorescence detector (Shimadzu RF-20Axs; excitation: 480, emission: 508). FSEC experiments were performed as described previously [137].

Strep Purification of DHHC20 enzymes – All *frog* DHHC20 constructs used for purification and subsequent crystallization experiments were made by cloning the DHHC20 cDNA into the pNGFP-FB3 or pCGFP-FB3 vectors to include an N-terminal GFP and Strep tags or a C-terminal GFP and Strep tags respectively. This cloning strategy resulted in insertions of two amino acids (Gly-Ser) right after the first methionine and three amino acids (Ala–Ser–Ser) before the stop codon. Additionally, these plasmids encode a thrombin cleavage site used to cleave the GFP and Streptavidin tags after the purification. All constructs were expressed using the Bac-to-Bac baculovirus-insect cell expression system. Sf9 cells were infected at 2.5 – 4.0 x $10^{\wedge 6}$ cells/mL with P2 virus. Cells were incubated at 27 °C for 48 h and then harvested by centrifugation of 500xg, washing twice with 200mL. Cells were then

disrupted in lysis buffers containing (50 mM Tris pH 7.4, 200 mM NaCl, 1% DDM, 10% glycerol, 1 mM TCEP and protease inhibitors (0.5 ug/mL leupeptin, 3 ug/mL aprotinin, 0.3 ug/mL pepstatin A, and 0.5 mM phenylmethylsulfonyl fluoride). Cleared lysate was then centrifuged at 100,000xg for 40 min. The soluble fraction was incubated with Streptactin sepharose High Performance resin (GE Healthcare) for 2 h by a batch method. The resin was pelleted by centrifugation and transferred to a gravity column (Bio Rad) and washed with 10 x column volumes of wash buffer containing 100 mM Tris HCl, pH 7.4, 150 mM NaCl, 10% glycerol, 0.5 mM DDM and 0.5 mM TCEP. The DHHC protein was eluted with buffer containing 100 mM Tris HCl, pH 7.4, 150 mM NaCl, 2.5 mM desthiobiotin, 0.5 mM TCEP, 10% glycerol and 0.5 mM DDM. The GFP and strep tags were removed by incubation with human thrombin (1:100) for 12 hours at 4 °C. Size exclusion chromatography (SEC) was done using a Superdex 200 (GE Healthcare) in SEC buffer (50 mM Tris pH 7.4, 150 mM NaCl, 0.5 mM TCEP, 10% glycerol, and 0.5 mM DDM). The protein concentration was determined by plotting elution samples along a linear curve generated with known concentrations of bovine serum albumin stained with Coomassie gel stain and quantified using a VersaDoc^{TM} 5000 imaging system.

Protein Acyl Transferase (PAT) Assay – Purified DHHC enzyme (30 nM) was assayed in a 50 µL reaction with 1 µM [^{3}H]-palmitoyl CoA and 1 µM myristoylated SH4-GFP at 25 °C for 0-30 min. The reaction was stopped with the addition of 5x sample buffer containing 10 mM TCEP and resolved on a Coomassie-stained gel. The substrate bands in the gel were excised, cut into 1 mm cubes and combined with 500 µL Soluene 500 (Perkin-Elmer, Waltham, MA). The excised bands were then heated at 37 °C overnight before being combined with 4.5 mL of Ultima Gold scintillation fluid (Perkin-Elmer) and counted in a scintillation counter.

Counting the Oligomeric States of DHHC Proteins by TIRF Microscopy – The data collection protocol [150] was developed with the guidance of Mark Richards and Rohit Singh in Dr. Susan Daniel's laboratory. The Matlab program was adapted from Julia Kumpf experiments on P2X proteins.

Plasma Membrane Bleb Preparation – Cell blebbing was performed by serum starving HeLa cells. Transfections were performed using 3 μg of DNA and 9 μg of polyethylenimine (PEI) transfection reagent followed by a 24 h incubation at 37 °C. HeLa cells were then washed with serum-free DMEM media and then incubated with 4 mL of serum-free DMEM media for 4 h before collection of the bleb-containing supernatant. Contaminating microsomes were removed by centrifugation using a 0.22-micron filter (Millipore). The blebs-containing solution that remained after filtration were used for the subsequent steps.

Liposome Preparation – 1-palmitoyl-2-oleoyl-glycero-3-phosphocholine (POPC) and 0.5% (mol/mol) 1,2-dipalmitoyl-sn-glycero-3-phosphoethanolamine-N-[methoxy(polyethyleneglycol)-5000] (PEG5000-PE) were used to formulate liposomes. Liposomes were prepared by dissolving components in chloroform (Sigma), mixing in appropriate ratios, and drying under a stream of nitrogen gas. Subsequently, lipid films were desiccated under vacuum for 3 h to remove trace solvent. Phosphate buffered saline (PBS) composed of 5 mM NaH_2PO4, 5 mM Na_2HPO_4, 150 mM NaCl at pH 7.4 was added to a lipid concentration of 2 mg/mL, and lipids were frozen. After thawing, liposomes were sonicated using a VWR B2500A-DTH bath sonicator for at least 60 min prior to use. Liposomes were stored at 4 °C until use.

Bleb Bilayer Formation for Fluorescence Microscopy – Glass slides (25 × 25 mm No. 1.5, VWR) were cleaned with piranha solution (mixture of 70% (v/v) H_2SO_4 (BDH) and 30% (v/v) H_2O_2 (Sigma) for 10 min and then rinsed for 20 min under 18.2 MΩ-cm water. Polydimethylsiloxane (PDMS) wells (5 mm diameter, 3 mm thick) were affixed to the clean, dry slides. The bleb-containing solution was then

added to the wells at approximately 4×10^8 blebs/mL. After a 10-min incubation, the well was rinsed vigorously with PBS buffer to remove excess, unadsorbed material. Bleb bilayer formation was induced by adding 70 µL of liposomes at 0.5 mg/mL into the well and incubating for 30 min before rinsing again with PBS buffer. An inverted Zeiss Axio Observer.Z1 microscope with α Plan-Apochromat objectives, a Hamamatsu EM-CCD camera (ImageEM, model C9100-13, Bridgewater, NJ) and X-Cite 120 microscope light source (Lumen Dynamics Group Inc., Canada) were used to visualize the bleb rupturing process. An ET MCH/TR filter cube (49008, c106274, Chromatech Inc.) was used to collect the fluorescence emitted from the R18 fluorophores. A 20 µm diameter spot in the supported lipid bilayer was bleached with a 4.7 mW 488 nm krypton/argon laser for 400 ms. The recovery of the intensity of the photobleached spot was recorded for 15 min at regular intervals. The fluorescence intensity of the bleached spot was determined after background subtraction and normalization for each image.

Data Analysis – The output is a video file composed of around 300-1500 frames, with each frame comprised of 512 x 512 pixels collected at 50 ms exposure time. A program in Matlab was designed to automate the detection, selection and quantification of fluorescence spots. This involves several image processing techniques including signal averaging, low/high pass filtering, and thresholding. The resulting output traces were exported to Microsoft Excel for manual counting. Several criteria were met in characterizing each trace. The fluorescent species was classified as either monomer, dimer, or higher oligomer based on the number of photobleaching steps observed in each trace. However, not all traces were analyzed. Traces were discarded under the following circumstances: a spot moved away from each original position at any time during the movie, a spot exhibited an elliptical shape, a spot was very close to other spots (<4 pixel) and therefore picked up some emission from these other spots, or a spot did not bleach completely by the end of acquisition time.

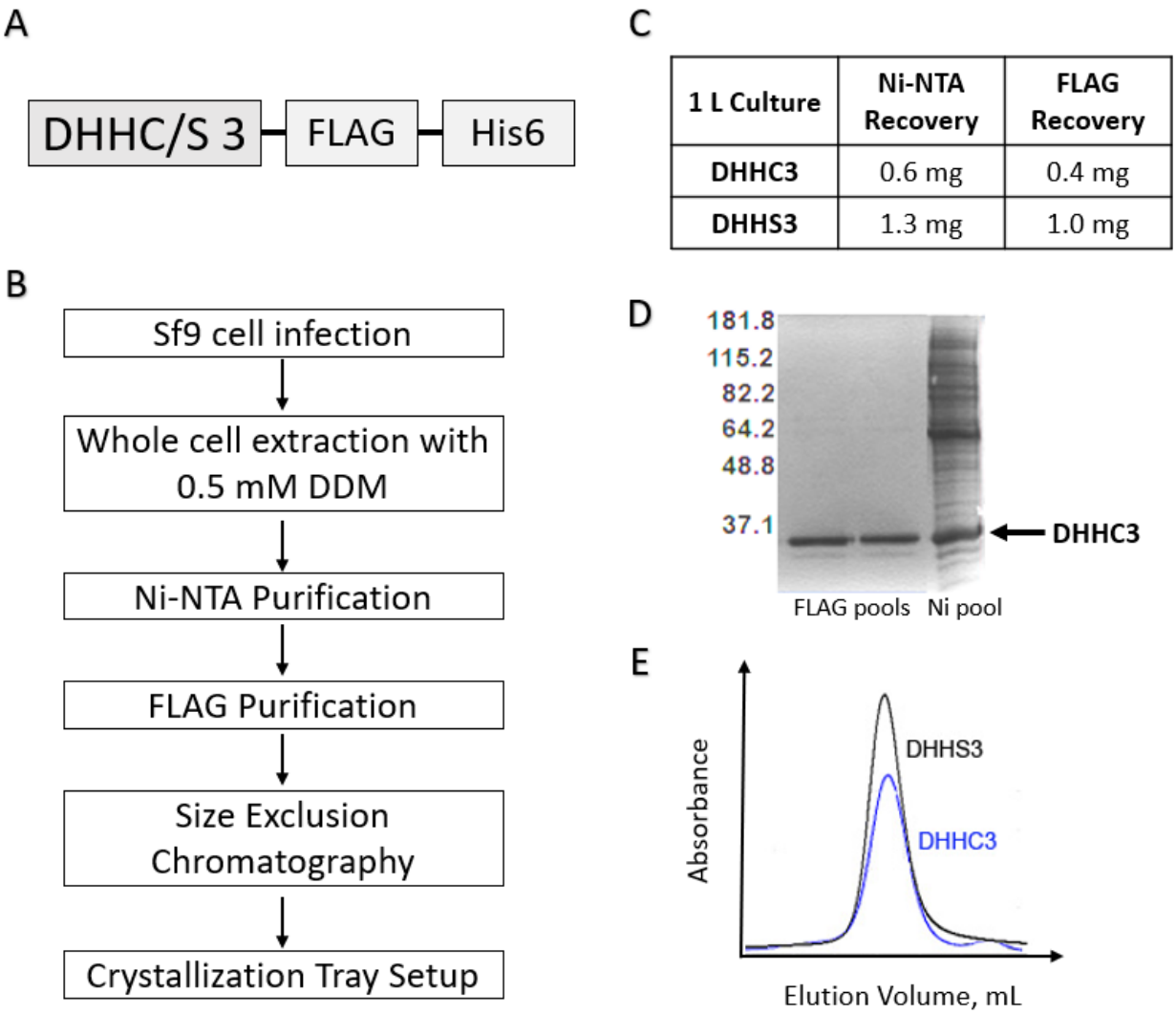

Figure 2.1 Preparation of full-length mouse DHHC3 and DHHS3 enzymes.

A. Mouse DHHC/**S**3 constructs were made with a FLAG epitope and a hexahistidine tag on the C-terminus of the enzyme.
B. Flowchart of DHHC3/**S**3 enzyme preparation.
C. Typical yields for a 1 L purification of DHHC/**S**3 after a two-step affinity purification.
D. Representative Coomassie-stained gel of DHHC3 after a two-step affinity purification.
E. SEC profiles of purified DHHC3 (0.1 mg/mL) and DHH**S**3 (0.15 mg/mL) show monodispersity of protein solution.

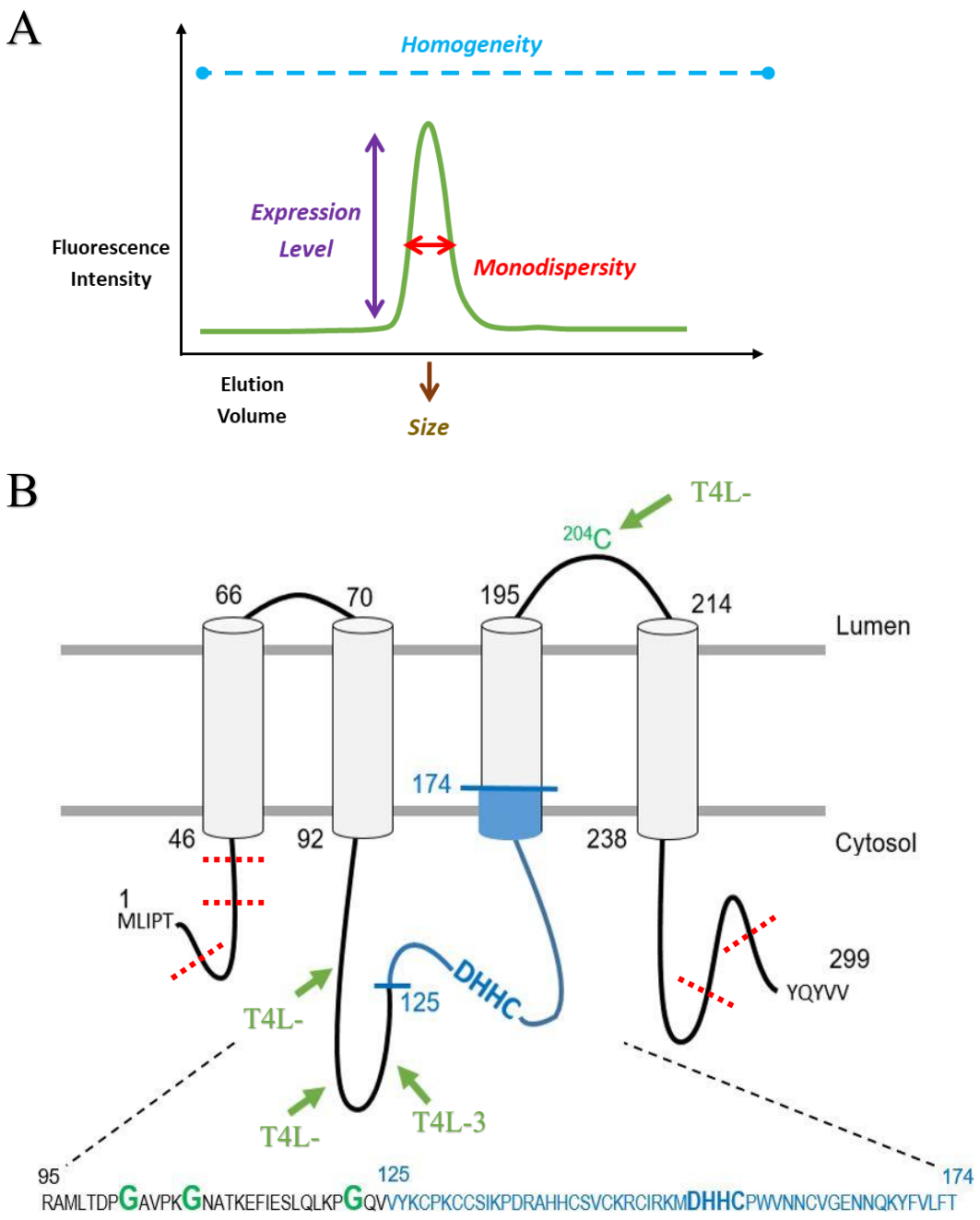

Figure 2.2 FSEC screening of truncated and T4 lysozyme-fused DHHS3 constructs.

A. FSEC profiles are evaluated by the homogeneity, expression level, monodispersity, and size of the protein peaks.

B. Topology of the DHHC3 enzyme showing the four TMDs and the DHHC-CRD domain (marked blue) between TMD2 and TMD3. Truncations (marked by red dashed lines) were made in both the N- and the C-termini of the DHH**S**3 version of the enzyme. T4 lysozyme was inserted internally in 4 different parts of DHH**S**3 (marked by green arrows).

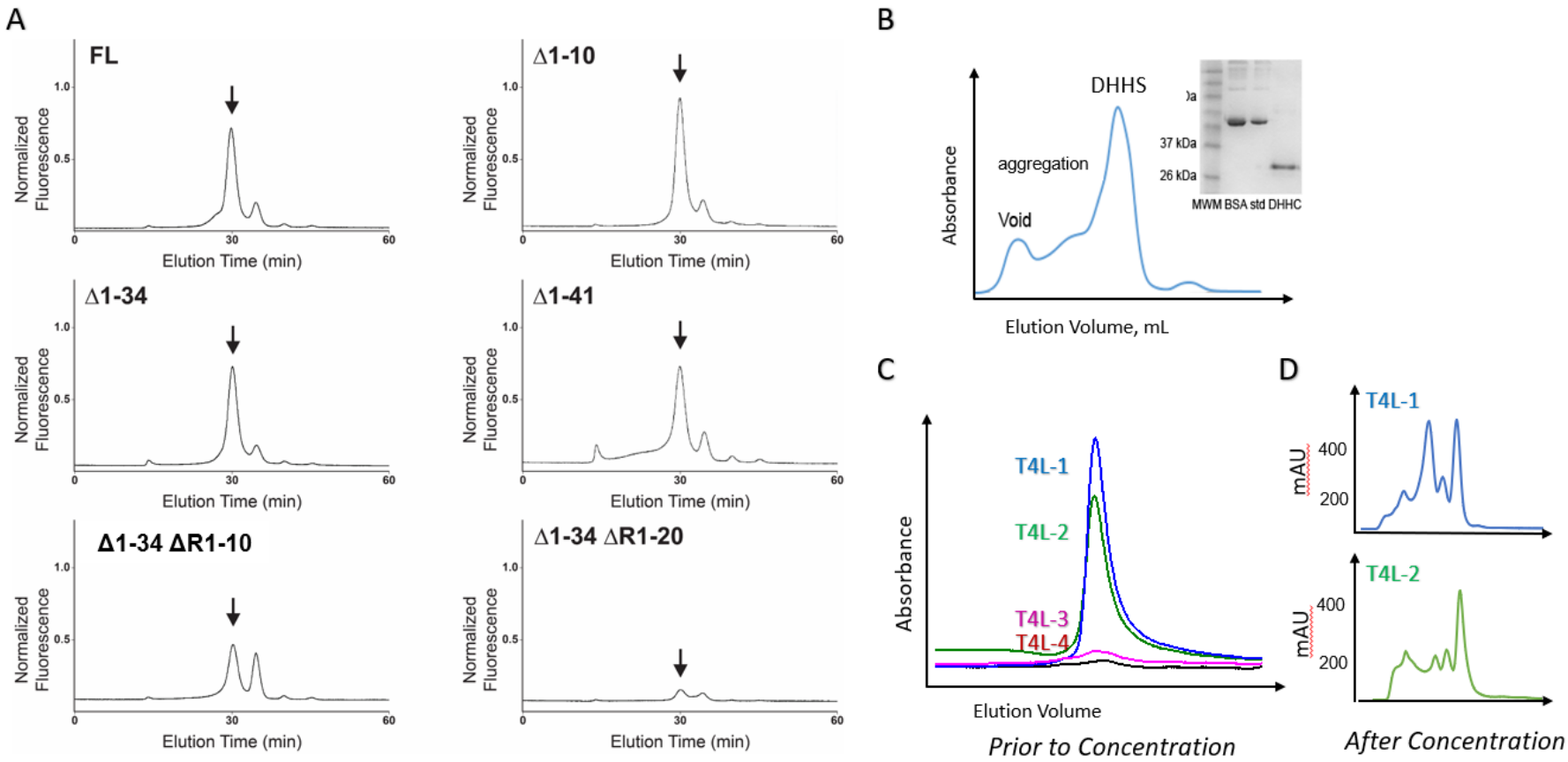

Figure 2.3 Truncated and lysozyme-fused mDHHS3 constructs aggregate at concentrations higher than 1 mg/mL.

A. FSEC traces of WT and truncated *m*DHH**S**3-GFP constructs. Δ1-10 means removing the first 10 amino acids in the N-terminus. ΔR1-20 means removing the last 20 amino acids of the C-terminus. The *m*DHH**S**3 Δ1-34 construct gave the best-looking profile.
B. SEC trace and Coomassie-stained gel of purified *m*DHH**S**3 Δ1-34 upon concentration to 1 mg/mL.
C. SEC traces of T4-lysozyme-fused *m*DHH**S**3 constructs.
D. SEC traces of purified T4L-1 and T4L-2 *m*DHH**S**3 fusion constructs after concentrating to 1 mg/mL.

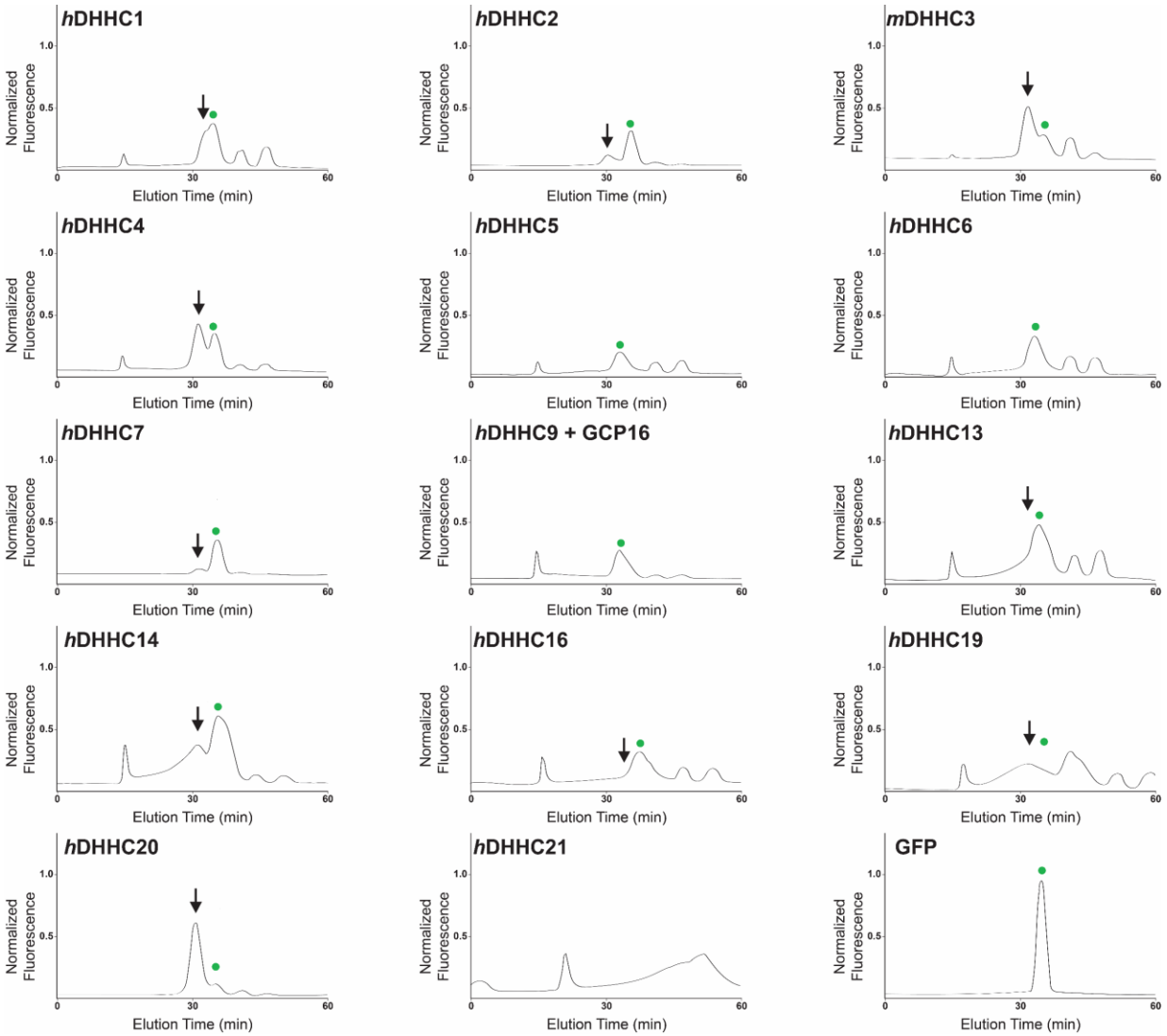

Figure 2.4 DHHC screening by FSEC.

Black arrow points to the DHHC peak and the green dot to the GFP peak in each chromatogram.

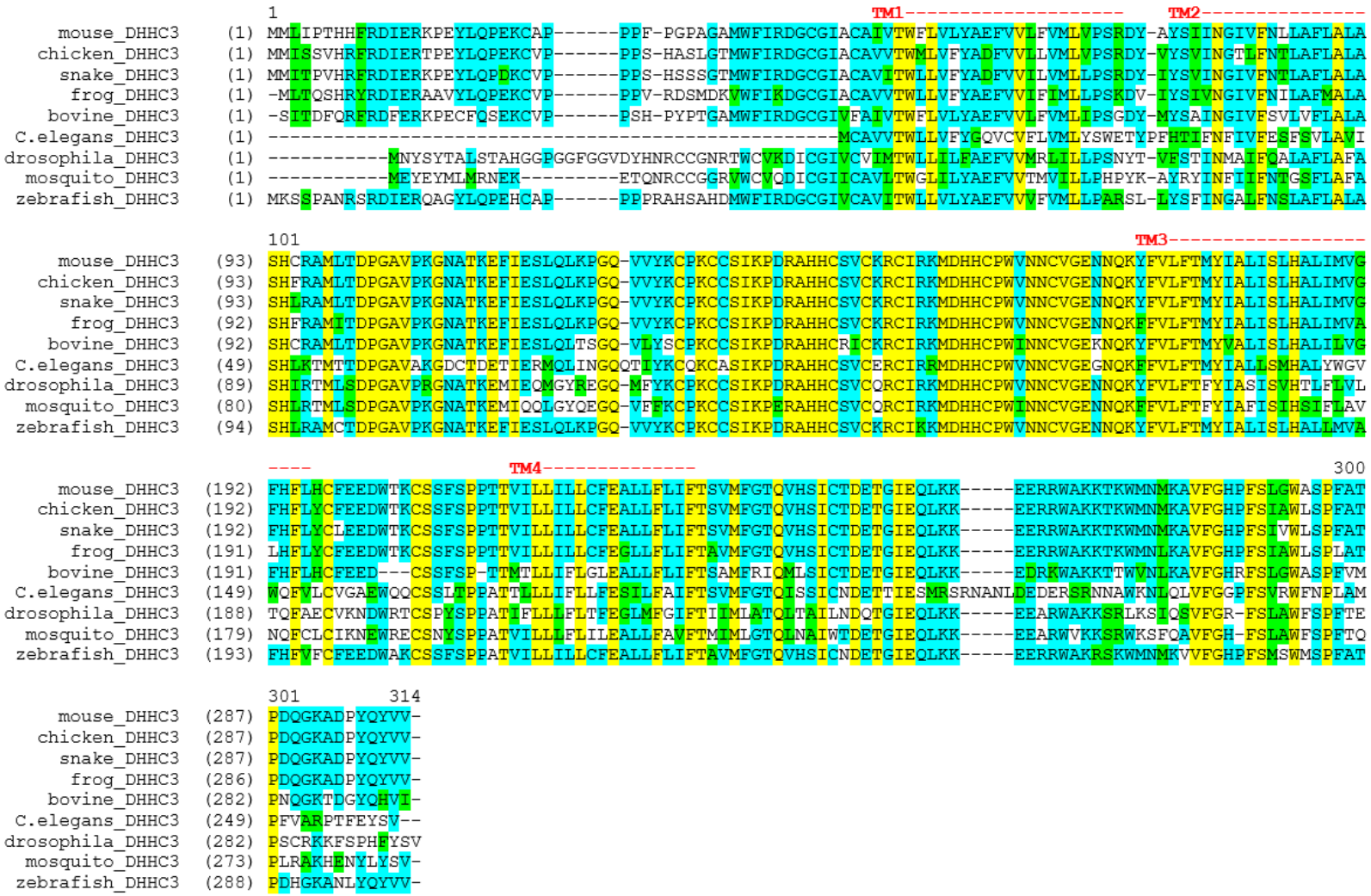

Figure 2.5 DHHC3 ortholog alignment.

Aligned using the Vector-NTI software. Sequence identity to *mouse* DHHC3 are as follows: *Chicken* –90%, *Snake* – 90%, *Frog* – 78%, *Bovine* – 81%, *C. elegans* – 57%, *Drosophila* – 61%, *Mosquito* – 57%, *Zebrafish* – 83%. Yellow marks conserved residues, blue marks very similar residues, green marks, slightly similar residues.

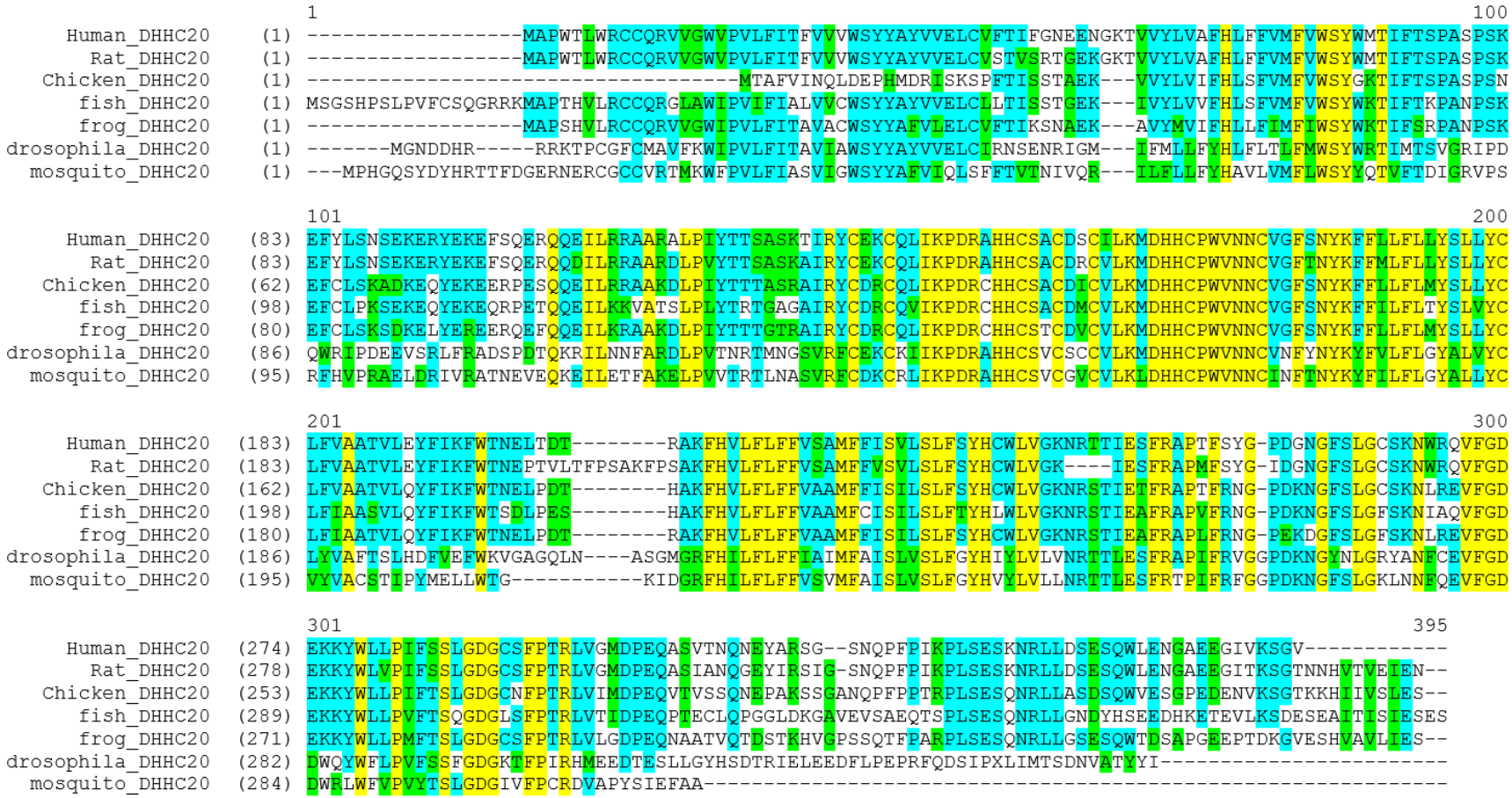

Figure 2.6 DHHC20 ortholog alignment.

Aligned using the Vector-NTI software. Sequence identity to *human* DHHC20 are as follows: *Rat* – 92%, *Chicken* – 74%, *Fish* – 66%, *Frog* – 73%, *Drosophila* – 46%, *Mosquito* – 48%. Yellow marks conserved residues, blue marks very similar residues, green marks, slightly similar residues.

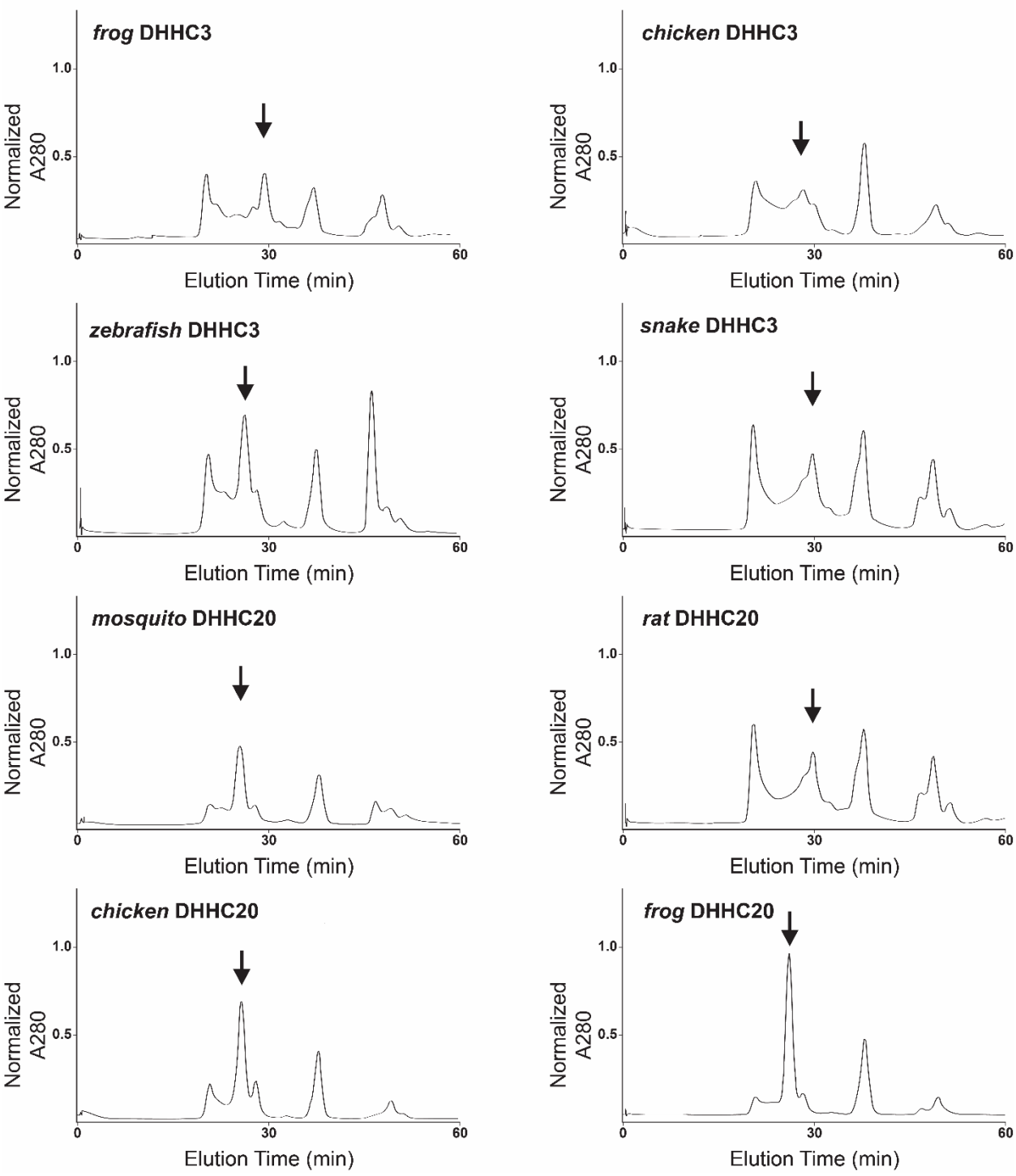

Figure 2.7 DHHC3 and DHHC20 ortholog screening by SEC.

Black arrows point to the DHHC peak in each chromatogram.

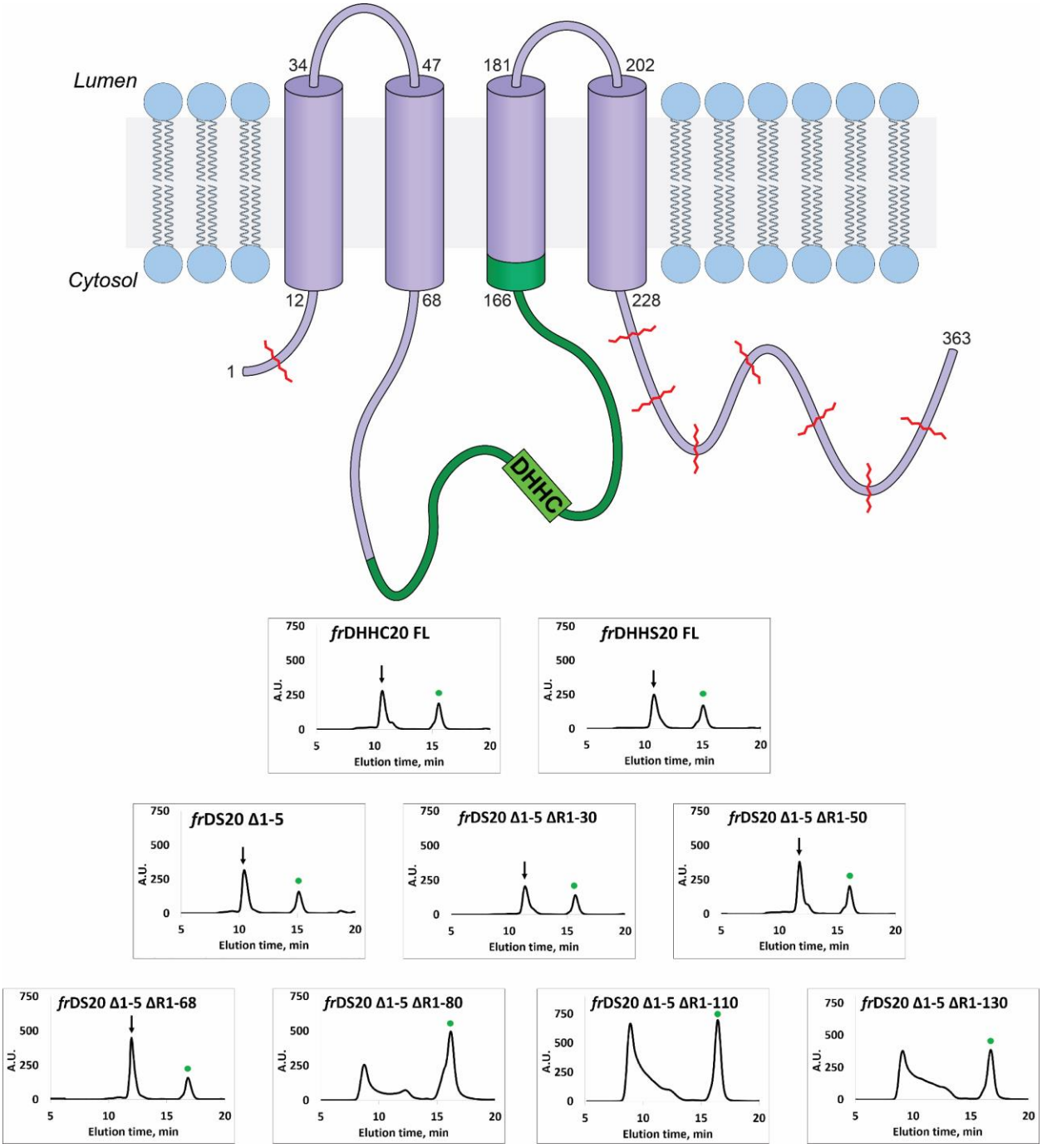

Figure 2.8 Screening truncations of frDHHS20 by SEC.

A. Sequence topology of FL *fr*DHHC20 (aa 1-363). The N- and C-terminal truncations included in the experiment are marked by red squiggly lines. The DHHC-CRD is marked green.

B. SEC traces of purified FL and truncated *fr*DHHC/**S**20 constructs. Black arrows point to the DHHC peak and green dots to the GFP peak in each chromatogram. Δ1-5 means removing the first five amino acids from the N-terminus. ΔR1-30 means removing 30 amino acids from the C-terminal tail. D**S** indicates DHH**S**.

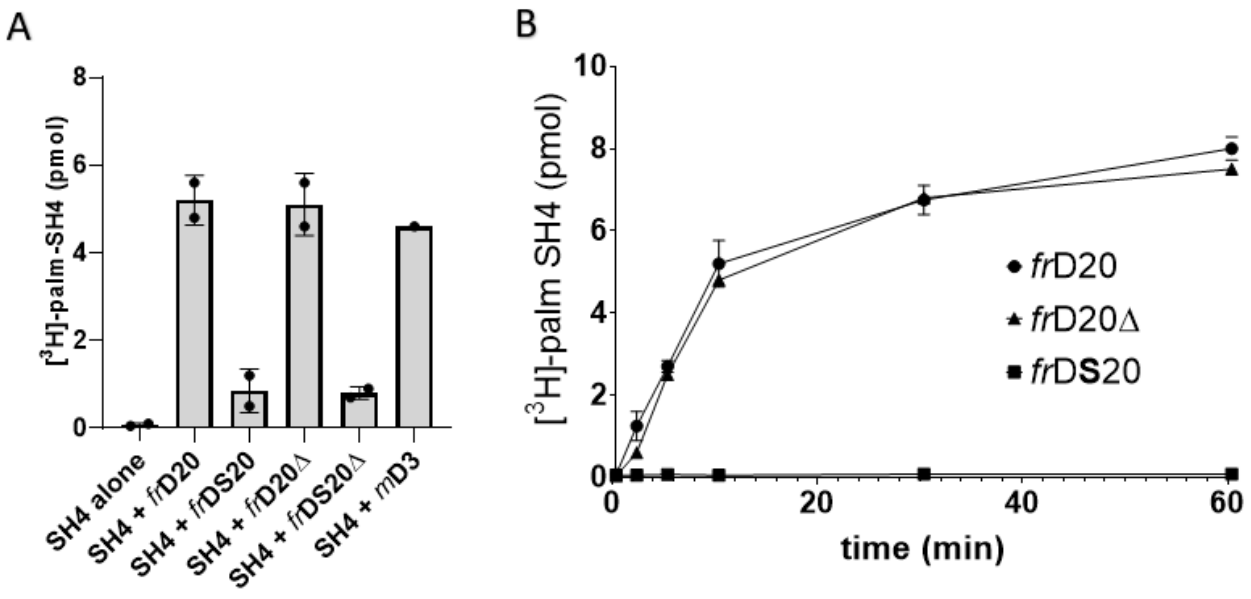

Figure 2.9 Functional characterization of frDHHC20 enzymes.

A. The activity of purified *fr*DHHC20 constructs was evaluated by combining 30 nM enzyme with 1 µM [^{3}H]-palmitoyl CoA and 1 µM myristoylated SH4-GFP substrate. For a single time-point assay, the PAT reaction was run for 10 min at room temperature. [^{3}H]-palmitate transferred to SH4 was then measured by liquid scintillation counting. *fr*D20 corresponds to FL *fr*DHHC20 enzyme. frD**S**20Δ corresponds to *fr*DHH**S**20 Δ1-5 ΔR1-68 (n=2).

B. Time-course PAT activity of *fr*DHHC20 constructs using SH4-GFP as a substrate (n=2).

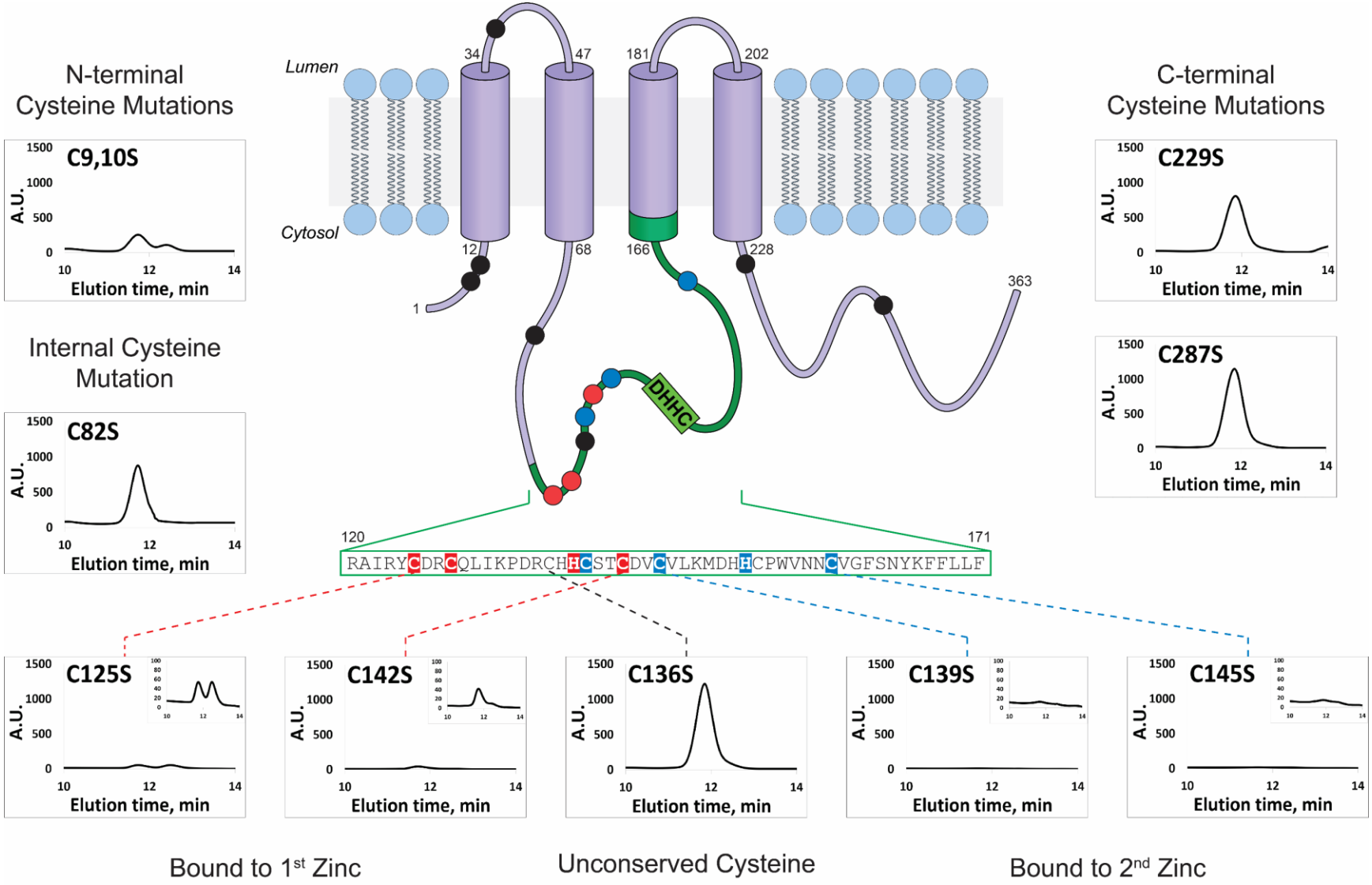

Figure 2.10 Mutagenic studies on the cysteine residues in frDHHS20 Δ1-5 ΔR1-68.

The arrows indicate the peak corresponding to the DHHC enzyme in each chromatogram.

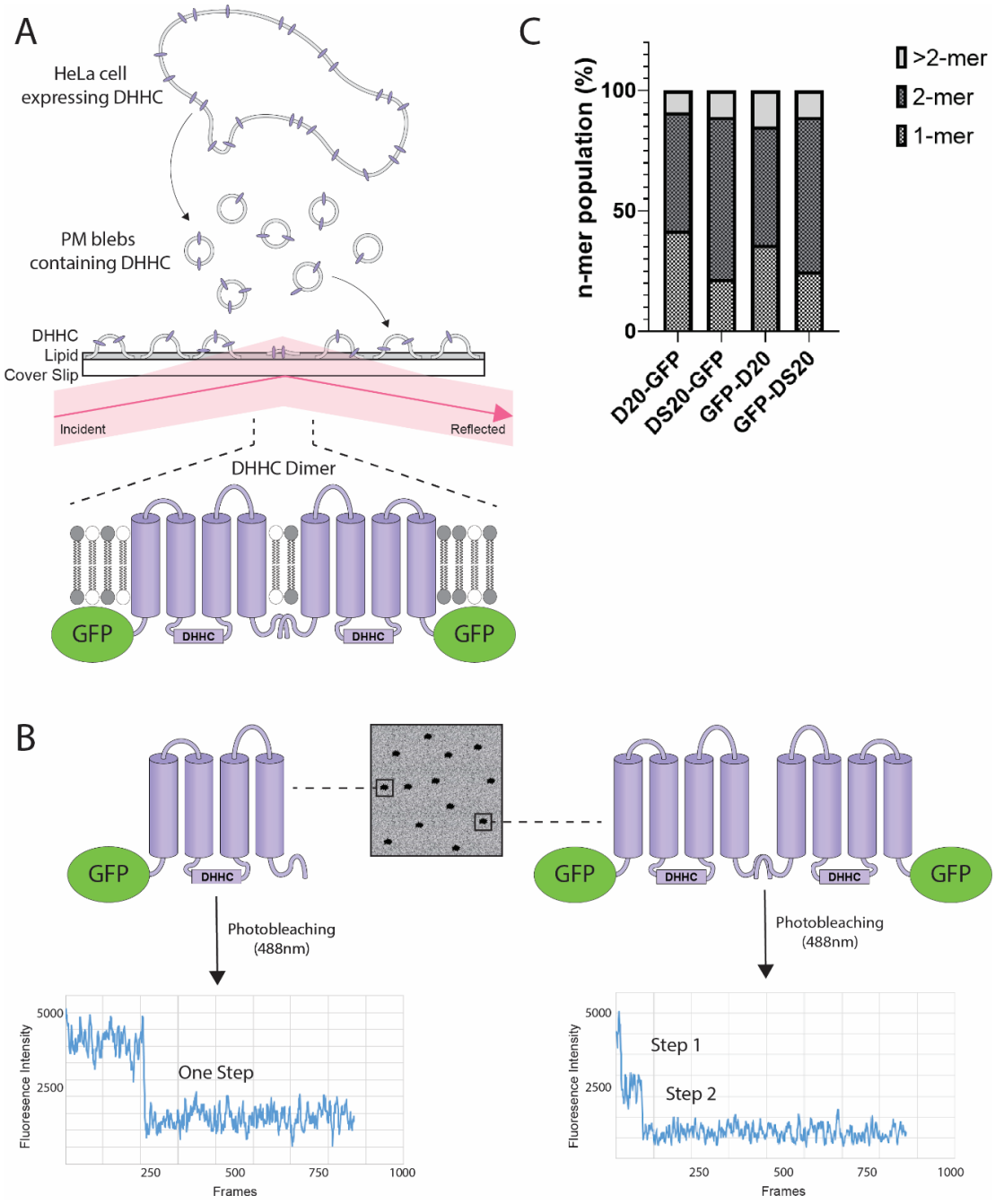

Figure 2.11 Counting the oligomeric states of DHHC proteins by TIRF microscopy.

A. Methodology of TIRF microscopy. TIRF provides a means to selectively excite fluorophores near an adherent surface (100 nm) while minimizing fluorescence from intracellular regions.
B. A fluorescent spot caused by a monomeric DHHC results in a single photobleaching event, while that of a dimeric DHHC results to a distinctly two-step photobleaching event.
C. Oligomeric populations of N- and C-terminally GFP-tagged human DHHC20 (D20), the catalytically inactive *human* DHH**S**20 (DS20), and C-terminally GFP-tagged DHHC2 (D2).

CHAPTER 3: CHARACTERIZATION OF THE PALMITOYLATION AND THE ACYL COA HYDROLASE ACTIVITY OF METALLO-β-LACTAMASE DOMAIN-CONTAINING PROTEIN 2 (MBLAC2)

INTRODUCTION

Protein S-palmitoylation refers to the post-translational addition of palmitate or other long-chain fatty acids to cysteine residues of a protein. In general, the palmitate moiety serves as a membrane anchor for proteins that lack transmembrane domains. Functionally, palmitoylation regulates the trafficking, stability, and activity of many peripheral and integral membrane proteins. To date, over 10,000 palmitoylated proteins have been catalogued in the SwissPalm palmitoylation database [123]. It is estimated that over 1,200 human genes (10% of the human genome) encode for palmitoylated proteins [151]. A substantial fraction of these proteins has been functionally characterized and implicated in the pathogenesis of a variety of human diseases, including disorders in the nervous system, cancer, and aberrant cellular metabolic processes. However, the biological relevance of many other palmitoylated proteins has yet to be uncovered, as is the case of the uncharacterized protein metallo-β-lactamase domain-containing protein 2 (MBLAC2).

When I started studying the MBLAC2 protein, very little information about the protein was known. There were no published structures nor any biochemical studies of the enzyme. Evidence for the palmitoylation of the human ortholog of MBLAC2 exists in 8 out of 17 published proteomic studies utilizing various biochemical techniques in several cell types (e.g. platelets, B-cells, HEK-293 cells) [123]. However, MBLAC2 palmitoylation has not been validated, nor its palmitoylation site/s mapped.

Furthermore, the palmitoyl transferase enzymes that catalyze MBLAC2 palmitoylation have not been identified. Recently, a comprehensive human interactome screen using affinity purification–mass spectrometry (APMS) showed an interaction between MBLAC2 (bait) and the palmitoyl transferase DHHC20 (hit) in total cell lysates of HEK-293 cells, suggesting that MBLAC2 is a potential substrate of DHHC20 [152]. In the first part of this chapter, I describe my examination of MBLAC2 palmitoylation and its relationship with the DHHC20 enzyme, both in cells and *in vitro*.

Structurally informed sequence analysis reveals that MBLAC2 belongs to the metallo-β-lactamase (MBL) superfamily of enzymes characterized by a highly conserved αββα fold. The MBL fold was first observed in prokaryotic enzymes that initiate the hydrolysis and inactivation of common β-lactam antibiotics but is now recognized to be widespread in biology. Of the 34,000 MBL-fold enzymes, only about 1,000 retain the classical antibiotic resistance activity as β-lactamases. The remaining enzymes have been implicated in various biological processes such as cell detoxification pathways, metabolism, and nucleic acid modifications [153], highlighting the prevalence and versatility of the MBL-fold domain in supporting a variety of enzymatic reactions.

The 18 known human MBL-fold proteins exhibit diverse sequences with as little as 25% identity between some enzymes [154]. Phylogenetic analyses cluster these proteins into three groups (Figure 3.1). Group 1 includes MBLAC2 and six other proteins. To date, four Group 1 MBL-fold proteins have been assigned a biochemical function: hydroxyacylglutathione hydrolase (HAGH), commonly called glyoxalase II, catalyzes a key step in the detoxification of 2-oxoaldehydes [155], ethylmalonic encephalopathy protein 1 (ETHE1) metabolizes the toxic H_2S gas in the mitochondria [156], β-lactamase-like protein 2 (LACTB2) acts as a mitochondrial endonuclease [157], and metallo-β-lactamase domain-containing protein 1 (MBLAC1) serves as a specific, high-affinity target for the glutamate transporter inducer, ceftriaxone [158]. The biochemical functions of MBLAC2, HAGHL, and

PNKD proteins are still unknown. The remaining members of the human MBL family also display diverse biological functions. For example, the survival motor neuron 1 (SNM1 A, B, and C) and cleavage stimulatory factor 73 (CSF73) proteins are involved in DNA repair pathways and RNA processing [153]. These enzymes contain an additional β-CPSF-Artemis-SNM1-Pso2 (β-CASP) domain, which along with the MBL-fold domain is important in nucleic acid binding and nuclease catalysis [159, 160].

In the second part of this chapter, I report how I characterized biochemically the hydrolytic activity of MBLAC2 using purified enzyme and a variety of small molecule and protein substrates. My results indicate that the MBLAC2 protein displays robust fatty acyl CoA thioesterase activity with a clear acyl chain length selectivity. Lastly, I identified key residues within the predicted zinc-binding active site in the MBL-fold domain of MBLAC2 that are necessary for the catalytic activity of the enzyme.

RESULTS

CHARACTERIZATION OF MBLAC2 PALMITOYLATION

MBLAC2 is palmitoylated at Cys–254

The SwissPalm palmitoylation database annotates MBLAC2 as a predicted palmitoylated protein, but the exact site/s of palmitoylation is/are unknown. Sequence alignment of human MBLAC2 and its orthologs shows three highly-conserved cysteines in its amino acid sequence that could potentially undergo palmitoylation: Cys–176, Cys–212, and Cys–254 (Figure 3.2A). To identify which of these cysteines is/are palmitoylated, I created N-terminally GFP-tagged constructs of the wild-type and of the individual cysteine mutants of MBLAC2 and expressed them in HEK-293 cells. A fifth construct containing a triple cysteine mutant was included in the experiment to assess any non-

specific signal. Using click chemistry, I measured the palmitoylation levels of each of these constructs (Figure 3.2B). The significant reduction in the 17-ODYA labeling of the C254A mutant indicated that Cys–254 is the main site of palmitoylation. Mutation of either Cys–176 or Cys–212 into an alanine residue did not affect the palmitoylation level of MBLAC2 (Figure 3.2C). To exclude the possibility of lysine-linked palmitoylation, I performed hydroxylamine (HA) treatment and showed that the palmitoylation of MBLAC2 is HA sensitive, indicating a legitimate thioester-linked MBLAC2 palmitoylation (Figure 3.2D).

DHHC20 increases the palmitoylation of MBLAC2 in HEK-293 cells and in vitro.

I then investigated if the observed palmitoylation in MBLAC2 was catalyzed by the DHHC enzymes, a family of palmitoyl transferases responsible for the palmitoylation of protein substrates in humans. An interactome screen in HEK-293 cells reported that MBLAC2 interacts with DHHC20, a prominent member of the DHHC family [152]. I validated this interaction by showing that N-terminally FLAG-tagged MBLAC2 consistently pulled down C-terminally GFP-tagged DHHC20 when the two proteins were co-expressed in HEK-293 cells and the MBLAC2 protein was purified by FLAG immunoprecipitation (Figure 3.3A,B). Interestingly, this interaction remained even when the palmitoylated cysteine in MBLAC2 was removed. Moreover, wild-type MBLAC2 could pull down DHH**S**20, in which the catalytically active cysteine of the DHHC20 is mutated into a serine residue. Together, these results suggest that the palmitoylation process is not crucial for the interaction of MBLAC2 with DHHC20.

Notably, the co-expression of FLAG-MBLAC2 with DHHC20-GFP, but not with DHH**S**20-GFP in HEK-293 cells resulted in roughly a threefold increase in the palmitoylation level of wild-type MBLAC2

(Figure 3.3C). As expected, the palmitoylation level of MBLAC2 C254A remained at background level and was not affected by co-expression with DHHC20-GFP. Interestingly, co-expression of FLAG-MBLAC2 with either DHHC2-GFP or DHHC3-GFP resulted in a minimal or no increase in MBLAC2 palmitoylation. Using purified enzyme preparations, I found that DHHC20, but not DHH**S**20 palmitoylated wild-type MBLAC2 *in vitro*, confirming that MBLAC2 is a DHHC20 substrate (Figure 3.4). Mutation of Cys–254, but not Cys–176 or Cys–212 significantly diminished DHHC20-mediated palmitoylation of the MBLAC2 protein, providing further support that Cys–254 is the relevant palmitoylation site. My *in vitro* results are consistent with MBLAC2 being a substrate of DHHC20, but it cannot be ruled out that other DHHC enzymes might also have palmitoyl transferase activity towards MBLAC2.

Palmitoylation does not affect the membrane localization of MBLAC2 by subcellular fractionation

In many cases, palmitoylation facilitates a controlled association of a soluble protein with a lipid membrane. In order to assess the relevance of palmitoylation in the membrane association of MBLAC2, I performed subcellular fractionation on HEK-293 cells transiently transfected with MBLAC2. Both the wild-type MBLAC2 and its palmitoylation deficient mutant, C254A showed a higher distribution in the membrane fraction than the soluble fraction (Figure 3.5A,B). The similar subcellular distribution pattern suggests that a different structural feature may play a role in the membrane localization of MBLAC2. I then asked if palmitoylation affects the organelle localization. I expressed N-terminally FLAG-tagged wild-type MBLAC2 and its C254A mutant in human bone osteosarcoma epithelial (U2OS) cells and visualized the fixed cells by immunofluorescence. My results suggest that both wild-type and palmitoylation-deficient MBLAC2 proteins are enriched in various

endomembranes (Figure 3.5C); however, the exact organelle of residency for either enzyme remains unclear.

CHARACTERIZATION OF THE BIOCHEMICAL FUNCTION OF MBLAC2

Expression and Purification of MBLAC2

After characterizing the palmitoylation of MBLAC2, I proceeded to discover the biological function of the enzyme using a biochemical approach. To study the activity of MBLAC2 *in vitro*, I made purified protein preparations of the MBLAC2 enzyme. MBL proteins used in activity assays are typically purified from bacterial cell cultures. However, the presence of palmitoylation in MBLAC2 necessitates its preparation in a mammalian expression system with the machinery for post-translational modifications. Indeed, my MBLAC2 preparations in an *E. coli* system resulted in a highly insoluble protein (data not shown). I then engineered a recombinant baculovirus of MBLAC2 that included a hexahistidine tag in the N-terminus and a FLAG epitope in the C-terminus to aid in protein purification. I found that MBLAC2 expressed in *Spodoptera frugiperda* (Sf9) insect cells and extracted using the nonionic detergent dodecylmaltoside (DDM) was highly purified after successive Ni-affinity and a FLAG-affinity purifications (Figure 3.6). By measuring the specific activity as an acyl CoA hydrolase in each step of the purification, I discovered that a two-step purification was necessary to remove contaminating hydrolases. This information proved critical in my subsequent analysis of the hydrolase activity of MBLAC2 towards various substrates.

MBLAC2 shows little to no hydrolase activity towards various small molecule substrates of related MBL-fold enzymes

MBLAC2 phylogenetically belongs to the human MBL-fold family of enzymes. Several members of this enzyme family have already been characterized and shown to exhibit hydrolase activity towards a diverse set of functional groups such as amides, esters, and thioesters. I initially tested the ability of MBLAC2 to hydrolyze two small molecules already known to be substrates of some related MBL-fold proteins: nitrocefin, a cephalosporin β-lactam antibiotic substrate routinely used to detect β-lactamase activity in microbes, and S-D-lactoyl glutathione, the physiological intermediate in the metabolism of various toxic aldehydes by the glyoxalase II enzyme. These substrates contain an amide and a thioester functional group, respectively, which can potentially be hydrolyzed by MBLAC2. In addition, because of the recently discovered association of human MBLAC1 with glutamate transport [158], I tested if MBLAC2 could hydrolyze the amide-containing small molecule glutamine (Figure 3.7A).

My purified preparations of MBLAC2 showed little to no hydrolase activity towards all the substrates tested (Figure 3.7). Recently, Smith et.al. reported that MBLAC2 has β-lactamase activity towards nitrocefin, a common β-lactam antibiotic. However, the kinetic values reported (kcat - 0.0004 s^{-1}, Km - 370 μM) were significantly lower compared to other established β-lactamases [161]. Although I could detect nitrocefin hydrolase activity in the Ni pool of MBLAC2, this activity was lost upon further purification by FLAG resin. Thus, I am not able to confirm that MBLAC2 has β-lactamase activity. I also did not observe MBLAC2 hydrolase activity towards S-D-lactoyl glutathione and glutamine.

MBLAC2 shows little to no hydrolase activity towards various palmitoylated protein substrates

My palmitoylation studies annotate MBLAC2 as the first human MBL-fold protein confirmed to undergo palmitoylation. Notably, none of the other 17 human MBL-fold proteins are predicted to be palmitoylated in the SwissPalm database [123], hinting at a somewhat unique role for MBLAC2. Interestingly, known protein depalmitoylases, acyl protein thioesterase 1 (APT1) and the α/β hydrolase domain protein 17 (ABHD17) are themselves palmitoylated proteins. Because of the association of MBLAC2 with palmitoylation, I decided to test whether MBLAC2's predicted hydrolase activity acts on palmitoylated proteins. I tested two palmitoylated protein substrates: the small G protein HRas that contains two palmitoylated cysteines, and the N-myristoylated SH4-GFP fusion protein, a model palmitoylation substrate that contains three cysteine residues. MBLAC2 did not show protein thioesterase activity towards SH4 radiolabeled with [^{3}H]-palmitate. In addition, MBLAC2 was only able to remove palmitate from HRas labeled with a palmitate analog at high enzyme concentration (1 μM range), suggesting that the reaction was not catalytic (Figure 3.8).

MBLAC2 exhibits acyl CoA thioesterase activity similar to Type I ACOTs

The lack of a conclusive hydrolase activity of MBLAC2 towards palmitoylated protein substrates prompted me to take a step back and look at other small molecules that also contain palmitate. It has long been appreciated that DHHC palmitoyl transferases typically use palmitoyl Coenzyme A (CoA), a 16-C fatty acyl CoA, as a donor for palmitate during the enzymatic palmitoylation of protein substrates both *in vitro* and in cells [28, 30]. Palmitoyl CoA is a fatty acyl molecule that contains a palmitate via a thioester linkage, and hence can potentially be hydrolyzed by the MBLAC2 enzyme. To test this, I incubated purified MBLAC2 with [^{3}H]-palmitoyl CoA. Following hydrolysis of the substrate, I extracted the [^{3}H]-palmitate released from the [^{3}H]-palmitoyl CoA and purified it by

solvent extraction with heptane. The extracted organic layer was then assayed for [^{3}H]-palmitic acid radioactivity using a scintillation counter. From this assay, I found that the MBLAC2 protein displayed robust thioesterase activity towards palmitoyl CoA (Figure 3.9A).

I investigated whether palmitoylation has an influence on the palmitoyl CoA hydrolase activity of MBLAC2. My results show that palmitoylation does not have a major effect the ability on the ability of MBLAC2 to act as an acyl CoA hydrolase *in vitro* (Figure 3.9B). The measured kinetic parameters showed only a slight reduction in the Vmax and the Km for the C254A mutant compared to wild-type MBLAC2 (Figure 3.9C). A limitation of my study is that the stoichiometry of palmitoylation of the purified wild-type MBLAC2 protein is unknown. It is possible that in the context of intact cells, palmitoylation may help increase the affinity of MBLAC2 in the membrane where it can access membrane-embedded acyl CoA molecules.

In the literature, thioesterase activity towards palmitoyl CoA and other fatty acyl CoA molecules has been largely attributed to a family of enzymes called acyl Coenzyme A thioesterases (ACOTs). In contrast to generic thioester hydrolases that cleave the thioester bond between a sulfur atom and carbonyl, most ACOTs specifically act on molecular substrates that contain CoA. There are two general types of ACOTs characterized by their response to peroxisome proliferator treatment and the fold of the catalytic active site. The kinetic parameters I measured for the palmitoyl CoA hydrolase activity of MBLAC2 are similar to those obtained for type I ACOTs. Members of type I ACOT enzymes are cytosolic thioesterases that contain an α/β-hydrolase domain in the active site. The pioneering member and most highly characterized enzyme in this family is ACOT1. The published kinetic parameters for ACOT1 for palmitoyl CoA (Km = 3.6 μM, Vmax = 600 nmol/min/mg) are comparable to the kinetic parameters I measured for MBLAC2 (Km = 0.6 μM, Vmax = 150 nmol/min/mg) (Figure 3.9C).

Notably, I found that both the wild-type and C254A MBLAC2 proteins are inhibited by high concentrations of palmitoyl CoA (Figure 3.9B). Not surprisingly, this substrate inhibition I observed for MBLAC2 is also seen in type I ACOT proteins. Because of this observation, the kinetic parameters for MBLAC2 were calculated using palmitoyl CoA concentrations between 0-5 μM (Figure 3.9A).

Additionally, ACOT1 has been shown to exhibit substrate selectivity for long chain (C12-C20) saturated and monounsaturated acyl CoAs. I examined if MBLAC2 could also hydrolyze fatty acyl CoA molecules other than palmitoyl CoA. Similar to some DHHC proteins [67, 68], MBLAC2 showed distinct selectivity towards various chain lengths of acyl CoA (Figure 3.10). I tested this by setting up a competition assay in which a 10-fold excess of nonradiolabeled acyl CoAs of various chain lengths and saturations was used to compete with [^{3}H]-palmitoyl CoA for hydrolysis by the MBLAC2 enzyme. The reduction of [^{3}H]-palmitic acid released was presumed to be because the competing nonradiolabeled acyl CoA were hydrolyzed instead. Similar to the acyl CoA substrate selectivity reported for the ACOT1 protein [162], my results showed that MBLAC2 showed preference towards saturated C12-C18 fatty acyl CoAs. Additionally, MBLAC2 also displayed hydrolase activity towards monounsaturated fatty acyl CoAs such as palmitoleoyl CoA (C16:1) and oleoyl CoA (C18:1). Interestingly, this acyl chain length selectivity I measured for MBLAC2 highly parallels that observed for DHHC20 [69].

MBLAC2 contains zinc ions that are important for enzymatic activity

After confirming that MBLAC2 was able to hydrolyze acyl CoAs, I sought to identify key residues that are crucial for this activity. I hypothesized that the mechanism of acyl CoA hydrolysis by MBLAC2 would involve analogous residues observed in the active sites of other MBL enzymes that catalyze the hydrolysis of various small molecule substrates. In many metallo-β-lactamase enzymes,

the active site is determined to be one or two zinc-binding domains, with the zinc playing a role in the catalysis.

Bacterial metallo-β-lactamase enzymes inactivate β-lactam drugs through a non-covalent mechanism in which one or two equivalents of zinc ions in the active site polarize a water molecule to form a nucleophilic hydroxide ion. The activated nucleophile then attacks the electrophilic carbon of the β-lactam ring transforming it into a ring-open product that is no longer active as an antibiotic. Variations in the chemical identity of the zinc coordination shell become the basis of classifying these bacterial MBL enzymes into three subclasses (Figure 3.11). Subclass B1 binds one zinc ion (Zn1) using three histidine residues and a second zinc ion (Zn2) using three different residues (aspartate, cysteine, and histidine). The zinc ligand residues in both the 3-His and Asp-Cys-His sites are strictly conserved among B1 enzymes. Subclass B2 lacks a Zn1 binding site due to a mutation in one of the histidine residues into an asparagine (H116N) but adopts a similar Zn2 site. Lastly, subclass B3 retains a traditional Zn1 binding site using three histidine residues but the Zn2 binding site replaces the cysteine residue with another histidine (H121). The differences in the zinc ion coordination in these three subclasses are reflected in variations in the catalytic properties of the enzymes. For example, B1 and B3 enzymes are most active with two zinc ions while the binding of the second zinc in the B2 enzymes inhibits catalysis [154]. Additionally, B1 and B3 enzymes have a broad-spectrum substrate profile that includes penicillin, cephalosporin, and carbapenem while the B2 enzymes can only hydrolyze carbapenem. While zinc is the most common metal ion found in the active site of these enzymes, some MBL enzymes are able to utilize other divalent metal ions such as iron and manganese [153, 163]. Despite having varied functions outside of β-lactam hydrolysis, the differences in the metal coordination of bacterial MBL family extend to the human proteins. For example, X-ray crystal structures show that both HAGH and LACTB2 proteins harbor two zinc ions in the active site [157,

164], while PNKD and SNM1A proteins contain only one zinc ion [153]. In addition, ETHE1 replaces zinc with iron.

While the structure of MBLAC2 has not been solved, the enzyme is predicted to belong to subclass B3 of MBL enzymes and harbor two zinc ions [1]. Zn1 is predicted to bind His–83, His–85, His–170 and Asp–189 and Zn2 is predicted to bind Asp–87, His–88, Asp–189, and His–231 (Figure 3.12A). I examined the significance of these zinc-binding residues in the catalytic activity of MBLAC2 by generating single point mutations of each of these residues and expressing them HEK-293 cells. Mutations of five of these residues resulted in insoluble protein that could not be further purified and assayed. Mutations D87A and H88A, both of which are Zn2-binding residues, yielded a detergent-extractable protein that was amenable to purification. I found that each of these two mutations significantly decreased the palmitoyl CoA activity of MBLAC2 to background levels. This strongly suggests that the Zn2-binding pocket is crucial for the acyl CoA hydrolase activity of MBLAC2. Notably, none of the Zn1 mutations were tested due to very low protein expression levels and insolubility. To exclude the possibility that the single point mutations caused a gross structural perturbation in the protein, I also tested a few mutations within the vicinity of the Zn2-binding pocket. Both S89A and Y93A mutations showed comparable palmitoyl CoA activities compared to the wild type protein (Figure 3.12B). To further confirm these results, I assayed highly purified protein preparations of the wild-type and D87A MBLAC2 enzymes and observed a similar inactivation of MBLAC2 acyl CoA hydrolase activity for the D87A mutant (Figure 3.13C). This confirms that the Asp-87 residue is required for the catalytic activity of MBLAC2.

DISCUSSION

My study provides the first biochemical characterization of the palmitoylation and the acyl CoA hydrolase activity of the MBLAC2 protein.

MBLAC2 Palmitoylation

Multiple palmitoyl-proteome studies in various cell lines predicted that MBLAC2 is a palmitoylated protein. However, the exact site of MBLAC2 palmitoylation has not been reported. Sequence analysis reveals that MBLAC2 contains three cysteine residues. Using click chemistry techniques in HEK-293 cells and *in vitro* PAT assays using purified enzyme preparations, I successfully mapped the palmitoylation site of MBLAC2 to Cys–254. I then proceeded to examine the relevance of MBLAC2 palmitoylation but did not find any major difference on the membrane association and subcellular localization between the wild-type MBLAC2 and its C254A mutant. While my immunofluorescence experiments suggest that MBLAC2 localizes primarily in endomembranes of U2OS, U87, and HEK cells, I have not characterized the exact organelle residency of MBLAC2 using specific organelle markers. Nevertheless, I found that the mutation of the palmitoylated cysteine does not exclude MBLAC2 from the membranes or cause a pronounced redistribution to another membrane compartment.

The question of what structural feature recruits MBLAC2 to the membrane remains unanswered. Aside from covalently bound lipid modification such as palmitoylation, there are other mechanisms by which a soluble protein can associate with membranes. For example, many proteins rely solely on an amphipathic α-helix in mediating associations with membranes. The non-palmitoylated proteins CTP:phosphocholine cytidylyltransferase (CCT) [165], prostaglandin

endoperoxide H synthases (PGHs 1 and 2) [166, 167], and G protein-coupled receptor kinase 5 (GRK5) [168] associate with the membrane as a result of an interaction between the membrane and an amphipathic patch in the protein. Notably, the helix serves only as a reversible membrane anchor for CCT but facilitates the stable membrane association of PGH and GRK5. A subset of the regulators of G protein signaling (RGS) proteins is another example of how an amphipathic helix can mediate protein-membrane association. Bernstein and Linder identified an amphipathic α-helix within the N-terminal domain of RGS4 to be responsible for membrane targeting [169]. Interestingly, RGS4 is a palmitoylated protein. Similar to my observations for MBLAC2, mutation of the palmitoylated cysteine in RGS4 does not interfere with the membrane association of the protein [170-172].

Secondary structure analysis suggests that a region situated in the C-terminus of MBLAC2 (residues 205-217) constitutes an amphipathic α-helix (Figure 3.13). This helix includes a hydrophobic patch of amino acids on one face of the helix, hydrophilic amino acids on the opposite face, and some basic amino acids. I hypothesize that this predicted helix of MBLAC2 may be the structural feature responsible for the observed membrane enrichment of MBLAC2. The hydrophobic residues in this helix can directly insert into membrane lipids, while the surrounding positively charged basic amino acids might further enhance membrane binding by electrostatic interaction with negatively charged phospholipids. In RGS4, the α-helix membrane targeting domain is both necessary and sufficient for membrane association and palmitoylation is a secondary effect. A similar case may be true for MBLAC2.

I also tested if palmitoylation has a role in the enzymatic activity of MBLAC2. However, I did not see any major change in the acyl CoA hydrolase activity between wild-type MBLAC2 and the C254A mutant. Notably, multiple structure threading programs consistently predict that the palmitoylated C-terminal Cys–254 is situated far away from the αββα MBL fold active site (Figure 3.13). This may

suggest that the palmitoylation and the acyl CoA hydrolase activity of MBLAC2 may exist independently.

Structure-function studies of MBLAC2

Structure-function analysis of the MBLAC2 protein had been greatly limited by the intolerance of the protein to single point mutations and truncations. Most of the protein sequence modifications caused a significantly reduced or highly aggregated protein expression in both HEK-293 and insect cell expression systems. The MBL fold domain in MBLAC2 corresponds to the 29^{th}-231^{st} residues of the 279 residue-long protein, which means bulk of the protein is the MBL fold site (Figure 3.13). This contrasts with the MBLAC1 and HAGH enzymes which both have a much longer C-terminus. In HAGH, the C-terminus is thought to be involved in recruiting its S-D-lactoyl-glutathione substrate, as determined by the crystal structure of the protein. I was not successful in expressing N- and C-terminal deletions of MBLAC2 and hence were unable to determine if the MBL fold domain was sufficient for the activity of the enzyme. This may suggest that the full sequence of MBLAC2 may be important in the over-all folding of the protein.

Similarity of MBLAC2 hydrolase activity to ACOT proteins

To date, thioesterase activity towards palmitoyl CoA and other fatty acyl CoA molecules has been largely attributed to a family of enzymes called acyl Coenzyme A thioesterases (ACOTs). My study identifies MBLAC2 as another enzyme that potentially plays a role in regulating cellular levels of acyl CoAs. When acyl CoAs are hydrolyzed, the thioester bond between the fatty acyl group and the Coenzyme A is broken forming a reduced CoA and a free fatty acid (FFA). FFAs are usually inactive and

require thioesterification into acyl CoAs for proper function. Acyl CoAs are widespread as intermediate substrates in diverse cellular metabolic pathways. These substrates are usually oxidized for energy production or incorporated into a variety of complex lipids [173]. The cycle of esterification and de-esterification of fatty acids serves as a regulatory mechanism for controlled lipid metabolism.

In cells, acyl-CoA binding protein (ACBP) binds long chain acyl CoAs with high affinity and is believed to play an important role in intracellular acyl CoA transport and pool formation. This binding is thought to regulate the function of long chain acyl CoAs as metabolites and regulators of cellular functions. I hypothesize that the hydrolytic activity of MBLAC2 towards acyl CoAs may be another means to control the local pool of acyl CoAs. In addition, it is possible that cellular levels of acyl CoA molecules can influence the activity of certain DHHC proteins. For example, Lai and Linder showed that DHHC3 and DHHC2 form palmitoylation-sensitive oligomers. Addition of palmitoyl CoA shifted the monomer-oligomer equilibrium in favor of the monomeric forms of these enzymes [82]. This effect was not seen in the catalytically inactive DHH**S** mutants of the enzymes. These results may suggest that DHHC protein activity is regulated by the availability of palmitoyl CoA. This hypothesis is supported by results showing that palmitoyl CoA addition to unfractionated bovine brain membrane fractions significantly increased the total amount of palmitoylation *in vitro* [174]. I found that MBLAC2 displays a preference for hydrolyzing longer chain acyl CoAs. This selectivity is remarkably parallel to that of the DHHC20 enzyme [69], suggesting that MBLAC2 may play a role in regulating the pool of acyl CoA available for the DHHC20 enzyme.

Implications and Future Directions

My characterization of the MBLAC2 protein is primarily biochemical, using purified protein preparations to study the properties and catalytic activity of the protein in an *in vitro* system. A future study for this project to understand the physiological relevance of both the palmitoylation and the acyl CoA hydrolase activity that I examined in this study using a biochemical approach.

While I have shown that the DHHC20 enzyme palmitoylates MBLAC2 both in cells and *in vitro*, I would like to verify that DHHC20 is the physiological enzyme of MBLAC2. Our lab has recently obtained DHHC20-knockout HAP1 cells. Measuring the palmitoylation level of MBLAC2 in this cell line will test if DHHC20 is the exclusive palmitoyltransferase for MBLAC2 or if other DHHC enzymes contribute to the palmitoylation of MBLAC2 *in vivo*. However, single knockdown experiments can be confounded by the inherent redundancies that allow for other DHHC enzymes to palmitoylate a protein substrate in the absence of the primary DHHC enzyme. In which case, I will knockdown multiple candidate DHHC proteins to identify the relevant DHHC enzymes.

Despite my kinetic data showing that MBLAC2 is an acyl CoA hydrolase in vitro, it will be crucial to identify if acyl CoA molecules are the physiological substrates of MBLAC2. Recently, Gibson and Blakely attempted to identify the physiological substrates of MBLAC1, another human metallo-β-lactamase enzyme of unknown function [158]. Both MBLAC1 and MBLAC2 belong to Group 1 of the human MBL-fold enzymes that also includes the Glyoxalase II enzyme. Using clustered regularly interspaced short palindromic repeats/CRISPR-associated protein 9 (CRISPR/Cas9) methods, the N-terminal coding sequence of the mouse *Mblac1* gene was disrupted. Afterwards, the serum small molecules responsive to loss of MBLAC1 expression were identified by hydrophilic interaction chromatography (HILIC) based ultra-performance liquid chromatography, coupled to mass spectrometry (UPLC-MS/MS). The study identified small molecules implicated in various metabolic

pathways, including bile acid biosynthesis and linoleate metabolism, pathways that share cell-protective actions in the face of metabolic and oxidative cellular stress [175]. MBLAC1 was initially identified as a specific, high-specific target for the glutamate transport inducer, ceftriaxone [158]. While it was hypothesized that ceftriaxone can potentially target MBLAC2 because of folding similarity and close phylogenetic relationship between MBLAC1 and MBLAC2, I did not find any evidence of Ceftriaxone binding to MBLAC2 (data not shown).

My studies of the MBLAC2 protein engender a better understanding of this previously uncharacterized protein. My findings are relevant in both the fields of palmitoylation and of the human MBL-fold enzymes. I demonstrated that MBLAC2 is a substrate for the DHHC20 palmitoyl transferase enzyme. MBLAC2 is unique among other human MBL enzymes because of its palmitoylation. I mapped the palmitoylation site in the protein and determined that the palmitoylated cysteine has little to no effect in the membrane distribution, subcellular localization, and enzymatic activity of MBLAC2. In addition, my study found a biochemical function for MBLAC2 as a robust acyl CoA thioesterase. My study adds to previous investigations demonstrating the versatility of the MBL-fold domain in supporting a variety of enzymatic reactions.

EXPERIMENTAL PROCEDURES

Reagents – Anti-FLAG® M2 affinity gel was purchased from Strategene. A 1000x polyethylenimine (PEI) transfection reagent (Sigma) was made in water. A 1000x protease inhibitor cocktail of 5 mg/mL leupeptin (Sigma-Aldrich, St. Louis, MO), 3 mg/mL aprotinin (Sigma), 1 M PMSF (MP Biomedicals, LLC, Solon, OH) and 1 mM pepstatin A (Amresco, Solon, OH) was mixed from individual components. Alexa-

flour®647 azide was purchased from Invitrogen (San Diego, CA). [^{3}H]-palmitoyl CoA was synthesized as previously described [82]. HEK-293 cells were cultured in DMEM (Gibco) media with 10% fetal bovine serum (Life Technologies). Cell were maintained at 37^{o}C in a humidified incubator supplemented with 5% CO_2.

Two-step Affinity Purification of MBLAC2 enzymes – MBLAC2 constructs were made using Bac-to-Bac baculovirus insect-cell expression system and expressed in Sf9 cells similar to the purification of DHHC enzymes [149]. Purified proteins were concentrated using Amicon® Ultra filter units (Millipore-sigma).

Protein Acyl Transferase (PAT) Assay – Purified DHHC20 enzyme (50 nM) was assayed in a 50 µL reaction with [^{3}H]-palmitoyl CoA (1 µM) and MBLAC2 (1 µM) at 25 °C for 0-30 min. The reaction was stopped with the addition of 5X sample buffer containing 10 mM TCEP and resolved on a Coomassie-stained gel. The substrate bands in the gel were excised, cut into 1 mm cubes and combined with 500 µL Soluene 500 (Perkin-Elmer, Waltham, MA). The excised bands were then heated at 37 °C overnight before being combined with 4.5 mL of Ultima Gold scintillation fluid (Perkin-Elmer) and counted in a scintillation counter.

Co-immunoprecipitation – MBLAC2 and DHHC constructs used in the experiment were cloned into the pCMV5-FLAG or pCGFP-EU2 vectors to include an N-terminal FLAG epitope or a C-terminal GFP tag respectively. The day before transfection, HEK-293 cells were plated onto a 10-cm plate at 40-50% confluency. The cells were incubated overnight at 37 °C. The next day, the cells were transfected with 3 ug each of DNA constructs and 18 ug of PEI transfection reagent. After 48 h, the DMEM media was

aspirated, and the cells were suspended and washed with 2 mL of ice-cold PBS. The cells were then disrupted in lysis buffers containing (50 mM Tris pH 7.4, 200 mM NaCl, 1% DDM, 10% glycerol, 1 mM TCEP and protease inhibitors (0.5 ug/mL leupeptin, 3 ug/mL aprotinin and 0.3 ug/mL pepstatin A). Cleared lysate was then centrifuged at 100,000 xg for 40 min. The soluble fraction was incubated with pre-equilibrated FLAG resin for 1 h. The resin was washed with 10 x column volumes of wash buffer containing 100 mM Tris HCl, pH 7.4, 150 mM NaCl, 0.5 mM DDM and 0.5 mM TCEP. The FLAG-tagged proteins were then eluted with elution buffer containing 100 mM Tris HCl, pH 7.4, 150 mM NaCl, 100 ug/mL 3xFLAG peptide, 0.5 mM TCEP and 0.5 mM DDM.

Detection of Palmitoylation in Cells by Click Chemistry – HEK-293 cells transfected with MBLAC2 DNA were cultured in DMEM with 10% FBS for 42 h. Cells were then incubated in DMEM containing 10% dialyzed FBS and 100 µM 17-ODYA for 6 h. Cells were washed with phosphate-buffered saline (PBS) and lysed with RIPA buffer (20 mM HEPES-NaOH [pH 7.4], 100 mM NaCl, 3 mM $MgCl_2$, 1% NP-40, 0.5% deoxycholate, and 0.1% SDS) supplemented with protease inhibitors (0.5 ug/mL leupeptin, 3 ug/mL aprotinin and 0.3 ug/mL pepstatin A). Cleared lysates were immunoprecipitated with anti-FLAG resin for 4 h. The FLAG immunoprecipitates were washed 3 times with RIPA buffer and suspended in 90 µL of PBS, and 10 µL of freshly premixed click chemistry reagent (final concentrations of 10 µM Alexa Fluor 647-azide, 1 mM tris(2-carboxyethyl)phosphine (TCEP), 100 µM tris[(1-benzyl-1H-1,2,3-triazol-4-yl)methyl]amine (TBTA), and 1 mM $CuSO_4$) was added. After 1 h at room temperature, the immunoprecipitates were washed twice with PBS containing and treated with sample buffer for SDS-PAGE. Probe-labeled proteins were detected by in-gel fluorescence. Relative protein amounts were compared by Western Blot.

Subcellular Fractionation **–** HEK-293 cells transfected with either FLAG epitope or GFP tag were washed in PBS and pelleted for resuspension in a digitonin buffer (150 mM NaCl, 50 mM HEPES, 200 µg/mL digitonin) for 10 min while rotating. Lysate was then spun at 2000 x g, and resultant supernatant was kept (cytosolic fraction). The remaining pellet was resuspended in an NP40 buffer (150 mM NaCl, 50 mM HEPES, 1% NP40), and lysate was left on ice in NP40 buffer for 30 min and then centrifuged at 7000 xg. The resultant supernatant was kept for membrane and organelle fraction, whereas the pellet was resuspended in RIPA buffer (150 mM NaCl, 50 mM HEPES, 0.5% Na-deoxycholate, 0.1% SDS) and rotated for 1 h at 4 °C then centrifuged for 10 min at 7000 x g. The supernatant was kept for nuclear protein fraction. Each fraction was then subjected to Western blot analysis using an appropriate antibody.

Nitrocefin Hydrolysis Assay **–** The hydrolysis of nitrocefin (Millipore) was monitored in a microplate reader (Biotek Gen5) using a 96-well plate (Costar 3912). The assay buffer contains 50 mM Tris pH 8, 300 mM NaCl, and 5% DMSO, at a final volume of 100 µL for each reaction. For a time-course hydrolysis assay, 50 µL of nitrocefin (1 mg/mL) is mixed with 50 µL of MBLAC2 enzyme solution. The hydrolysis reaction was monitored for 60 minutes by following the absorbance at 486 nm (nitrocefin $\varepsilon 486 = 20500\ M^{-1}\ cm^{-1}$), corresponding to the appearance of a red product. For kinetic studies, 50 µL of nitrocefin (0.0-2.0 mM) is mixed with 50 µL of MBLAC2 enzyme solution (1 µM).

Glyoxalase II Assay **–** The Glyoxalase II assay was performed using a Colorimetric Glyoxalase II Assay Kit (BioVision) following manufacturer's standard protocol.

HRas Protein Thioesterase Assay – 6xHis-HRas was purified from total cell lysates of baculovirus-infected Sf9 cells using Ni-NTA agarose. Infected Sf9 cells were incubated with a standard Sf9 medium (Expression Systems) containing 100 µM 17-ODYA for 6 h. To initiate the hydrolysis reaction, HRas-ODYA (2 µM) was mixed with MBLAC2 or APT1 (200 nM) at 25 °C in HNMC buffer (50 mm HEPES pH 7.0, 150 mM NaCl, 50 mM $MgCl_2$, 1 mM $CaCl_2$). The hydrolysis reaction was stopped by adding 4% SDS followed by boiling for 2 min. A click chemistry reaction was performed by adding a freshly prepared click chemistry reaction mix (final concentrations of 10 µM Alexa Fluor 647-azide, 1 mM tris(2-carboxyethyl)phosphine (TCEP), 100 µM tris[(1-benzyl-1H-1,2,3-triazol-4-yl)methyl]amine (TBTA), and 1 mM $CuSO_4$). HRas-ODYA labeling was detected by in-gel fluorescence and quantified by using the densitometry functionality of the VersaDoc software. The hydrolase activity of MBLAC2 or APT1 towards HRas was indicated by the time-dependent or enzyme concentration-dependent decrease in the ODYA labeling of the HRas protein during hydrolysis.

SH4-GFP Protein Thioesterase Assay – The SH4-GFP substrate used in this assay was prepared by labeling myr-Vac[SH4]-meGFP-6xHis (2 µM) with [^{3}H]-palmitoyl CoA (1 µM) using the palmitoyltransferase DHHC20 enzyme (50 nM). The labeling reaction was performed for 1 h in MES buffer (50 mM, pH 6.4). The [^{3}H]-palmitoyl-SH4-GFP (2,000 dpm/pmol) was then purified using Ni-affinity purification. For the hydrolysis assay, APT1 or MBLAC2 (0-400 nM) was mixed with [^{3}H]-palmitoyl-SH4-GFP (200 nM) and incubated at 25 °C for 10 min. The hydrolysis reaction was then halted by adding a buffer containing 2% SDS and 2 mg/mL cytochrome C. The unreacted substrate was precipitated with 500 µL of isopropyl alcohol followed by centrifugation at 16,000 xg for 10 min. The free [^{3}H]-palmitate released from the reaction was assayed for radioactivity using a liquid scintillation counter. The hydrolase activity of MBLAC2 or APT1 towards SH4-GFP was indicated by the

enzyme concentration-dependent increase in the [^{3}H]-palmitate released by the [^{3}H]-palmitoyl-SH4-GFP during hydrolysis.

Acyl CoA Hydrolase Assay **–** Palmitoyl CoA and other acyl Coenzyme A's were purchased from Sigma and stored using manufacturer's protocol. For the hydrolysis of palmitoyl CoA, a reaction hot mix (RHM) was prepared by mixing non-radioactive palmitoyl CoA with [^{3}H]-palmitoyl CoA to a final concentration of 12.5 µM (specific activity 1,000 dpm/pmol). The reaction was initiated by adding 400 µL of the RHM to 100 µL of the enzyme solution (500 nM) at 30 °C. For a time-course experiment, the reaction was monitored for 30 min. The reaction was stopped with 1 mL of Dole's reagent (25 2-propanol: 5 heptane: 1 M H_2SO_4). The [^{3}H]-palmitic acid product was isolated by extraction with 500 µL heptane followed by vigorously shaking for one hour. The organic layer collected then assayed for radioactivity using a liquid scintillation counter. For a competition assay, 1.25 µM [^{3}H]-palmitoyl CoA was mixed with 11.25 µM of competing acyl CoA prior to adding the enzyme to form the RHM.

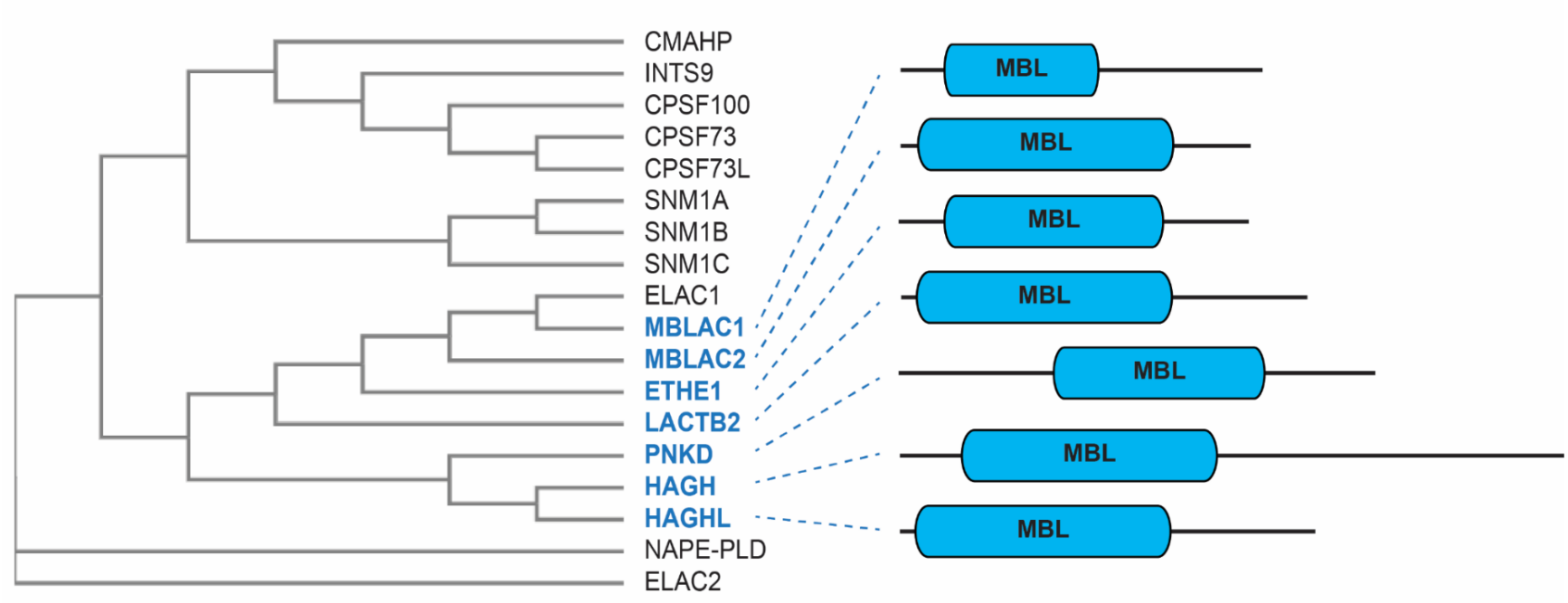

Figure 3.1 MBLAC2 belongs to the human metallo-β-lactamase (MBL) fold enzyme family.

A. Phylogenetic tree representation of the 18 human MBL-fold enzymes. Protein sequences were obtained from the UniProt database and aligned using Clustal Omega multisequence alignment tool [176]. Group 1 enzymes, which include MBLAC2, are written in blue.

B. Domain architecture of Group 1 MBL-fold enzymes. The MBL fold domain is represented as a blue cylinder. The sequence lengths and secondary structures of N- and C-termini vary widely within the enzyme family.

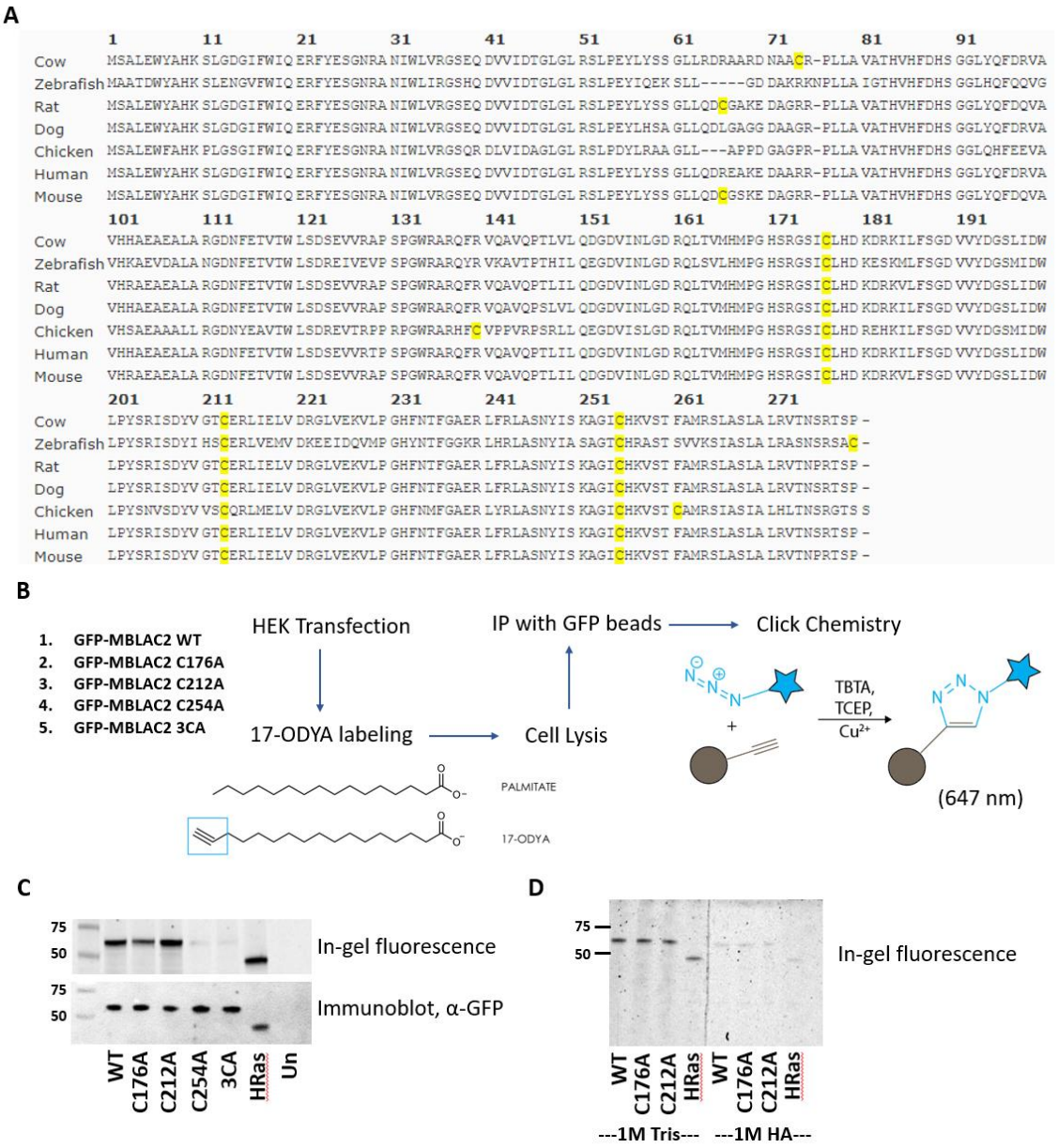

Figure 3.2 Mapping the Palmitoylation Sites of MBLAC2 by Click Chemistry.

A. Sequence alignment reveals three highly-conserved cysteines in vertebrate orthologs of MBLAC2: Cys–176, Cys–212, and Cys–254 (highlighted in yellow).

B. Schematic diagram of the Click Chemistry method used to detect the palmitoylation of GFP-MBLAC2 in HEK-293 cells. In this technique, palmitate is exchanged with an alkyne-containing analog, 17-ODYA. The alkyne functional group then undergoes a cycloaddition reaction with a fluorescent azide.

C. Palmitoylation levels of GFP-MBLAC2 are measured by in-gel fluorescence at 647 nm. Protein levels are compared by immunoblotting using a GFP antibody. HRas is a well-known palmitoylated protein used as a positive control. 3CA means mutating all three cysteine residues into alanine (n=4).

D. Treatment with 1M hydroxylamine (HA) removes the palmitate of MBLAC2 (n=2).

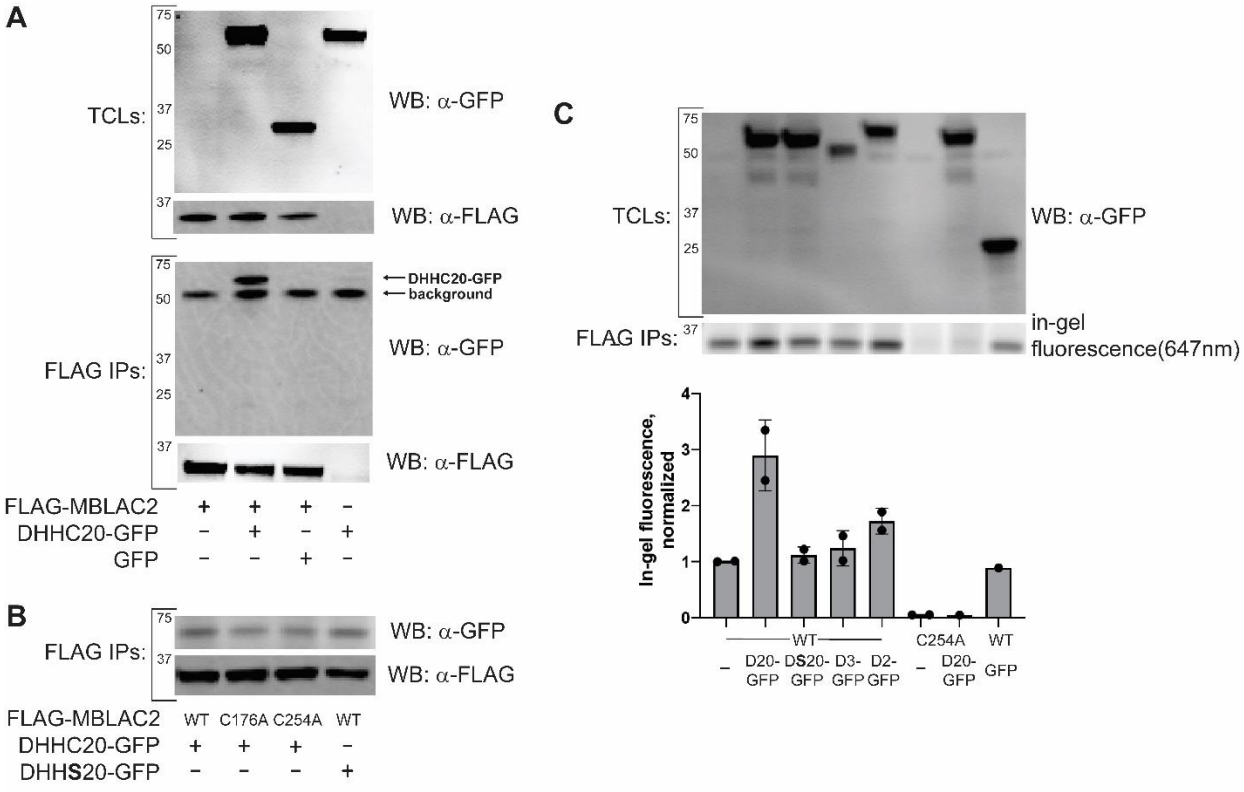

Figure 3.3 DHHC20 interacts with and increases the palmitoylation of MBLAC2 when co-expressed in HEK-293 cells.

A. FLAG-MBLAC2 and DHHC20-GFP were co-expressed in HEK-293 cells. After cell lysis, FLAG-MBLAC2 was purified using FLAG beads. The FLAG immunoprecipitates (IPs) were then blotted with either the FLAG antibody to detect MBLAC2 or GFP antibody to detect DHHC20. The protein levels in the total cell lysates (TCLs) were also compared by immunoblotting with the appropriate antibodies. Monomeric GFP was used as a negative control (n=3).

B. The palmitoylation process is not crucial for the interaction of MBLAC2 with DHHC20. This interaction remained even with the removal of the palmitoylated cysteine in MBLAC2 (C254A) or the catalytic cysteine in the DHHC20 enzyme (n=2).

C. Co-expression with DHHC20-GFP (D20), but not with DHH**S**20-GFP (D**S**20) increases the palmitoylation of wild-type FLAG-MBLAC2 in HEK-293 cells. MBLAC2 C254A palmitoylation was not detected even after co-expression with D20. Other DHHC enzymes tested were DHHC3-GFP (D3) and DHHC2-GFP (D2), both of which only slightly increased palmitoylation in wild-type MBLAC2 (n=2).

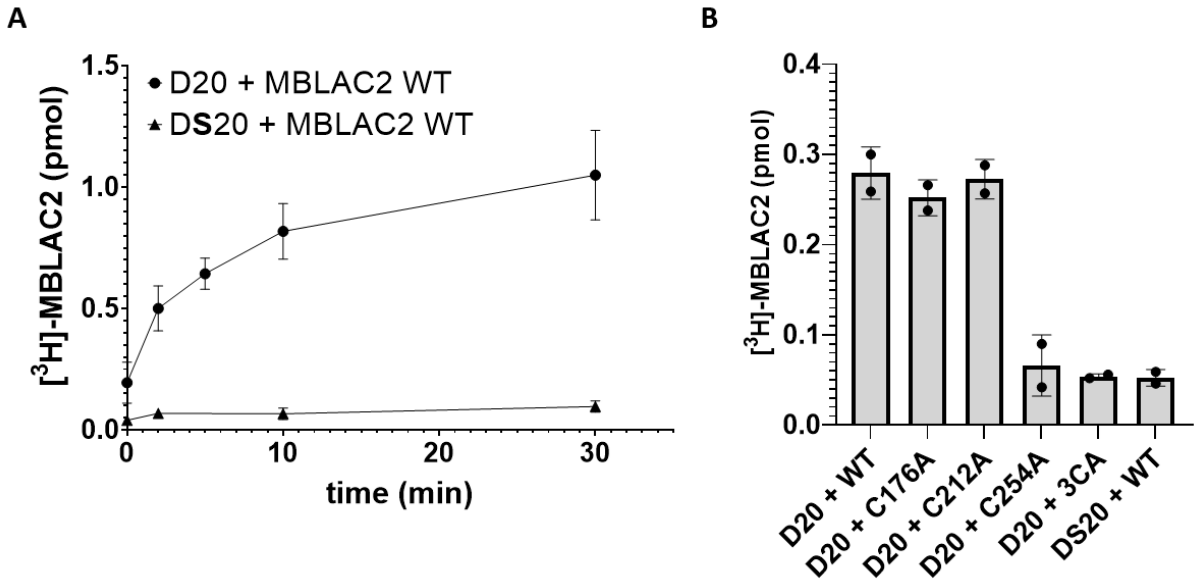

Figure 3.4 DHHC20 palmitoylates wild-type MBLAC2 in vitro.

A. Time-dependent incorporation of [^{3}H]-palmitate (1 µM) into wild-type MBLAC2 (1 µM) by either DHHC20 (50 nM) or DHH**S**20 (50 nM) enzyme at 25 °C.

B. Mutation of Cys−254 residue in MBLAC2 is sufficient to prevent palmitoylation of MBLAC2 by the DHHC20 enzyme.

Data are displayed as the mean ± SEM, n=2

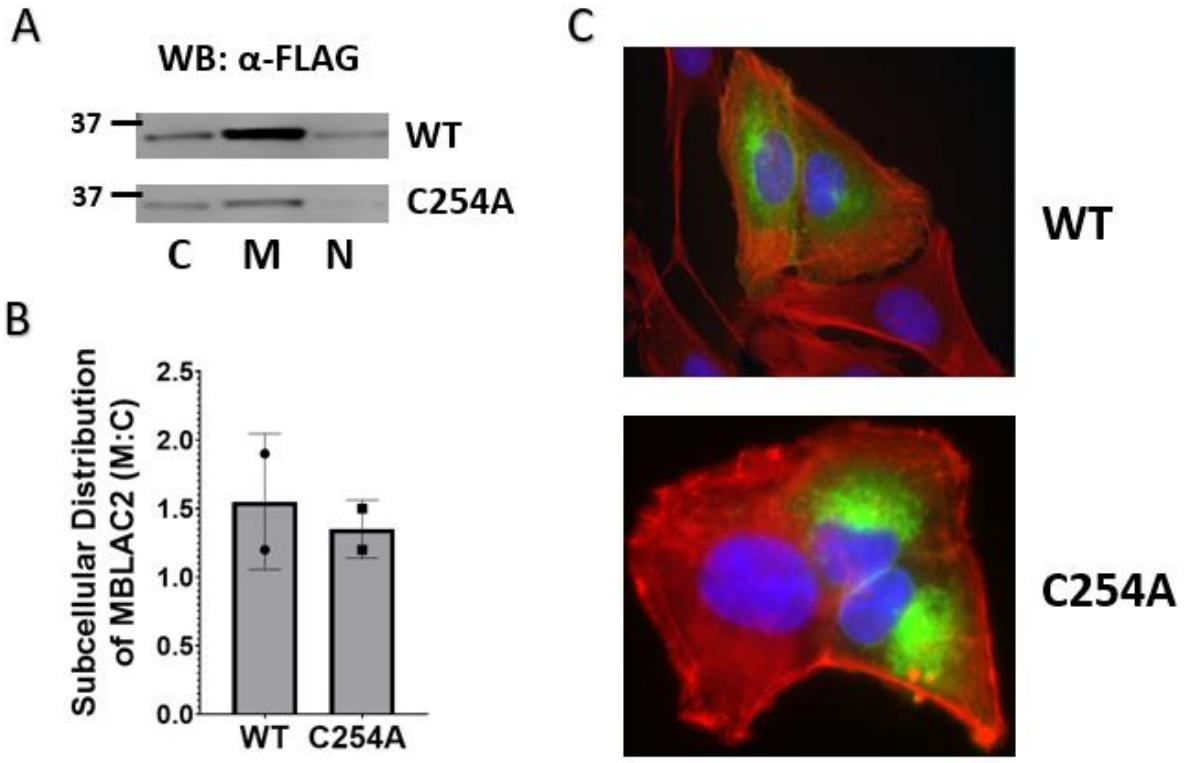

Figure 3.5 Palmitoylation has minimal effect on the membrane association or subcellular localization of MBLAC2.

A. HEK-293 cells expressing either FLAG-MBLAC2 WT or the palmitoylation-deficient mutant, FLAG-MBLAC2 C254A were subjected to subcellular fraction to separate the membrane (M), cytosol (C), and nuclear fractions. MBLAC2 was detected by immunoblotting with the FLAG antibody.

B. Quantification of the subcellular distribution of wild-type and palmitoylation-deficient MBLAC2 (n=2).

C. Representative immunofluorescence images of U2OS cells expressing FLAG-MBLAC2 WT and FLAG-MBLAC2 C254A. Blue – nuclei (DAPI), red – actin (Rh phalloidin), green – MBLAC2 (α-FLAG).

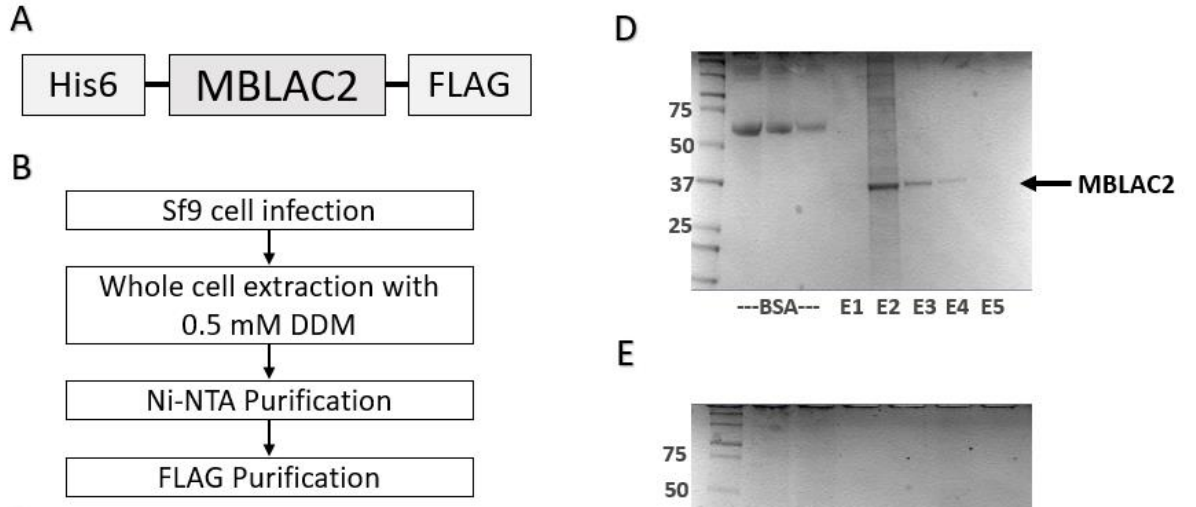

C

Purification Step	Protein (µg)	Specific Activity (nmol/min/mg)
Ni-NTA Purification		
• Ni input	25,600	21
• Ni FT	23,200	20
• Ni washes	1,860	19
• Ni pool	220	25
FLAG Purification		
• FLAG input	185	26
• FLAG FT	65	19
• FLAG washes	26	10
• FLAG pool	120	170

Figure 3.6 Two-step affinity purification of MBLAC2 yields a highly purified protein.

A. MBLAC2 constructs were engineered with an N-terminal hexahistidine tag and a C-terminal FLAG epitope.

B. Flowchart of MBLAC2 two-step affinity purification.

C. Purification table of wild-type MBLAC2. The total protein amount was measured by Bradford assay and the specific activity as an acyl CoA hydrolase was determined in each step of MBLAC2 purification.

D. Representative Coomassie-stained gel after Ni-NTA affinity purification of MBLAC2.

E. Representative Coomassie-stained gel after FLAG affinity purification of MBLAC2.

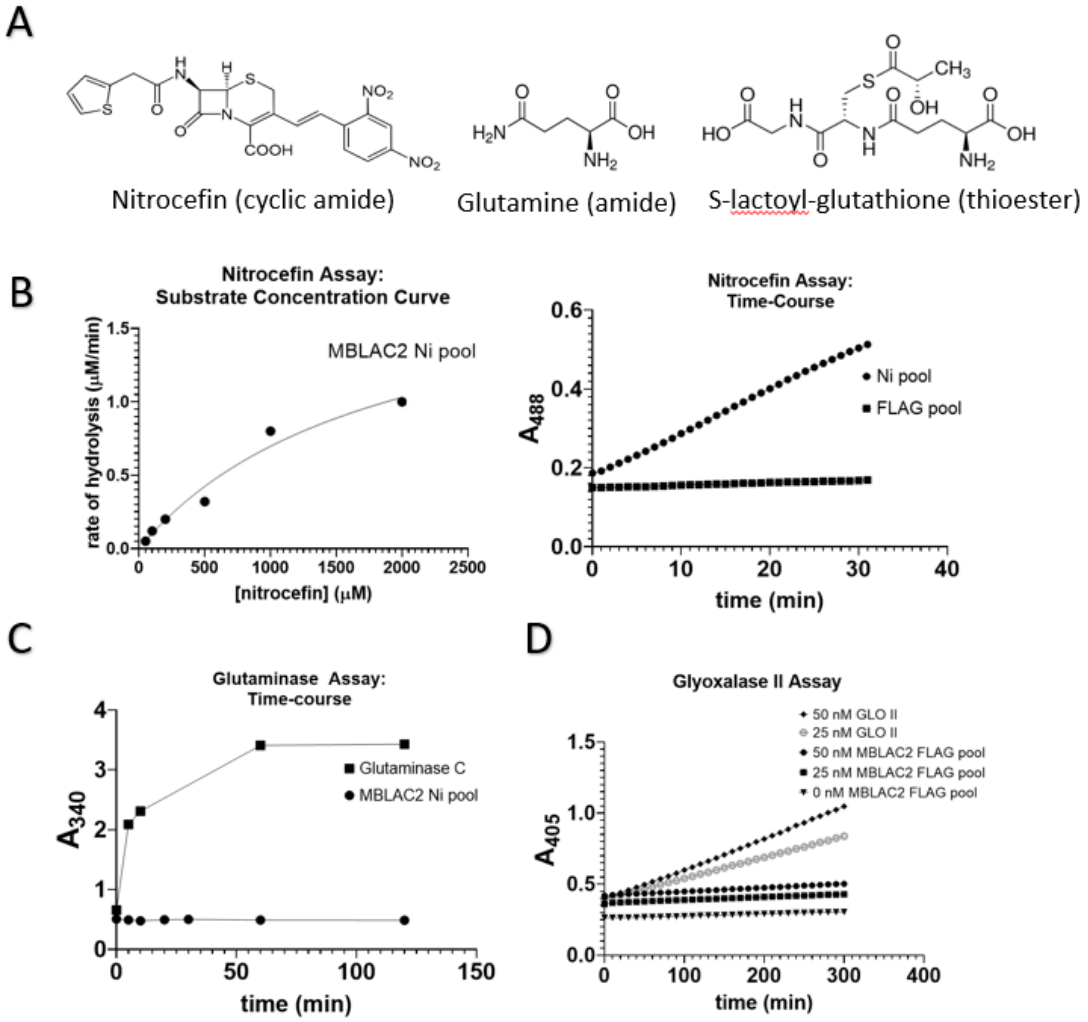

Figure 3.7 MBLAC2 showed little to no activity as a a hydrolase to nitrocefin, glutamine, and S-lactoyl-glutathione.

A. Structures of three small molecules tested as hydrolysis substrates of MBLAC2.

B. Nitrocefin hydrolysis assay. MBLAC2 purified by either one step (Ni pool) or two steps (FLAG pool) was used to hydrolyze nitrocefin. The hydrolysis reaction was monitored by measuring the absorbance of the acyclic product at 488 nm (n=2). The nitrocefin amidase activity seen in MBLAC2 Ni pool was undetectable in MBLAC2 FLAG pool.

C. Glutaminase assay. 50 nM of either MBLAC2 Ni pool or Glutaminase C (positive control) was used to hydrolyze 20 mM glutamine at room temperature. The reaction was monitored by measuring the absorbance at 340 nm of the hydrolyzed carboxylic acid product (n=1).

D. Glyoxalase II assay. Increasing concentrations of either MBLAC2 FLAG pool or commercial recombinant Glyoxalase II (positive control) were used to hydrolyze 1 mM S-lactoyl-glutathione (n=2).

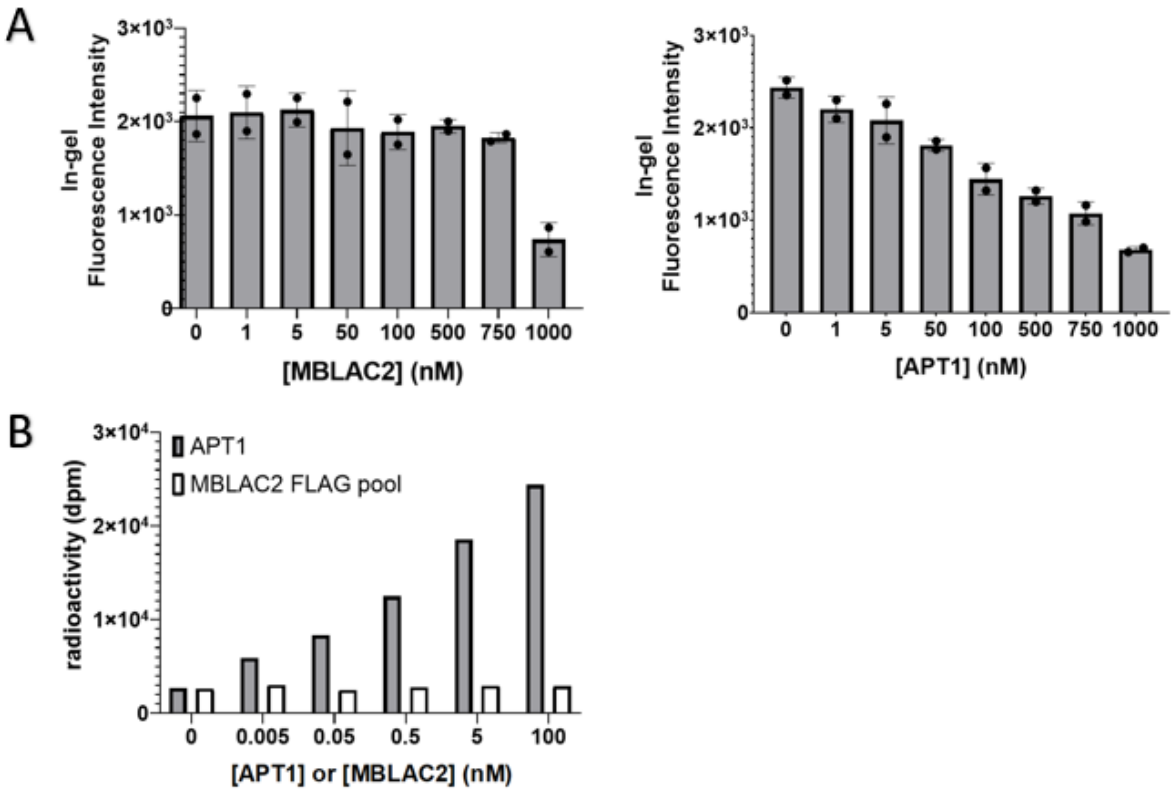

Figure 3.8 MBLAC2 showed little to no activity as a protein thioesterase towards HRas and SH4-GFP.

A. Protein Thioesterase Assay on HRas. Purified 17-ODYA-labeled HRas (1 µM) was incubated with either MBLAC2 FLAG pool or APT1 (positive control) at 25 °C for 10 min to initiate hydrolysis. After a click chemistry reaction and gel electrophoresis, the 17-ODYA labeling that remained in HRas was measured by in-gel fluorescence (n=2).

B. Protein Thioesterase Assay on SH4-GFP. Purified [^{3}H]-palmitate-labeled SH4-GFP (1 µM) was incubated with different concentrations of either MBLAC2 FLAG pool or APT1 at 25 °C for 10 min to initiate hydrolysis. The [^{3}H]-palmitic acid released from SH4-GFP was then extracted and the radioactivity was counted using a scintillation counter (n=2).

A

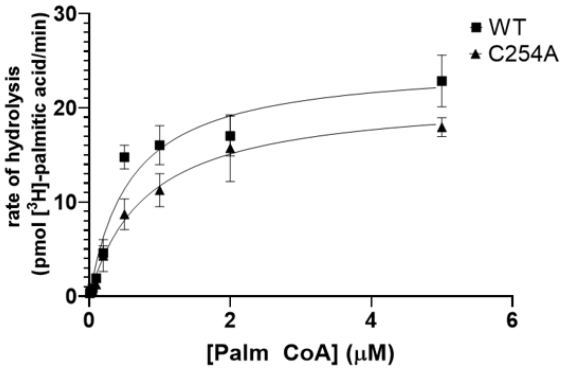

B

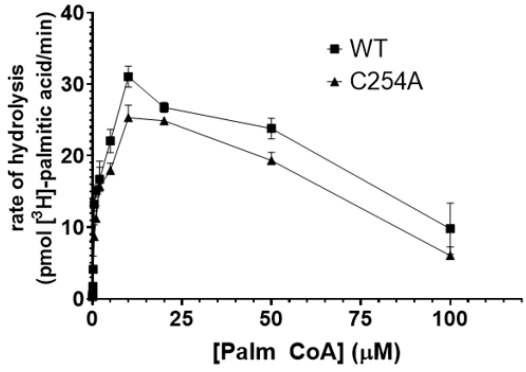

C

	WT	C254A
kcat	2,478	2,271
Km (μM)	0.5877	0.8179
Vmax (pmol/min)	24.78	21.28
Vmax (nmol/min/mg)	134	115
R^2	0.9477	0.9652

Figure 3.9 Palmitoyl CoA hydrolase activity of wild-type and C254A mutant of MBLAC2.

A. MBLAC2 WT and C254A proteins exhibit Michaelis-Menten kinetics between 0-5 μM palmitoyl CoA concentration (n=2).

B. Both MBLAC2 WT and C254A proteins are inhibited by high concentrations of palmitoyl CoA (n=2).

C. Kinetic parameters of MBLAC2 WT and C254A as palmitoyl CoA hydrolase (n=2).

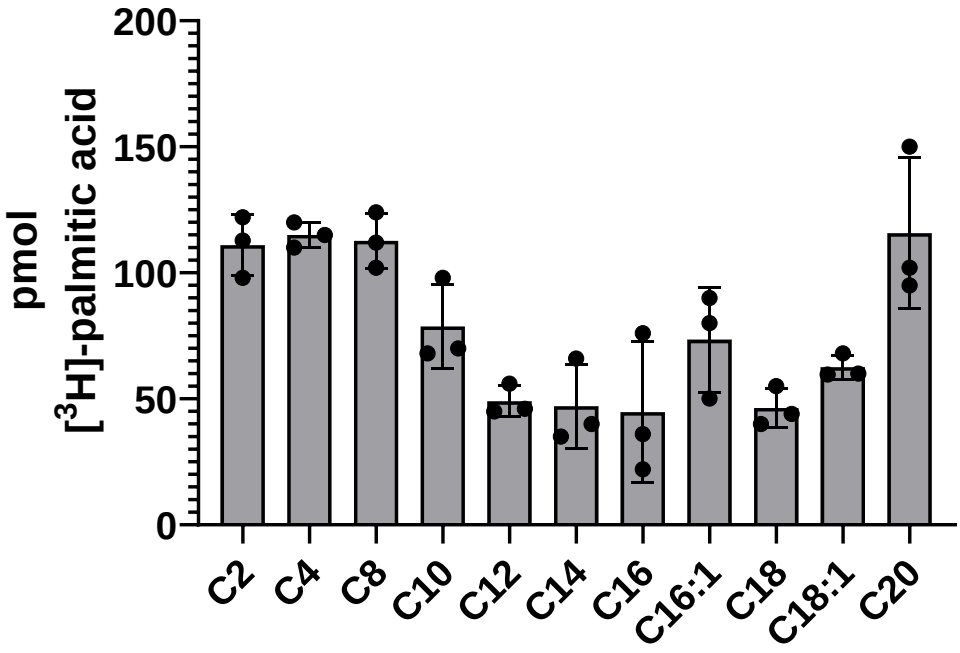

Figure 3.10 Acyl chain length selectivity of MBLAC2.

To examine the acyl chain length selectivity of MBLAC2, [^{3}H]-palmitoyl CoA (1 µM) was made to compete with various unlabeled acyl CoAs (9 µM) for hydrolysis by MBLAC2 (50 nM). The [^{3}H]-palmitic acid produced by the hydrolysis reaction was then extracted and counted using a scintillation counter. Using this assay, I found that MBLAC2 exhibits acyl CoA hydrolase selectivity towards C12-C18 acyl CoAs. Moreover, MBLAC2 can also hydrolyze monounsaturated acyl CoAs such as palmitoleoyl CoA (C16:1) and oleoyl CoA (C18:1) (n=3).

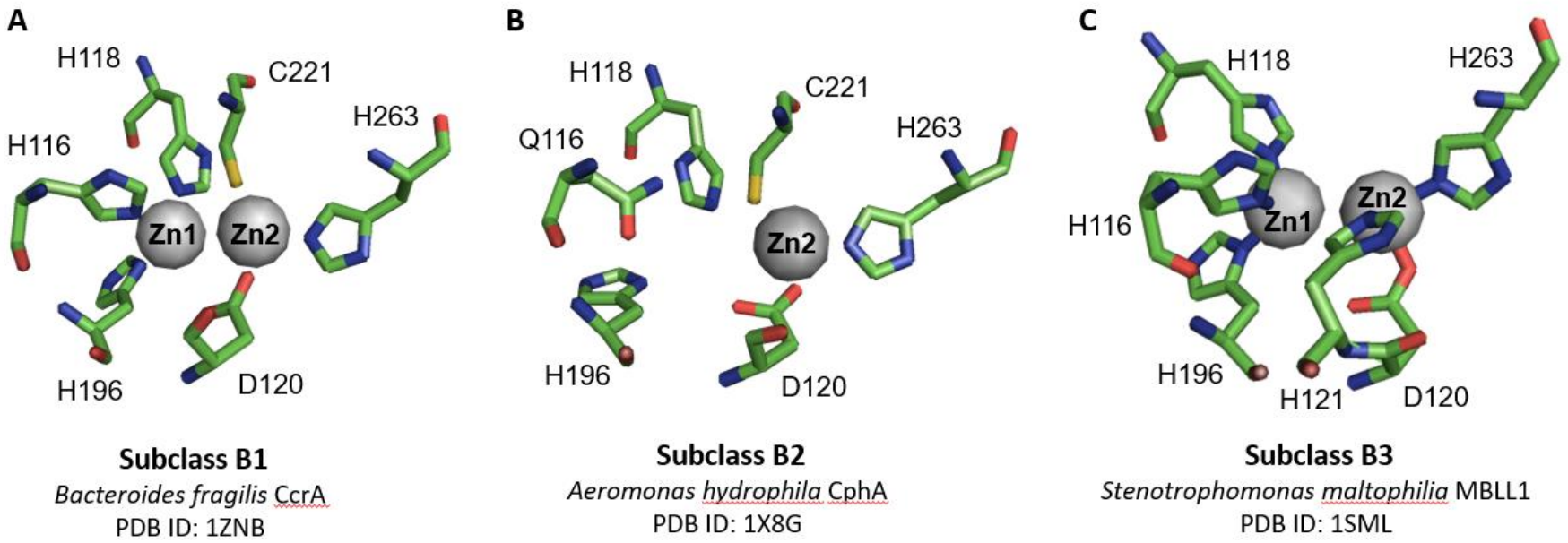

Figure 3.11 **MBL enzymes are categorized based on zinc coordination.**

Schematic illustration of the amino acid residues bound to zinc ions in MBLs subclass B1, B2, and B3 using representative proteins of known structures. Structural coordinates from the Protein Data Bank were analyzed using Pymol. Zinc ions are represented by gray spheres. Amino acid residues are colored by element (C-green, N-blue, O-red, S-yellow).

A. Cassette chromosome recombinase A1 (CcrA1) contains two Zn-binding motifs – one containing three histidines and one containing a histidine, a cysteine, and an aspartic acid [177].

B. One of the histidines in CphA is mutated into a glutamine preventing the binding of Zn1. Zn2 binding residues are conserved [178].

C. Metallo-β-lactamase like 1 (MBLL1) contains the same 3-His motif present in the Zn1 binding site of subclass B1 proteins but replaces the cysteine residue with a histidine in the Zn2 binding site [163].

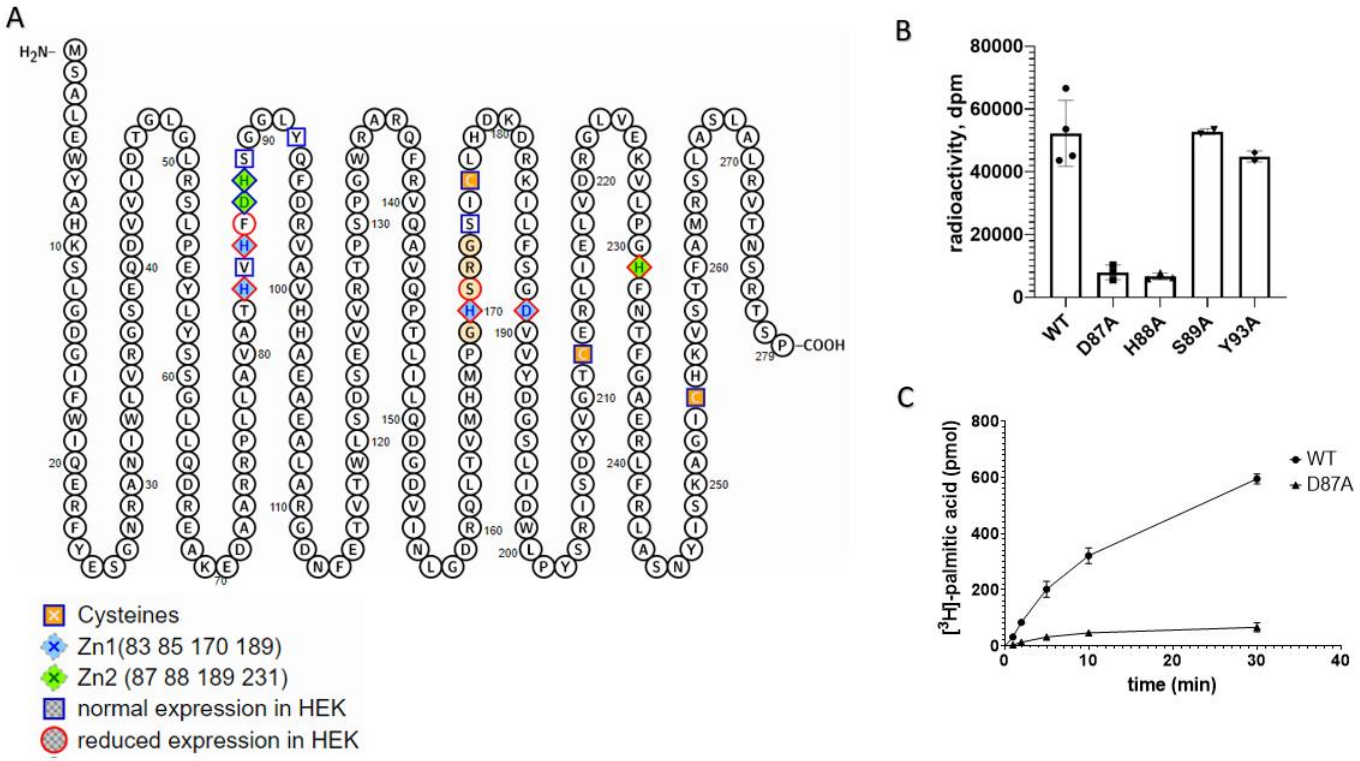

Figure 3.12 Some of the predicted zinc-binding residues are important for the acyl CoA hydrolase of MBLAC2.

A. MBLAC2 amino acid sequence showing key residues predicted to be involved in acyl CoA hydrolysis. Zn1 binding residues are highlighted in blue (H83, H85, H170, D189). Zn2 binding residues are highlighted in green (D87, H88, D189, H231). Mutations that showed good expression in HEK-293 cells are traced in blue (V84A, D87A, H88A, S89A, Y93A). Mutations that showed reduced expression in HEK-293 cells are traced in red (H83A, H85A, F86A, H171A, D189A, H231A). The cysteine mutants are also shown and are highlighted in orange (C176A, C212A, C254A).

B. Acyl CoA hydrolase activity of wild-type and MBLAC2 mutants immunoprecipitated using FLAG beads from transfected HEK-293 cells (n=4).

C. Time-course of acyl CoA hydrolase activity of wild-type MBLAC2 and D87A mutant purified from insect cells (n=2), confirming with highly purified enzyme that D87A is required for catalytic activity.

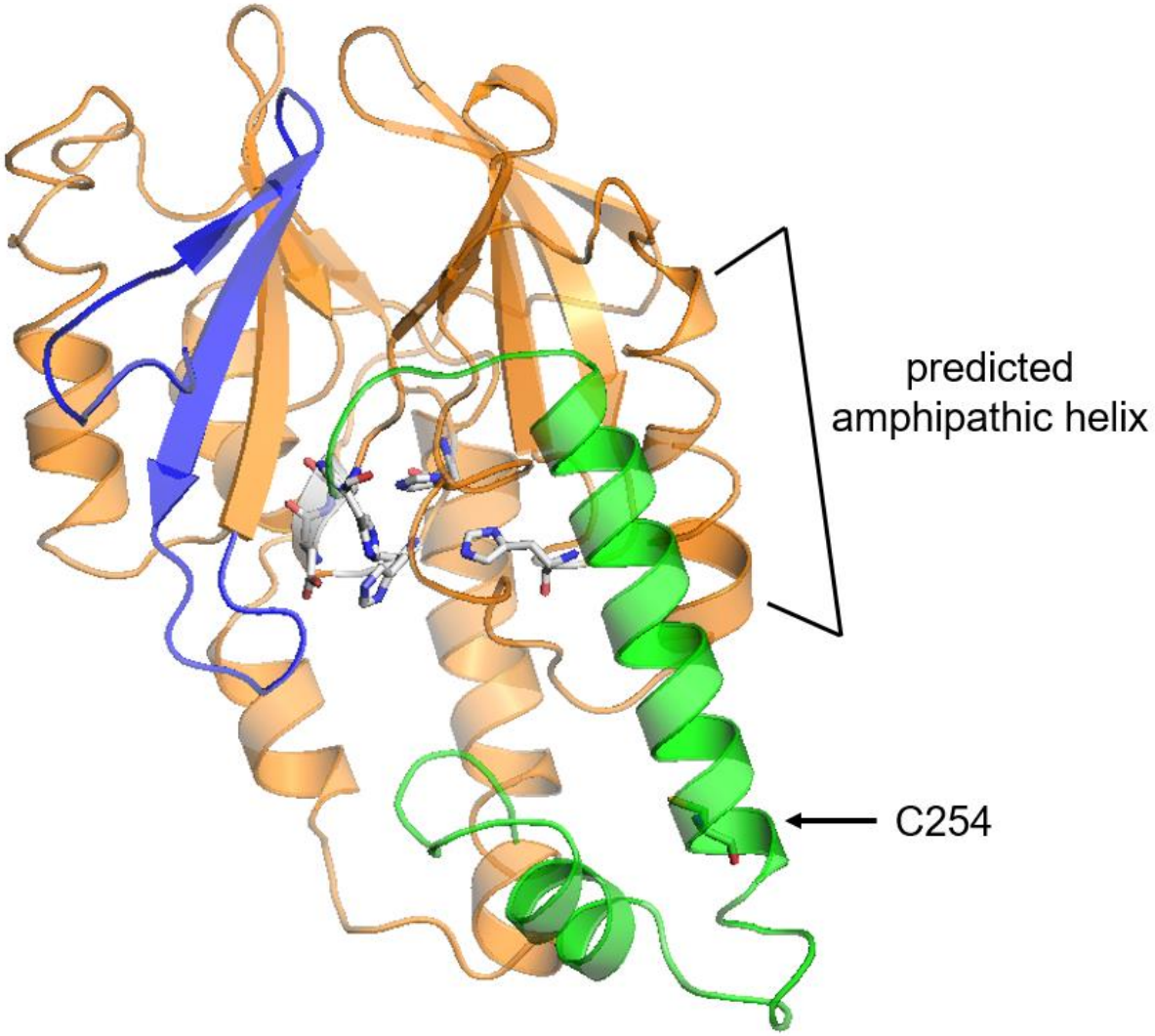

Figure 3.13 Predicted three-dimensional fold of the human MBLAC2 protein.
Structure threading was performed in I-TASSER, a software that models unknown protein structures using templates available from the PDB library. Each candidate structure is given a C-score [-5 to 2], with 2 indicating the highest confidence. The highest C-score (0.2) obtained during the threading was for the crystal structure of β-lactamase domain protein from *Burkhoderia ambifaria* (PDB ID: 5I0P) [179, 180] and hence was used as a template in this figure. The resulting MBLAC2 structure was visualized using Pymol. The MBL-fold domain is represented by orange, the N-terminus by blue, and the C-terminus by green. The predicted zinc-binding side chains in the active site are represented as sticks and colored by the element (C-gray, N-blue, O-red). The Cys−254 residue seen distant from the active site and a predicted amphipathic within the MBL-fold domain are labeled (see discussion).

REFERENCES

1. Chen, B., et al., *Protein Lipidation in Cell Signaling and Diseases: Function, Regulation, and Therapeutic Opportunities.* Cell Chemical Biology, 2018. **25**(7): p. 817-831.
2. Resh, M.D., *Covalent lipid modifications of proteins.* Current biology : CB, 2013. **23**(10): p. R431-R435.
3. Nadolski, M.J. and M.E. Linder, *Protein lipidation.* The FEBS Journal, 2007. **274**(20): p. 5202-5210.
4. Jiang, H., et al., *Protein Lipidation: Occurrence, Mechanisms, Biological Functions, and Enabling Technologies.* Chemical Reviews, 2018. **118**(3): p. 919-988.
5. Hosseini, V., et al., *Wnt lipidation: Roles in trafficking, modulation, and function.* J Cell Physiol, 2019. **234**(6): p. 8040-8054.
6. Ferguson, M.A.J., G.W. Hart, and T. Kinoshita, *Glycosylphosphatidylinositol Anchors*, in *Essentials of Glycobiology*, rd, et al., Editors. 2015, Cold Spring Harbor Laboratory Press
7. Bursten, S.L., et al., *Acylation of monocyte and glomerular mesangial cell proteins. Myristyl acylation of the interleukin 1 precursors.* J Clin Invest, 1988. **82**(5): p. 1479-88.
8. Hedo, J.A., E. Collier, and A. Watkinson, *Myristyl and palmityl acylation of the insulin receptor.* J Biol Chem, 1987. **262**(3): p. 954-7.
9. Pillai, S. and D. Baltimore, *Myristoylation and the post-translational acquisition of hydrophobicity by the membrane immunoglobulin heavy-chain polypeptide in B lymphocytes.* Proc Natl Acad Sci U S A, 1987. **84**(21): p. 7654-8.
10. Stevenson, F.T., et al., *Myristyl Acylation of the Tumor Necrosis Factor Alpha Precursor on Specific Lysine Residues.* J. Exp. Med., 1992. **176**: p. 1053.
11. Haigis, M.C. and D.A. Sinclair, *Mammalian Sirtuins: Biological Insights and Disease Relevance.* Annu. Rev. Pathol.: Mech. Dis., 2010. **5**: p. 253.
12. Jiang, H., et al., *Sirt6 Regulates Tnf-α Secretion through Hydrolysis of Long-Chain Fatty Acyl Lysine.* Nature, 2013. **496**: p. 110.
13. Zhang, X., et al., *SIRT6 Regulates Ras-Related Protein R-Ras2 by Lysine Defatty-Acylation.* eLife, 2017. **6**.
14. Jing, H., et al., *SIRT2 and lysine fatty acylation regulate the transforming activity of K-Ras4a.* eLife, 2017. **6**: p. e32436.
15. Buglino, J.A. and M.D. Resh, *Hhat Is a Palmitoylacyltransferase with Specificity for N-Palmitoylation of Sonic Hedgehog.* Journal of Biological Chemistry, 2008. **283**(32): p. 22076-22088.
16. Clevers, H. and R. Nusse, *Wnt/β-Catenin Signaling and Disease.* Cell, 2012. **149**(6): p. 1192-1205.
17. Takada, R., et al., *Monounsaturated fatty acid modification of Wnt protein: its role in Wnt secretion.* Dev Cell, 2006. **11**(6): p. 791-801.
18. Rocks, O., et al., *The palmitoylation machinery is a spatially organizing system for peripheral membrane proteins.* Cell, 2010. **141**(3): p. 458-71.
19. Won, S.J. and B.R. Martin, *Temporal Profiling Establishes a Dynamic S-Palmitoylation Cycle.* ACS Chem Biol, 2018. **13**(6): p. 1560-1568.
20. Stoffyn, P., and Folch-Pi, J., *On the tpe of linkage binding fatty acids present in brain white matter proteolipid apoprotein.* Biochemical and Biophysical Research Coomunications, 1971. **44**: p. 157-161.
21. Schmidt, M.F., M. Bracha, and M.J. Schlesinger, *Evidence for covalent attachment of fatty acids to Sindbis virus glycoproteins.* Proc Natl Acad Sci U S A, 1979. **76**(4): p. 1687-91.

22. Kaufman, J.F., M.S. Krangel, and J.L. Strominger, *Cysteines in the transmembrane region of major histocompatibility complex antigens are fatty acylated via thioester bonds.* J Biol Chem, 1984. **259**(11): p. 7230-8.
23. Magee, A.I., et al., *Release of fatty acids from virus glycoproteins by hydroxylamine.* Biochim Biophys Acta, 1984. **798**(2): p. 156-66.
24. Reuter, C.W.M., M.A. Morgan, and L. Bergmann, *Targeting the Ras signaling pathway: a rational, mechanism-based treatment for hematologic malignancies?* Blood, 2000. **96**(5): p. 1655-1669.
25. Hancock, J.F., et al., *All ras proteins are polyisoprenylated but only some are palmitoylated.* Cell, 1989. **57**(7): p. 1167-77.
26. Rocks, O., et al., *An Acylation Cycle Regulates Localization and Activity of Palmitoylated Ras Isoforms.* Science, 2005. **307**(5716): p. 1746-1752.
27. Mitchell, D.A., et al., *A polybasic domain allows nonprenylated Ras proteins to function in Saccharomyces cerevisiae.* Journal of Biological Chemistry, 1994. **269**(34): p. 21540-21546.
28. Bartels, D.J., et al., *Erf2, a novel gene product that affects the localization and palmitoylation of Ras2 in Saccharomyces cerevisiae.* Molecular and cellular biology, 1999. **19**(10): p. 6775-6787.
29. Zhao, L., et al., *Erf4p and Erf2p Form an Endoplasmic Reticulum-associated Complex Involved in the Plasma Membrane Localization of Yeast Ras Proteins.* Journal of Biological Chemistry, 2002. **277**(51): p. 49352-49359.
30. Lobo, S., et al., *Identification of a Ras Palmitoyltransferase in Saccharomyces cerevisiae.* Journal of Biological Chemistry, 2002. **277**(43): p. 41268-41273.
31. Roth, A.F., et al., *The yeast DHHC cysteine-rich domain protein Akr1p is a palmitoyl transferase.* The Journal of cell biology, 2002. **159**(1): p. 23-28.
32. Mitchell, D.A., et al., *Thematic review series: Lipid Posttranslational Modifications. Protein palmitoylation by a family of DHHC protein S-acyltransferases.* Journal of Lipid Research, 2006. **47**(6): p. 1118-1127.
33. Hemsley, P.A. and C.S. Grierson, *Multiple roles for protein palmitoylation in plants.* Trends in Plant Science, 2008. **13**(6): p. 295-302.
34. Bannan, B.A., et al., *The Drosophila protein palmitoylome: Characterizing palmitoyl-thioesterases and DHHC palmitoyl-transferases.* Fly, 2008. **2**(4): p. 198-214.
35. Hicks, Stuart W., et al., *Subcellular Targeting of Salmonella Virulence Proteins by Host-Mediated S-Palmitoylation.* Cell Host & Microbe, 2011. **10**(1): p. 9-20.
36. Lin, Y.-H., et al., *Host Cell-catalyzed S-Palmitoylation Mediates Golgi Targeting of the Legionella Ubiquitin Ligase GobX.* Journal of Biological Chemistry, 2015. **290**(42): p. 25766-25781.
37. Rana, M.S., C.-J. Lee, and A. Banerjee, *The molecular mechanism of DHHC protein acyltransferases.* Biochemical Society Transactions, 2019. **47**(1): p. 157-167.
38. González Montoro, A., et al., *A novel motif at the C-terminus of palmitoyltransferases is essential for Swf1 and Pfa3 function in vivo.* Biochemical Journal, 2009. **419**(2): p. 301-308.
39. Zaballa, M.-E. and F.G. van der Goot, *The molecular era of protein S-acylation: spotlight on structure, mechanisms, and dynamics.* Critical Reviews in Biochemistry and Molecular Biology, 2018. **53**(4): p. 420-451.
40. Putilina, T., P. Wong, and S. Gentleman, *The DHHC domain: A new highly conserved cysteine-rich motif.* Molecular and Cellular Biochemistry, 1999. **195**(1): p. 219-226.

41. Gottlieb, C.D., S. Zhang, and M.E. Linder, *The Cysteine-rich Domain of the DHHC3 Palmitoyltransferase is Palmitoylated and Contains Tightly Bound Zinc.* Journal of Biological Chemistry, 2015.
42. González Montoro, A., S. Chumpen Ramirez, and J. Valdez Taubas, *The Canonical DHHC Motif Is Not Absolutely Required for the Activity of the Yeast S-acyltransferases Swf1 and Pfa4.* Journal of Biological Chemistry, 2015. **290**(37): p. 22448-22459.
43. Böhm, S., D. Frishman, and H.W. Mewes, *Variations of the C2H2 zinc finger motif in the yeast genome and classification of yeast zinc finger proteins.* Nucleic acids research, 1997. **25**(12): p. 2464-2469.
44. González Montoro, A., R. Quiroga, and J. Valdez Taubas, *Zinc co-ordination by the DHHC cysteine-rich domain of the palmitoyltransferase Swf1.* Biochemical Journal, 2013. **454**(3): p. 427-435.
45. Ohno, Y., et al., *Analysis of substrate specificity of human DHHC protein acyltransferases using a yeast expression system.* Molecular biology of the cell, 2012. **23**(23): p. 4543-4551.
46. Ohno, Y., et al., *Intracellular localization and tissue-specific distribution of human and yeast DHHC cysteine-rich domain-containing proteins.* Biochimica et Biophysica Acta (BBA) - Molecular and Cell Biology of Lipids, 2006. **1761**(4): p. 474-483.
47. Draper, J.M. and C.D. Smith, *Dhhc20: A Human Palmitoyl Acyltransferase That Causes Cellular Transformation.* Mol. Membr. Biol., 2010. **27**: p. 123.
48. Greaves, J., J.A. Carmichael, and L.H. Chamberlain, *The palmitoyl transferase DHHC2 targets a dynamic membrane cycling pathway: regulation by a C-terminal domain.* Molecular biology of the cell, 2011. **22**(11): p. 1887-1895.
49. Greaves, J., et al., *Palmitoylation of the SNAP25 Protein Family: SPECIFICITY AND REGULATION BY DHHC PALMITOYL TRANSFERASES.* Journal of Biological Chemistry, 2010. **285**(32): p. 24629-24638.
50. Jia, L., M.E. Linder, and K.J. Blumer, *Gi/o signaling and the palmitoyltransferase DHHC2 regulate palmitate cycling and shuttling of RGS7 family-binding protein.* The Journal of biological chemistry, 2011. **286**(15): p. 13695-13703.
51. Mill, P., et al., *Palmitoylation Regulates Epidermal Homeostasis and Hair Follicle Differentiation.* PLOS Genetics, 2009. **5**(11): p. e1000748.
52. Fernández-Hernando, C., et al., *Identification of Golgi-localized acyl transferases that palmitoylate and regulate endothelial nitric oxide synthase.* The Journal of Cell Biology, 2006. **174**(3): p. 369-377.
53. Gorleku, O.A., et al., *Endoplasmic Reticulum Localization of DHHC Palmitoyltransferases Mediated by Lysine-based Sorting Signals.* Journal of Biological Chemistry, 2011. **286**(45): p. 39573-39584.
54. Noritake, J., et al., *Mobile DHHC palmitoylating enzyme mediates activity-sensitive synaptic targeting of PSD-95.* J Cell Biol, 2009. **186**(1): p. 147-60.
55. Roth, A.F., et al., *Global analysis of protein palmitoylation in yeast.* Cell, 2006. **125**(5): p. 1003-13.
56. Fukata, Y., T. Iwanaga, and M. Fukata, *Systematic screening for palmitoyl transferase activity of the DHHC protein family in mammalian cells.* Methods, 2006. **40**(2): p. 177-82.
57. Kilpatrick, C.L., et al., *Dissociation of Golgi-Associated Dhhc-Type Zinc Finger Protein (Godz)-and Sertoli Cell Gene with a Zinc Finger Domain-Beta (Serz-Beta)-Mediated Palmitoylation by Loss of Function Analyses in Knock-out Mice.* J. Biol. Chem., 2016. **291**: p. 27371.
58. Liu, P., et al., *Palmitoylacyltransferase Zdhhc9 Inactivation Mitigates Leukemogenic Potential of Oncogenic Nras.* Leukemia, 2016. **30**: p. 1225.

59. Lee, H.-J. and J.J. Zheng, *PDZ domains and their binding partners: structure, specificity, and modification.* Cell Communication and Signaling, 2010. **8**(1): p. 8.
60. Fukata, Y. and M. Fukata, *Protein palmitoylation in neuronal development and synaptic plasticity.* Nat Rev Neurosci, 2010. **11**(3): p. 161-75.
61. Thomas, G.M., et al., *Dhhc8-Dependent Pick1 Palmitoylation Is Required for Induction of Cerebellar Long-Term Synaptic Depression.* J. Neurosci., 2013. **33**: p. 15401.
62. Fredericks, G.J., et al., *Stable Expression and Function of the Inositol 1,4,5-Triphosphate Receptor Requires Palmitoylation by a Dhhc6/Selenoprotein K Complex.* Proc. Natl. Acad. Sci. U. S. A., 2014. **111**: p. 16478.
63. Meiler, S., et al., *Selenoprotein K is required for palmitoylation of CD36 in macrophages: implications in foam cell formation and atherogenesis.* J Leukoc Biol, 2013. **93**(5): p. 771-80.
64. Singaraja, R.R., et al., *HIP14, a novel ankyrin domain-containing protein, links huntingtin to intracellular trafficking and endocytosis.* Hum Mol Genet, 2002. **11**(23): p. 2815-28.
65. Lemonidis, K., M.C. Sanchez-Perez, and L.H. Chamberlain, *Identification of a Novel Sequence Motif Recognized by the Ankyrin Repeat Domain of Zdhhc17/13 S-Acyltransferases.* J. Biol. Chem., 2015. **290**: p. 21939.
66. Verardi, R., et al., *Structural Basis for Substrate Recognition by the Ankyrin Repeat Domain of Human Dhhc17 Palmitoyltransferase.* Structure, 2017. **25**: p. 1337.
67. Jennings, B.C. and M.E. Linder, *Dhhc Protein S-Acyltransferases Use Similar Ping-Pong Kinetic Mechanisms but Display Different Acyl-Coa Specificities.* J. Biol. Chem., 2012. **287**: p. 7236.
68. Greaves, J., et al., *Molecular Basis of Fatty Acid Selectivity in the Zdhhc Family of S-Acyltransferases Revealed by Click Chemistry.* Proc. Natl. Acad. Sci. U. S. A., 2017. **114**: p. E1365.
69. Rana, M.S., et al., *Fatty acyl recognition and transfer by an integral membrane S-acyltransferase.* Science, 2018. **359**(6372): p. eaao6326.
70. Muszbek, L., et al., *The pool of fatty acids covalently bound to platelet proteins by thioester linkages can be altered by exogenously supplied fatty acids.* Lipids, 1999. **34**(S1Part3): p. S331-S337.
71. Haynes, C.A., et al., *Quantitation of fatty acyl-coenzyme As in mammalian cells by liquid chromatography-electrospray ionization tandem mass spectrometry.* Journal of Lipid Research, 2008. **49**(5): p. 1113-1125.
72. Liang, X., et al., *Heterogeneous Fatty Acylation of Src Family Kinases with Polyunsaturated Fatty Acids Regulates Raft Localization and Signal Transduction.* Journal of Biological Chemistry, 2001. **276**(33): p. 30987-30994.
73. Fukata, M., et al., *Identification of Psd-95 Palmitoylating Enzymes.* Neuron, 2004. **44**: p. 987.
74. Mitchell, D.A., et al., *Mutational Analysis of Saccharomyces Cerevisiae Erf2 Reveals a Two-Step Reaction Mechanism for Protein Palmitoylation by Dhhc Enzymes.* J. Biol. Chem., 2010. **285**: p. 38104.
75. Rana, M.S., et al., *Fatty acyl recognition and transfer by an integral membrane S-acyltransferase.* Science, 2018. **359**(6372).
76. Gonzalez Montoro, A., S. Chumpen Ramirez, and J. Valdez Taubas, *The Canonical Dhhc Motif Is Not Absolutely Required for the Activity of the Yeast S-Acyltransferases Swf1 and Pfa4.* J. Biol. Chem., 2015. **290**: p. 22448.
77. Wedegaertner, P.B. and H.R. Bourne, *Activation and depalmitoylation of Gs alpha.* Cell, 1994. **77**(7): p. 1063-70.
78. Swarthout, J.T., et al., *Dhhc9 and Gcp16 Constitute a Human Protein Fatty Acyltransferase with Specificity for H- and N-Ras.* J. Biol. Chem., 2005. **280**: p. 31141.

79. Zhang, M.M., et al., *Quantitative Control of Protein S-Palmitoylation Regulates Meiotic Entry in Fission Yeast.* PLOS Biology, 2013. **11**(7): p. e1001597.
80. Charych, E.I., et al., *Interplay of Palmitoylation and Phosphorylation in the Trafficking and Localization of Phosphodiesterase 10a: Implications for the Treatment of Schizophrenia.* J. Neurosci., 2010. **30**: p. 9027.
81. Lievens, P.M.-J., et al., *ZDHHC3 Tyrosine Phosphorylation Regulates Neural Cell Adhesion Molecule Palmitoylation.* Molecular and cellular biology, 2016. **36**(17): p. 2208-2225.
82. Lai, J. and M.E. Linder, *Oligomerization of Dhhc Protein S-Acyltransferases.* J. Biol. Chem., 2013. **288**: p. 22862.
83. Singaraja, R.R., et al., *Palmitoylation of Atp-Binding Cassette Transporter A1 Is Essential for Its Trafficking and Function.* Circ. Res., 2009. **105**: p. 138.
84. Keith, D.J., et al., *Palmitoylation of a-Kinase Anchoring Protein 79/150 Regulates Dendritic Endosomal Targeting and Synaptic Plasticity Mechanisms.* J. Neurosci., 2012. **32**: p. 7119.
85. Delint-Ramirez, I., et al., *Palmitoylation targets AKAP79 protein to lipid rafts and promotes its regulation of calcium-sensitive adenylyl cyclase type 8.* J Biol Chem, 2011. **286**(38): p. 32962-75.
86. Yanai, A., et al., *Palmitoylation of huntingtin by HIP14 is essential for its trafficking and function.* Nat Neurosci, 2006. **9**(6): p. 824-31.
87. Yang, H., et al., *Palmitoylation participates in G protein coupled signal transduction by affecting its oligomerization.* Mol Membr Biol, 2008. **25**(1): p. 58-71.
88. Yanai, A., et al., *Palmitoylation of Huntingtin by Hip14 Is Essential for Its Trafficking and Function.* Nat. Neurosci., 2006. **9**: p. 824.
89. Hayashi, T., G. Rumbaugh, and R.L. Huganir, *Differential regulation of AMPA receptor subunit trafficking by palmitoylation of two distinct sites.* Neuron, 2005. **47**(5): p. 709-23.
90. Magee, A.I., et al., *Dynamic fatty acylation of p21N-ras.* Embo j, 1987. **6**(11): p. 3353-7.
91. Staufenbiel, M., *Ankyrin-bound fatty acid turns over rapidly at the erythrocyte plasma membrane.* Mol Cell Biol, 1987. **7**(8): p. 2981-4.
92. Camp, L.A. and S.L. Hofmann, *Purification and properties of a palmitoyl-protein thioesterase that cleaves palmitate from H-Ras.* Journal of Biological Chemistry, 1993. **268**(30): p. 22566-74.
93. Camp, L.A., et al., *Molecular cloning and expression of palmitoyl-protein thioesterase.* Journal of Biological Chemistry, 1994. **269**(37): p. 23212-23219.
94. Bellizzi, J.J., et al., *The crystal structure of palmitoyl protein thioesterase 1 and the molecular basis of infantile neuronal ceroid lipofuscinosis.* Proceedings of the National Academy of Sciences, 2000. **97**(9): p. 4573-4578.
95. Hellsten, E., et al., *Human palmitoyl protein thioesterase: evidence for lysosomal targeting of the enzyme and disturbed cellular routing in infantile neuronal ceroid lipofuscinosis.* Embo j, 1996. **15**(19): p. 5240-5.
96. Verkruyse, L.A. and S.L. Hofmann, *Lysosomal Targeting of Palmitoyl-protein Thioesterase.* Journal of Biological Chemistry, 1996. **271**(26): p. 15831-15836.
97. Vesa, J., et al., *Mutations in the palmitoyl protein thioesterase gene causing infantile neuronal ceroid lipofuscinosis.* Nature, 1995. **376**(6541): p. 584-587.
98. Duncan, J.A. and A.G. Gilman, *A Cytoplasmic Acyl-Protein Thioesterase That Removes Palmitate from G Protein A Subunits and P21ras.* J. Biol. Chem., 1998. **273**: p. 15830.
99. Sugimoto, H., H. Hayashi, and S. Yamashita, *Purification, cDNA Cloning, and Regulation of Lysophospholipase from Rat Liver.* Journal of Biological Chemistry, 1996. **271**(13): p. 7705-7711.

100. Hirano, T., et al., *Thioesterase activity and subcellular localization of acylprotein thioesterase 1/lysophospholipase 1.* Biochim Biophys Acta, 2009. **1791**(8): p. 797-805.
101. Devedjiev, Y., et al., *Crystal Structure of the Human Acyl Protein Thioesterase I from a Single X-Ray Data Set to 1.5 Å.* Structure, 2000. **8**(11): p. 1137-1146.
102. Veit, M. and M.F. Schmidt, *Enzymatic depalmitoylation of viral glycoproteins with acyl-protein thioesterase 1 in vitro.* Virology, 2001. **288**(1): p. 89-95.
103. Flaumenhaft, R., et al., *SNAP-23 and syntaxin-2 localize to the extracellular surface of the platelet plasma membrane.* Blood, 2007. **110**(5): p. 1492-1501.
104. Dekker, F.J., et al., *Small-Molecule Inhibition of Apt1 Affects Ras Localization and Signaling.* Nat. Chem. Biol., 2010. **6**: p. 449.
105. Kong, E., et al., *Dynamic Palmitoylation Links Cytosol-Membrane Shuttling of Acyl-Protein Thioesterase-1 and Acyl-Protein Thioesterase-2 with That of Proto-Oncogene H-Ras Product and Growth-Associated Protein-43.* J. Biol. Chem., 2013. **288**: p. 9112.
106. Yeh, D.C., et al., *Depalmitoylation of Endothelial Nitric-Oxide Synthase by Acyl-Protein Thioesterase 1 Is Potentiated by Ca2+-Calmodulin.* J. Biol. Chem., 1999. **274**: p. 33148.
107. Manna, J.D., et al., *Identification of the major prostaglandin glycerol ester hydrolase in human cancer cells.* J Biol Chem, 2014. **289**(49): p. 33741-53.
108. Abrami, L., et al., *Identification and Dynamics of the Human Zdhhc16-Zdhhc6 Palmitoylation Cascade.* eLife, 2017. **6**.
109. Adachi, N., et al., *S-Palmitoylation of a Novel Site in the beta2-Adrenergic Receptor Associated with a Novel Intracellular Itinerary.* J Biol Chem, 2016. **291**(38): p. 20232-46.
110. Rusch, M., et al., *Identification of Acyl Protein Thioesterases 1 and 2 as the Cellulartargets of the Ras-Signaling Modulators Palmostatin B and M.* Angew. Chem., Int. Ed., 2011. **50**: p. 9838.
111. Vartak, N., et al., *The Autodepalmitoylating Activity of Apt Maintains the Spatial Organization of Palmitoylated Membrane Proteins.* Biophys. J., 2014. **106**: p. 93.
112. Kathayat, R.S., et al., *Active and dynamic mitochondrial S-depalmitoylation revealed by targeted fluorescent probes.* Nature Communications, 2018. **9**(1): p. 334.
113. Peikert, C.D., et al., *Charting organellar importomes by quantitative mass spectrometry.* Nat Commun, 2017. **8**: p. 15272.
114. Morgenstern, M., et al., *Definition of a High-Confidence Mitochondrial Proteome at Quantitative Scale.* Cell Rep, 2017. **19**(13): p. 2836-2852.
115. Lindgren, C.M., et al., *Genome-wide association scan meta-analysis identifies three Loci influencing adiposity and fat distribution.* PLoS Genet, 2009. **5**(6): p. e1000508.
116. Speliotes, E.K., et al., *Genome-wide association analysis identifies variants associated with nonalcoholic fatty liver disease that have distinct effects on metabolic traits.* PLoS Genet, 2011. **7**(3): p. e1001324.
117. Bürger, M., et al., *Crystal structure of the predicted phospholipase LYPLAL1 reveals unexpected functional plasticity despite close relationship to acyl protein thioesterases.* Journal of Lipid Research, 2012. **53**(1): p. 43-50.
118. Lin, D.T. and E. Conibear, *Abhd17 Proteins Are Novel Protein Depalmitoylases That Regulate N-Ras Palmitate Turnover and Subcellular Localization.* eLife, 2015. **4**: p. e11306.
119. Vujic, I., et al., *Acyl Protein Thioesterase 1 and 2 (Apt-1, Apt-2) Inhibitors Palmostatin B, Ml348 and Ml349 Have Different Effects on Nras Mutant Melanoma Cells.* Oncotarget, 2016. **7**: p. 7297.
120. Hernandez, J.L., et al., *Apt2 Inhibition Restores Scribble Localization and S-Palmitoylation in Snail-Transformed Cells.* Cell Chem. Biol., 2017. **24**: p. 87.

121. Ahearn, I.M., et al., *FKBP12 binds to acylated H-ras and promotes depalmitoylation.* Mol Cell, 2011. **41**(2): p. 173-85.
122. Simon, G.M. and B.F. Cravatt, *Activity-based Proteomics of Enzyme Superfamilies: Serine Hydrolases as a Case Study.* Journal of Biological Chemistry, 2010. **285**(15): p. 11051-11055.
123. Blanc, M., F.P.A. David, and F.G. van der Goot, *SwissPalm 2: Protein S-Palmitoylation Database*, in *Protein Lipidation: Methods and Protocols*, M.E. Linder, Editor. 2019, Springer New York: New York, NY. p. 203-214.
124. Won, S.J., M. Cheung See Kit, and B.R. Martin, *Protein depalmitoylases.* Critical Reviews in Biochemistry and Molecular Biology, 2018. **53**(1): p. 83-98.
125. Raymond, F.L., et al., *Mutations in Zdhhc9, Which Encodes a Palmitoyltransferase of Nras and Hras, Cause X-Linked Mental Retardation Associated with a Marfanoid Habitus.* Am. J. Hum. Genet., 2007. **80**: p. 982.
126. Mansouri, M.R., et al., *Loss of Zdhhc15 Expression in a Woman with a Balanced Translocation T(X;15)(Q13.3;Cen) and Severe Mental Retardation.* Eur. J. Hum. Genet., 2005. **13**: p. 970.
127. Sutton, L.M., et al., *Hip14l-Deficient Mice Develop Neuropathological and Behavioural Features of Huntington Disease.* Hum. Mol. Genet., 2013. **22**: p. 452.
128. Ota, V.K., et al., *Zdhhc8 Gene May Play a Role in Cortical Volumes of Patients with Schizophrenia.* Schizophr. Res., 2013. **145**: p. 33.
129. Xu, M., D. St Clair, and L. He, *Testing for Genetic Association between the Zdhhc8 Gene Locus and Susceptibility to Schizophrenia: An Integrated Analysis of Multiple Datasets.* Am. J. Med. Genet., Part B, 2010. **153B**: p. 1266.
130. Oo, H.Z., et al., *Overexpression of Zdhhc14 Promotes Migration and Invasion of Scirrhous Type Gastric Cancer.* Oncol. Rep., 2014. **32**: p. 403.
131. Greaves, J. and L.H. Chamberlain, *DHHC palmitoyl transferases: substrate interactions and (patho)physiology.* Trends in Biochemical Sciences, 2011. **36**(5): p. 245-253.
132. Mukai, J., et al., *Evidence That the Gene Encoding Zdhhc8 Contributes to the Risk of Schizophrenia.* Nat. Genet., 2004. **36**: p. 725.
133. Saleem, A.N., et al., *Mice with Alopecia, Osteoporosis, and Systemic Amyloidosis Due to Mutation in Zdhhc13, a Gene Coding for Palmitoyl Acyltransferase.* PLoS Genet., 2010. **6**: p. e1000985.
134. Milnerwood, A.J., et al., *Memory and Synaptic Deficits in Hip14/Dhhc17 Knockout Mice.* Proc. Natl. Acad. Sci. U. S. A., 2013. **110**: p. 20296.
135. Gonzalez Montoro, A., R. Quiroga, and J. Valdez Taubas, *Zinc Co-Ordination by the Dhhc Cysteine-Rich Domain of the Palmitoyltransferase Swf1.* Biochem. J., 2013. **454**: p. 427.
136. Runkle, K.B., et al., *Inhibition of Dhhc20-Mediated Egfr Palmitoylation Creates a Dependence on Egfr Signaling.* Mol. Cell, 2016. **62**: p. 385.
137. Kawate, T. and E. Gouaux, *Fluorescence-detection size-exclusion chromatography for precrystallization screening of integral membrane proteins.* Structure, 2006. **14**(4): p. 673-81.
138. Zou, Y., W.I. Weis, and B.K. Kobilka, *N-Terminal T4 Lysozyme Fusion Facilitates Crystallization of a G Protein Coupled Receptor.* PLOS ONE, 2012. **7**(10): p. e46039.
139. Nadolski, M.J. and M.E. Linder, *Molecular Recognition of the Palmitoylation Substrate Vac8 by Its Palmitoyltransferase Pfa3.* Journal of Biological Chemistry, 2009. **284**(26): p. 17720-17730.
140. Fang, C., et al., *GODZ-Mediated Palmitoylation of GABA_A Receptors Is Required for Normal Assembly and Function of GABAergic Inhibitory Synapses.* The Journal of Neuroscience, 2006. **26**(49): p. 12758-12768.

141. Noritake, J., et al., *Mobile Dhhc Palmitoylating Enzyme Mediates Activity-Sensitive Synaptic Targeting of Psd-95.* J. Cell Biol., 2009. **186**: p. 147.
142. Ulbrich, M.H. and E.Y. Isacoff, *Subunit counting in membrane-bound proteins.* Nat Methods, 2007. **4**(4): p. 319-21.
143. Caffrey, M. and V. Cherezov, *Crystallizing membrane proteins using lipidic mesophases.* Nat Protoc, 2009. **4**(5): p. 706-31.
144. Rayment, I., *[12] Reductive alkylation of lysine residues to alter crystallization properties of proteins*, in *Methods in Enzymology*. 1997, Academic Press. p. 171-179.
145. Reddy, K.D., et al., *Physicochemical sequence characteristics that influence S-palmitoylation propensity.* J Biomol Struct Dyn, 2017. **35**(11): p. 2337-2350.
146. Gamsjaeger, R., et al., *Sticky fingers: zinc-fingers as protein-recognition motifs.* Trends in Biochemical Sciences, 2007. **32**(2): p. 63-70.
147. Manglik, A. and B. Kobilka, *The role of protein dynamics in GPCR function: insights from the β2AR and rhodopsin.* Current Opinion in Cell Biology, 2014. **27**: p. 136-143.
148. Oswald, C., et al., *Intracellular allosteric antagonism of the CCR9 receptor.* Nature, 2016. **540**: p. 462.
149. Malgapo, M.I.P. and M.E. Linder, *Purification of Recombinant DHHC Proteins Using an Insect Cell Expression System.* Methods Mol Biol, 2019. **2009**: p. 179-189.
150. Richards, M.J., et al., *Membrane Protein Mobility and Orientation Preserved in Supported Bilayers Created Directly from Cell Plasma Membrane Blebs.* Langmuir, 2016. **32**(12): p. 2963-2974.
151. Sanders, S.S., et al., *Curation of the Mammalian Palmitoylome Indicates a Pivotal Role for Palmitoylation in Diseases and Disorders of the Nervous System and Cancers.* PLOS Computational Biology, 2015. **11**(8): p. e1004405.
152. Huttlin, E.L., et al., *Architecture of the human interactome defines protein communities and disease networks.* Nature, 2017. **545**: p. 505.
153. Pettinati, I., et al., *The Chemical Biology of Human Metallo-beta-Lactamase Fold Proteins.* Trends Biochem Sci, 2016. **41**(4): p. 338-355.
154. Palzkill, T., *Metallo-β-lactamase structure and function.* Annals of the New York Academy of Sciences, 2013. **1277**: p. 91-104.
155. Xue, M., N. Rabbani, and P.J. Thornalley, *Glyoxalase in ageing.* Semin Cell Dev Biol, 2011. **22**(3): p. 293-301.
156. Kabil, O. and R. Banerjee, *Characterization of patient mutations in human persulfide dioxygenase (ETHE1) involved in H2S catabolism.* J Biol Chem, 2012. **287**(53): p. 44561-7.
157. Levy, S., et al., *Identification of LACTB2, a metallo-β-lactamase protein, as a human mitochondrial endoribonuclease.* Nucleic acids research, 2016. **44**(4): p. 1813-1832.
158. Retzlaff, C.L., et al., *Metallo-beta-lactamase Domain-Containing Protein 1 (MBLAC1) Is a Specific, High-Affinity Target for the Glutamate Transporter Inducer Ceftriaxone.* ACS Chem Neurosci, 2017. **8**(10): p. 2132-2138.
159. Aravind, L., D.R. Walker, and E.V. Koonin, *Conserved domains in DNA repair proteins and evolution of repair systems.* Nucleic Acids Res, 1999. **27**(5): p. 1223-42.
160. Callebaut, I., et al., *Metallo-beta-lactamase fold within nucleic acids processing enzymes: the beta-CASP family.* Nucleic Acids Res, 2002. **30**(16): p. 3592-601.
161. Diene, S.M., et al., *Human metallo-beta-lactamase enzymes degrade penicillin.* Sci Rep, 2019. **9**(1): p. 12173.

162. Hunt, M.C., et al., *Analysis of the mouse and human acyl-CoA thioesterase (ACOT) gene clusters shows that convergent, functional evolution results in a reduced number of human peroxisomal ACOTs.* Faseb j, 2006. **20**(11): p. 1855-64.
163. Ullah, J.H., et al., *The crystal structure of the L1 metallo-beta-lactamase from Stenotrophomonas maltophilia at 1.7 A resolution.* J Mol Biol, 1998. **284**(1): p. 125-36.
164. Cameron, A.D., et al., *Crystal structure of human glyoxalase II and its complex with a glutathione thiolester substrate analogue.* Structure, 1999. **7**(9): p. 1067-1078.
165. Dunne, S.J., et al., *Structure of the Membrane Binding Domain of CTP:Phosphocholine Cytidylyltransferase.* Biochemistry, 1996. **35**(37): p. 11975-11984.
166. Picot, D., P.J. Loll, and R.M. Garavito, *The X-ray crystal structure of the membrane protein prostaglandin H2 synthase-1.* Nature, 1994. **367**(6460): p. 243-249.
167. Li, Y., et al., *The Membrane Association Sequences of the Prostaglandin Endoperoxide Synthases-1 and -2 Isozymes.* Journal of Biological Chemistry, 1998. **273**(45): p. 29830-29837.
168. Thiyagarajan, M.M., et al., *A Predicted Amphipathic Helix Mediates Plasma Membrane Localization of GRK5.* Journal of Biological Chemistry, 2004. **279**(17): p. 17989-17995.
169. Bernstein, L.S., et al., *RGS4 Binds to Membranes through an Amphipathic α-Helix.* Journal of Biological Chemistry, 2000. **275**(24): p. 18520-18526.
170. Chen, C., et al., *The Membrane Association Domain of RGS16 Contains Unique Amphipathic Features That Are Conserved in RGS4 and RGS5.* Journal of Biological Chemistry, 1999. **274**(28): p. 19799-19806.
171. Druey, K.M., et al., *Amino-terminal Cysteine Residues of RGS16 Are Required for Palmitoylation and Modulation of Gi- and Gq-mediated Signaling.* Journal of Biological Chemistry, 1999. **274**(26): p. 18836-18842.
172. Srinivasa, S.P., et al., *Plasma membrane localization is required for RGS4 function in Saccharomyces cerevisiae.* Proceedings of the National Academy of Sciences, 1998. **95**(10): p. 5584-5589.
173. Tillander, V., S.E.H. Alexson, and D.E. Cohen, *Deactivating Fatty Acids: Acyl-CoA Thioesterase-Mediated Control of Lipid Metabolism.* Trends in Endocrinology & Metabolism, 2017. **28**(7): p. 473-484.
174. Dunphy, J.T., et al., *Differential effects of acyl-CoA binding protein on enzymatic and non-enzymatic thioacylation of protein and peptide substrates.* Biochimica et Biophysica Acta (BBA) - Molecular and Cell Biology of Lipids, 2000. **1485**(2): p. 185-198.
175. Gibson, C.L., et al., *Global untargeted serum metabolomic analyses nominate metabolic pathways responsive to loss of expression of the orphan metallo beta-lactamase, MBLAC1.* Mol Omics, 2018. **14**(3): p. 142-155.
176. Madeira, F., et al., *The EMBL-EBI search and sequence analysis tools APIs in 2019.* Nucleic acids research, 2019. **47**(W1): p. W636-W641.
177. Concha, N.O., et al., *Crystal structure of the wide-spectrum binuclear zinc beta-lactamase from Bacteroides fragilis.* Structure, 1996. **4**(7): p. 823-36.
178. Garau, G., et al., *A metallo-beta-lactamase enzyme in action: crystal structures of the monozinc carbapenemase CphA and its complex with biapenem.* J Mol Biol, 2005. **345**(4): p. 785-95.
179. Zhang, Y., *I-TASSER: fully automated protein structure prediction in CASP8.* Proteins, 2009. **77 Suppl 9**: p. 100-13.
180. *Crystal Structure of a Beta-lactamase domain protein from Burkholderia ambifaria*. http://www.rcsb.org/structure/5I0P.

APPENDIX

This appended section on the Purification of Recombinant DHHC Proteins Using an Insect Cell Expression System was published as a chapter in the *Methods in Molecular Biology* book series (MIMB, volume 2009). My contribution in this chapter includes performing the experiment and writing up the protocol and the results.

Chapter 14

Purification of Recombinant DHHC Proteins Using an Insect Cell Expression System

Martin Ian P. Malgapo and Maurine E. Linder

Abstract

DHHC enzymes are a family of integral membrane proteins that catalyze the posttranslational addition of palmitate, a 16-carbon fatty acid, onto a cysteine residue of a protein. While the library of identified palmitoylated proteins has grown tremendously over the years, biochemical and mechanistic studies on DHHC proteins are challenged by the innate difficulty of purifying the enzyme in large amounts. Here we describe our protocol for preparing recombinant DHHC proteins tagged with a hexahistidine sequence and a FLAG epitope that aid in the purification. This procedure has been tested successfully in purifying several members of the enzyme family; DHHC3 and its catalytically inactive cysteine mutant, DHHS3 are used as examples. The recombinant protein is extracted from whole cell lysates using the detergent dodecylmaltoside (DDM) and is subjected to a two-column purification. Homogeneity and monodispersity of the purified protein are checked by size exclusion chromatography (SEC). A preparation from a 400-mL infection of Sf9 insect cell culture typically yields 0.5 mg of DHHC3 and 1.0 mg of catalytically inactive DHHS3. Both forms appear monodisperse up to a concentration of 1 mg/mL by SEC.

Key words DHHC protein, Palmitoylation, Protein acyltransferase, Immobilized metal affinity chromatography, Affinity chromatography, Size exclusion chromatography

1 Introduction

Palmitoylation refers to the posttranslational attachment of a fatty acid onto a cysteine residue of a protein. Although fatty acids of varying degrees of unsaturation and chain lengths can be added to cysteines, the 16-carbon fatty acid, palmitate, is the most commonly observed and hence most well studied. Palmitoylation can occur in both soluble and integral membrane proteins. In soluble proteins, the addition of palmitate increases the hydrophobic character of the protein at the site of palmitoylation, allowing for specific membrane targeting. The consequences of palmitoylating an integral membrane protein include alterations in the conformation of transmembrane domains, association with specific membrane domains such as lipid rafts, controlled interactions with

Maurine E. Linder (ed.), *Protein Lipidation: Methods and Protocols*, Methods in Molecular Biology, vol. 2009,
https://doi.org/10.1007/978-1-4939-9532-5_14,

other proteins, and controlled interplay with other posttranslational modifications [1]. Current estimates suggest that more than 10% of the human proteome undergoes palmitoylation [2].

Although protein palmitoylation had been known for several decades, the identity of the family of enzymes that catalyze palmitoylation in cells remained unknown until 2002, with the discovery of the two founding members of the DHHC enzyme family in yeast. The Erf2/Erf4 (Effect on Ras function) protein complex was found to palmitoylate the Ras2 protein [3], and ankyrin repeat-containing protein 1 was found to palmitoylate yeast casein kinase 2 [4]. DHHC enzymes act as protein acyltransferases and are highly conserved throughout eukaryotes with families ranging in size from 5 members in *Schizosaccharomyces pombe* [5] to 23 in humans [6].

DHHC enzymes are polytopic integral membrane proteins characterized by their highly conserved DHHC (Asp-His-His-Cys) motif within its catalytic 51-amino acid cysteine-rich domain (CRD) [7]. The typical membrane topology is four transmembrane domains with the N- and C-termini exposed to the cytoplasm. A few DHHC enzymes have six transmembrane helices [8]. The N- and C-terminal regions vary in sequence and size, potentially allowing specific protein–protein interactions. It is now appreciated that DHHC proteins generally function via a kinetic ping-pong mechanism [9, 10]. The enzyme first undergoes autopalmitoylation on the cysteine of the DHHC motif using palmitoyl-coenzyme A (CoA) as a palmitoyl donor, the palmitate is then transferred to a cysteine residue on the substrate. Mutating the cysteine in the catalytic DHHC motif into a serine or alanine typically inactivates the enzyme, although there are exceptions [11].

The innate difficulty of expressing and purifying sufficient quantities of DHHC proteins has served as a bottleneck in the biochemical, mechanistic, and structural characterization of these enzymes. Standard bacterial expression systems lack the enzymes required for posttranslational modification, and hence are not suited for purifying these eukaryotic membrane enzymes. Moreover, preservation of their biological and functional activities during the isolation process can be compromised. One key consideration is the use of an appropriate detergent such as dodecylmaltoside (DDM) during solubilization to prevent the protein from aggregating upon extraction from the membrane. Solubilized with amphiphilic detergents and purified as protein–detergent complexes, the detergent micelle covers the hydrophobic surface of the membrane protein as would the hydrophobic lipids in the native membrane bilayer.

In this chapter we describe a protocol for purifying recombinant DHHC proteins. We have used this protocol to routinely prepare DHHC2, DHHC3, DHHC20, and their catalytically inactive DHHS mutants. The DHHC constructs are cloned to include

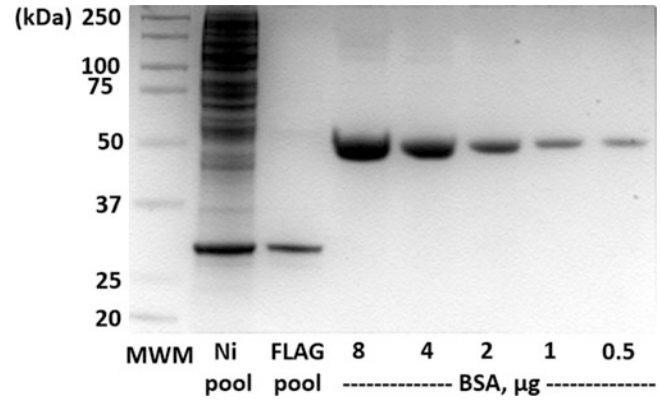

Fig. 1 Coomassie Blue-stained gel of DHHC3 Ni and FLAG pools with a BSA standard curve for protein yield quantification

a hexahistidine sequence and a FLAG tag at the C-terminus and are expressed and purified using a two-step column purification to give a preparation of high yield and good protein purity. Immobilized metal affinity chromatography (IMAC) is used as the first step. Histidine residues in the hexahistidine tag of the DHHC protein bind to the vacant positions in the coordination sphere of the nickel ions immobilized on the nitrilotriacetic acid agarose resin. After washing to remove nonspecifically bound proteins, the enzyme is eluted using 200–500 mM imidazole as a binding competitor under nondenaturing conditions. While Ni IMAC purification is effective in removing most contaminants in the whole cell lysate, following it with FLAG affinity purification significantly increases the purity of the enzyme (Fig. 1). The FLAG (N-DYKDDDDK-C epitope) tag of DHHC binds to the FLAG M2 monoclonal antibody covalently cross-linked to agarose. FLAG-tagged proteins bind to the resin while contaminants pass through. After washing to remove nonspecifically bound proteins, FLAG-DHHC3 is eluted using 100 µg/mL FLAG peptide as a binding competitor under nondenaturing conditions. A final step of size exclusion chromatography (SEC) enables removal of FLAG peptide and buffer exchange, as well as serving to check the monodispersity of the preparation.

2 Materials

Prepare all solutions and buffers using analytical grade reagents and ultrapure water (18.2 MΩ•cm at 25 °C).

2.1 Baculovirus Stocks and Insect Cell Culture

1. Bacmid encoding His- and FLAG-tagged DHHC protein (*see* **Note 1**).
2. Bacvector Sf9 cells (Novagen).

3. TriEx Sf9 cells (Novagen).
4. Unsupplemented Grace's Insect Medium.
5. Growth Medium: Grace's Medium, 10% heat-inactivated fetal bovine serum (HI-FBS) (*see* **Note 2**).
6. ESF 921 medium (Expression Systems).
7. Cellfectin® II transfection reagent.
8. 6-well sterile tissue culture plates.
9. Phosphate-buffered saline (PBS): 137 mM NaCl, 2.7 mM KCl, 8 mM Na_2HPO_4, and 2 mM KH_2PO_4.

2.2 Ni-NTA Purification

1. Nickel-nitrilotriacetic acid (Ni-NTA) agarose (Qiagen).
2. 1.5 × 15 cm glass chromatography column (cross-sectional area 1.77 cm^2).
3. DDM Extraction Buffer: 50 mM Tris–HCl, pH 7.4, 200 mM NaCl, 10% glycerol, 1 mM (tris(2-carboxyethyl)phosphine) (TCEP), pH 7.4, 1% dodecylmaltoside (DDM), 1 μg/mL aprotinin, 1 μg/mL leupeptin, 1 μg/mL pepstatin A, 0.25 mM PMSF, 1 mM benzamidine (*see* **Note 3**).
4. Ni Equilibration Buffer: 50 mM Tris–HCl, pH 7.4, 200 mM NaCl, 10% glycerol, 1 mM TCEP, pH 7.4, 0.05% DDM, 1 μg/mL aprotinin, 1 μg/mL leupeptin, 1 μg/mL pepstatin A, 0.25 mM PMSF, 1 mM benzamidine.
5. Ni Wash Buffer: 50 mM Tris–HCl, pH 7.4, 200 mM NaCl, 10% glycerol, 0.5 mM TCEP, pH 7.4, 0.05% DDM, 1 μg/mL aprotinin, 1 μg/mL leupeptin, 1 μg/mL pepstatin A, 0.25 mM PMSF, 1 mM benzamidine, 15 mM imidazole, pH 7.4 (*see* **Note 4**).
6. Ni Elution Buffer A: 50 mM Tris–HCl, pH 7.4, 100 mM NaCl, 10% glycerol, 0.25 mM TCEP, pH 7.4, 0.05% DDM, 200 mM imidazole.
7. Ni Elution Buffer B: 50 mM Tris–HCl, pH 7.4, 100 mM NaCl, 10% glycerol, 0.25 mM TCEP, pH 7.4, 0.05% DDM, 500 mM imidazole.
8. 5× Protein Sample Buffer: 250 mM Tris–HCl, pH 6.8, 50% glycerol, 5% SDS, 0.1% bromophenol blue.

2.3 FLAG Purification

1. Anti-FLAG M2 Affinity Gel (Sigma).
2. 1.5 × 15 cm glass chromatography column (cross-sectional area 1.77 cm^2).
3. Tris-buffered Saline (TBS) Buffer: 50 mM Tris–HCl, pH 7.4, 150 mM NaCl.
4. 30 mg/mL 3× FLAG peptide (Sigma) in TBS.

5. FLAG Equilibration Buffer: 50 mM Tris–HCl, pH 7.4, 150 mM NaCl, 10% glycerol, 1 mM EDTA, 1 mM TCEP, pH 7.4, 0.05% DDM.
6. FLAG Elution Buffer: 50 mM Tris–HCl, pH 7.4, 150 mM NaCl, 10% glycerol, 1 mM EDTA, 1 mM TCEP, pH 7.4, 0.05% DDM, 100 μg/mL FLAG peptide.
7. FLAG Column Regeneration Buffer: 100 mM glycine, pH 3.5.
8. FLAG Column Storage Buffer: TBS, 50% glycerol, 0.02% sodium azide.

2.4 Size Exclusion Chromatography

1. Superdex® 200 10/300 GL analytical SEC column.
2. Running Buffer: 50 mM Tris–HCl, pH 7.4, 150 mM NaCl, 1 mM TCEP, pH 7.4, 0.05% DDM.

3 Methods

3.1 Baculovirus Stock and Insect Cell Culture

1. Create a suspension culture of Bacvector Sf9 cells at a concentration of 4×10^5 cells/mL with unsupplemented Grace's Insect Medium (*see* **Note 5**).
2. Seed each 2-cm well with 8×10^5 cells.
3. Allow the cells to attach onto the bottom of the well for 15 min.
4. Dilute 8 μL of Cellfectin in 100 μL of unsupplemented Grace's Insect Medium in a 1.5 mL-eppendorf tube.
5. Dilute 1 μg of bacmid DNA in 100 μL unsupplemented Grace's Insect Medium in a separate 1.5 mL-eppendorf tube.
6. Combine the two solutions and incubate for 15–30 min at room temperature.
7. Pipette the combined DNA–Cellfectin–Grace's mixture dropwise onto the cells (*see* **Note 6**).
8. Incubate for 3–5 h.
9. Vacuum aspirate the transfection mixture and replace with 2 mL of Growth Medium.
10. Incubate the cells at 27 °C for 4–6 days or until signs of viral infection become apparent (*see* **Note 7**).
11. Centrifuge the cells at $500 \times g$ for 10 min and collect the supernatant. This is designated P1 virus.
12. Add HI-FBS to the P1 virus to a concentration of 10% and store at 4 °C in the dark (*see* **Note 8**).
13. Create a 50-mL suspension culture of Triex Sf9 cells in ESF 921 medium at a logarithmic growth phase (*see* **Note 5**).
14. Dilute the P1 virus 1:1000 into the Triex Sf9 cell culture.

15. Incubate the cells at 27 °C with shaking at 125 rpm for 4–6 days or until signs of viral infection become apparent (*see* **Note 7**).
16. Centrifuge the cells at 500 × *g* for 10 min and collect the supernatant. This is designated P2 virus.
17. Add HI-FBS to the P2 virus to a concentration of 10% and store at 4 °C in the dark (*see* **Note 9**).
18. Use the P2 virus to infect Sf9 cells in ESF 921 medium for a large-scale preparation.
19. Infect a 400-mL culture of Triex Sf9 cells in logarithmic growth phase at a density of 1.5–2.0 × 10^6 cells/mL using a ratio of 1:50 (P2 virus–cell culture volume).
20. Incubate the culture with shaking (125 rpm) in a 27 °C incubator for 48 h for optimal expression while limiting proteolysis. Before harvesting, check the cells for signs of infection (i.e., enlarged nuclei, enlarged cells) and count using a hemocytometer. The cell counts postinfection typically range from 2.5 to 3.5 × 10^6 cells/mL.
21. Collect the cells by centrifugation at 1000 × *g* for 10 min at 4 °C. Wash twice with 40 mL PBS.
22. Flash freeze the cell pellets with liquid nitrogen and store at −80 °C.

3.2 Ni IMAC Purification

Carry out all procedures at 4 °C in the cold room unless otherwise specified.

1. Pour the Ni agarose resin into a column. Let the resin settle at the bottom of the column and wash with 10 column volumes (CV) of water to remove the ethanol from the beads (*see* **Notes 10–12**).
2. Wash the resin with 10 CV of Ni Equilibration Buffer (*see* **Notes 13** and **14**).
3. Thaw the frozen cell pellet in a 25 °C water bath, flicking frequently to ensure homogeneous thawing. Once thawed, keep the tube on ice.
4. Resuspend pellet in the DDM Extraction Buffer by pipetting up and down. For DHHC3, the tested ratio of cell pellet to volume of extraction buffer is 3.5 × 10^6 cells/100 μL (*see* **Notes 15** and **16**).
5. Transfer the suspension into a conical tube and rotate end over end for 120 min to lyse the cells.
6. Centrifuge the lysate at 100,000 × *g* for 35 min (*see* **Note 17**).
7. Collect the supernatant (S100).

8. Resuspend a fraction of the pellet (P100) with protein sample buffer containing 0.5 mM TCEP for later **analysis** (*see* **Note 18**).
9. Apply S100 to the column and allow to pass through dropwise at a flow rate of less than 3 mL/min. Collect flow-through (FT) (*see* **Note 19**).
10. Apply FT to column and allow to pass through in a dropwise fashion; collect and reapply for a total of three times. Save the final FT.
11. Wash the column with 10 CV of DDM Extraction Buffer (contains no imidazole) to elute unbound proteins. Save XT wash.
12. Wash the column with 10 CV of Ni Wash Buffer (contains 15 mM imidazole) to elute proteins weakly bound to resin. Save buffer wash (*see* **Notes 20** and **21**).
13. Collect a total of six 2-mL elutions, the first two using Ni Elution Buffer A (containing 200 mM imidazole) and the remaining four using Ni Elution Buffer B (containing 500 mM imidazole) (*see* **Note 22**).
14. If continuing with the FLAG purification on the same day, hold Ni elutions at 4 °C. Otherwise, flash freeze the elutions and store at −80 °C (*see* **Note 23**).
15. Save 40-μL aliquots of each elution. Run SDS-PAGE on half of the gel samples of the six Ni elutions with bovine serum albumin (BSA) protein standards. Stain with Coomassie. Estimate DHHC3 protein concentrations in each of the elutions by comparing it with a linear protein band concentration curve generated with known concentrations of BSA standards (*see* **Note 24**).
16. Run a western blot with aliquots of the P100, XT, Ni FT, and the other half of the elutions to determine the efficiency of extraction, efficiency of binding to the Ni column, and elution profile.
17. Identify peak fractions for FLAG purification based on purity and DHHC3 protein concentration.
18. The Ni-NTA agarose resin can be regenerated by successively washing with 5 CV of the following: water, 0.1 M EDTA pH 8.0, water, 0.1 M $NiSO_4$, 20% ethanol. Store the resin at 4 °C.

3.3 FLAG Purification

Carry out all procedures at 4 °C in the cold room unless otherwise specified.

1. Rinse an empty glass column twice with 5 mL of FLAG Equilibration Buffer. Drain the column and leave about 1 mL residual buffer in the column to aid in packing the gel.
2. Pipette 500 μL FLAG resin (50% suspension) into the column (*see* **Note 25**).
3. Allow the gel bed to drain. The resin buffer will flow slowly and the flow rate will increase as the glycerol is removed.
4. Prime the gel by applying three sequential CV of FLAG Column Regeneration Buffer (*see* **Note 26**).
5. Wash the resin three times with 10 CV of FLAG Equilibration Buffer.
6. If Ni elution samples were frozen, quickly thaw in a 25 °C water bath and place on ice.
7. Dilute the pooled fractions: 1 part Ni pool–4 parts FLAG Equilibration Buffer.
8. Apply pooled fractions to the column resin under gravity flow and collect the FT. Reapply the FT for a total of three times as multiple passes improve binding.
9. Wash the column with 10 CV of FLAG Equilibration Buffer. This should remove contaminating proteins nonspecifically bound to the FLAG M2 antibody.
10. Collect a total of six 500-μL elutions using FLAG Elution Buffer. Save 40 μL aliquots for gel analysis.
11. Elute any remaining protein from the FLAG resin by washing the column three times with 1 CV of FLAG Column Regeneration Buffer and save the fractions (*see* **Note 27**).
12. Immediately add 500 μL of FLAG Equilibration Buffer to each fraction to achieve neutral pH.
13. Rinse the column with FLAG Equilibration Buffer until the pH of effluent is neutral.
14. Prepare the column for storage by washing with 10 CV of FLAG Column Storage Buffer.
15. Add 5 mL of FLAG Column Storage Buffer. Do not drain. Label and store the column at 4 °C for future use (*see* **Note 28**).
16. Run SDS-PAGE on half of the gel samples of the six nickel elutions with bovine serum albumin (BSA) protein standards. Stain with Coomassie. Estimate DHHC3 protein concentrations in each of the elutions by comparing it with a linear protein band concentration curve generated with known concentrations of BSA standards (*see* **Note 29**).

3.4 Size Exclusion Chromatography

1. Pool FLAG elutions and concentrate to 1 mg/mL.
2. Apply 25 μg of protein diluted to 100 μL with running buffer to a size exclusion column at a flow rate of 0.5 mL/min.
3. Check for monodispersity based on the intrinsic tryptophan fluorescence at A280.

4 Notes

1. Bacmids are constructed using the Bac-to-Bac Insect Cell Expression System from Invitrogen.
2. Fetal bovine serum is heat inactivated by incubating at 56 °C for 30 min.
3. Protease Inhibitors are made up as 1000× stocks as follows: 1 mg/mL aprotinin in H_2O, 1 mg/mL leupeptin in H_2O, 1 mg/mL pepstatin A in absolute ethanol, 250 mM PMSF in absolute ethanol, 1 M benzamidine in H_2O.
4. Adding 1 M imidazole to the wash and elution buffers will change the overall pH of the solution. Adjust the final pH of the solution to 7.4 with 12 M HCl.
5. Before setting up the transfection or infection, ensure that the BacVector/Triex Sf9 cells are in the log phase of cell growth (target concentration = 1.5–2.5 × 10^6 cells/mL).
6. It is important to add the solution dropwise to not detach the cells from the bottom of the well.
7. Signs of viral infection include clearings in the well, enlarged cells, and enlarged cell nuclei. Having a negative control (without the transfection mixture) in a separate well is recommended. In the control well, the cells will keep growing and minimal clearing of the monolayer will be seen.
8. We have determined that the P1 virus remains potent for at least 3 months if stored in the dark at 4 °C.
9. We have determined that the P2 virus remains potent for 2 weeks if stored in the dark at 4 °C.
10. For efficient column packing, make sure that both the column and the resin are equilibrated at 4 °C before starting. For a 400 mL cell culture, we typically use 2 mL of Ni-NTA agarose packed in a 1.5 × 15 cm, cross-sectional area 1.77 cm^2 glass chromatography column. The theoretical binding capacity of the Qiagen Ni-NTA agarose beads is 50 mg/mL.
11. Ni-NTA agarose comes as a 50% suspension in 20% ethanol. Resuspend the resin by inverting the bottle several times.
12. Do not let the agarose resin run dry at any point in the purification.

13. Ni purification buffers can be prepared a day in advance in the bench and kept at 4 °C until the next day. However, the reducing agent (TCEP), detergent (DDM), and protease inhibitors must be added just before use on the same day of purification.
14. Increasing the pH of the equilibration buffer to pH 8 will increase protein binding to the NTA beads but will also increase nonspecific binding of other proteins.
15. For a 400 mL prep harvested at 3.5×10^6 cells/mL, we extract with about 40 mL of extraction buffer.
16. Pipetting up and down ensures that there are no clumps of unbroken cells left during the extraction.
17. Thick-wall polycarbonate tubes can be partially filled and centrifuged. Thin-walled ultracentrifuge tubes must be filled completely, or they will collapse during centrifugation. For ultracentrifugation, the tubes must be balanced such that the masses of the tubes with the sample must be within ± 0.1 g.
18. If P100 is hard to solubilize, use a syringe needle (25G) to let the SDS get into the pellet.
19. Ensure that S100 clear and not cloudy to avoid clogging the column.
20. It is recommended to include 15 mM imidazole in the Ni Wash Buffer to remove proteins nonspecifically bound to the resin.
21. Although 10 CV of wash buffer is usually sufficient, the total protein concentration in the washes can be monitored by measuring the absorbance at 280 nm (A_{280}). Ensure that the final wash fraction has a baseline A_{280} value before proceeding with the elution.
22. Most of the protein typically elutes in Ni elutions 2 and 3.
23. It is recommended to keep the Ni column at 4 °C until the results of the gel analysis are available.
24. We use the VersaDoc™ 5000 imaging system to quantify protein bands in a gel using volume density determination followed by linear regression analysis.
25. The ANTI-FLAG M2 affinity gel resin is stored in 50% glycerol. The glycerol must be removed just prior to use and the resin equilibrated with the equilibration buffer. Because the gel is very viscous, it is very important to thoroughly resuspend the resin. Make sure the bottle is a uniform suspension of the gel beads before pipetting. Vortex if necessary.
26. Avoid disturbing the gel bed while applying the FLAG Column Regeneration Buffer. Let each aliquot drain completely before adding the next. Do not leave the column in glycine HCl for longer than 20 min.

27. This step serves a dual purpose. The glycine in the FLAG Column Regeneration Buffer elutes any remaining protein and regenerates the FLAG resin for future use.
28. Do not allow the resin to remain in TBS buffer for >24 h without an antimicrobial agent, 0.02% NaN_3.
29. For a 400-mL preparation, the typical yields are 0.5 mg for DHHC3 and 1 mg of DHHS3.

Acknowledgements

This work was supported by the National Institutes of Health (R01 GM121540).

References

1. Sanja B, Mathieu B, Gisou GF (2013) What does S-palmitoylation do to membrane proteins? FEBS J 280(12):2766–2774
2. Blanc M et al (2015) SwissPalm: Protein Palmitoylation database [version 1; referees: 3 approved]. F1000Res 4:261
3. Lobo S et al (2002) Identification of a Ras Palmitoyltransferase in *Saccharomyces cerevisiae*. J Biol Chem 277(43):41268–41273
4. Roth AF et al (2002) The yeast DHHC cysteine-rich domain protein Akr1p is a palmitoyl transferase. J Cell Biol 159(1):23–28
5. Zhang MM et al (2013) Quantitative control of protein S-palmitoylation regulates meiotic entry in fission yeast. PLoS Biol 11(7): e1001597
6. Mitchell DA et al (2006) Thematic review series: lipid posttranslational modifications. Protein palmitoylation by a family of DHHC protein S-acyltransferases. J Lipid Res 47 (6):1118–1127
7. Gottlieb CD, Linder ME (2017) Structure and function of DHHC protein S–acyltransferases. Biochem Soc Trans 45(4):923–928
8. Politis EG, Roth AF, Davis NG (2005) Transmembrane topology of the protein palmitoyl transferase Akr1. J Biol Chem 280 (11):10156–10163
9. Mitchell DA et al (2010) Mutational analysis of *Saccharomyces cerevisiae* Erf2 reveals a two-step reaction mechanism for protein palmitoylation by DHHC enzymes. J Biol Chem 285 (49):38104–38114
10. Jennings BC, Linder ME (2012) DHHC protein S-acyltransferases use similar ping-pong kinetic mechanisms but display different acyl-CoA specificities. J Biol Chem 287 (10):7236–7245
11. González Montoro A, Chumpen Ramirez S, Valdez Taubas J (2015) The canonical DHHC motif is not absolutely required for the activity of the yeast S-acyltransferases Swf1 and Pfa4. J Biol Chem 290(37):22448–22459